JYU DISSERTATIONS 220

Kalle Kolari

Metal-Metal Contacts in Late Transition Metal Polymers

UNIVERSITY OF JYVÄSKYLÄ
FACULTY OF MATHEMATICS
AND SCIENCE

JYU DISSERTATIONS 220

Kalle Kolari

Metal-Metal Contacts in Late Transition Metal Polymers

Esitetään Jyväskylän yliopiston matemaattis-luonnontieteellisen tiedekunnan suostumuksella
julkisesti tarkastettavaksi
toukokuun 22. päivänä 2020 kello 13.

Academic dissertation to be publicly discussed, by permission of
the Faculty of Mathematics and Science of the University of Jyväskylä,
on May 22, 2020 at 13 o'clock.

JYVÄSKYLÄN YLIOPISTO
UNIVERSITY OF JYVÄSKYLÄ

JYVÄSKYLÄ 2020

Editors
Matti Haukka
Department of Chemistry, University of Jyväskylä
Päivi Vuorio
Open Science Centre, University of Jyväskylä

.

Permanent link to this publication: http://urn.fi/URN:ISBN:978-951-39-8162-4

ISBN 978-951-39-8162-4 (PDF)
URN:ISBN:978-951-39-8162-4
ISSN 2489-9003

ABSTRACT

Kolari, Kalle
Metal-metal contacts in late transition metal polymers
Jyväskylä: University of Jyväskylä, 2020, 60 p.
(JYU Dissertations
ISSN 2489-9003; 220)
ISBN 978-951-39-8162-4 (PDF)

This thesis titled 'Metal-metal contacts in late transition metal polymers' contains two main parts: the introductory section, and a section presenting and discussing the key results of the study. A concluding section, summarising the study's findings, is also provided. The introduction gives a classification of metallopolymers based on parameters such as structure, metal-ion bonding interaction with the polymeric framework, and electronic interactions that polymers may express. Additionally, structural and crystal-packing features of metallopolymers—namely, extended metal atom chains (EMACs)—are presented. Moreover, first section of the thesis contains a brief introduction to metal-metal interactions. It also describes the solid state structure of compounds in which group 11 (Cu, Ag and Au), Rh, and Pt contacts with aromatic N, S-, or N-donor ligands are present. Finally, properties and applications of metal-metal contact containing compounds are presented.

The second main part of thesis presents the results of the syntheses and characterisation of group 11, Rh, and Pt polymers. Either ditopic bridging ligands or chelating polypyridines were utilised to promote polymeric structures with close metal-metal contacts. Nine compouds were synthesized and characterized with single crystal x-ray diffraction. Metal-metal contacts were analysed with computational chemistry, distance criteria, or spectroscopy. Metal-metal distances with a sub sum of Bondi's Van der Waals radii were present in 8 of obtained structures. In addition to Pt-Pt contacts, platinum polymer were found to be luminescent and act as a metallogelator. Fluorophilic interactions were found to impact on gelation behaviour of metallogelator. Mechanical and thermal stability and self-healing properties of obtained gel were investigated with rheology.

In sum, the results presented highlight the great importance of ligand selection for the formation of structural and chemical features of one-dimensional polymeric materials that contain close metal-metal separations and interactions.

Keywords: Metallopolymers, metal-metal contacts, metal-metal interaction.

TIIVISTELMÄ

Kolari, Kalle
Metalli-metalli kontaktit siirtymämetalli polymeereissä
Jyväskylä: University of Jyväskylä, 2020, 60 p.
(JYU Dissertations
ISSN 2489-9003; 220)
ISBN 978-951-39-8162-4 (PDF)

Väitöskirja Metalli-metalli kontaktit siirtymämetalli polymeereissä jakautuu kahteen osaan: Johdantoon sekä tuloksiin ja johtopäätöksiin. Johdanto-osiossa käydään läpi väitöskirjatyön kannalta keskeisimpiä aihealueita, joihin kuuluvat metallopolymeerit sekä metalli-metalli vuorovaikutukset. Metallopolymeerit kappaleessa havainnollistetaan yhdisteryhmille keskeisimmät luokittelutavat sekä rakenteelliset ominaisuudet. Metalli-metalli vuorovaikutusten muodostumismekanismia käsitellään lyhyesti yhdisteille tyypillisimpien ominaisuuksien sekä sovelluskohteiden ohessa.

Tulokset ja johtopäätökset kappale sisältää väitöskirjatyön keskeisimmät tulokset. Ryhmän 11, Rh sekä Pt metallopolymeerejä syntetisoitiin käyttäen joko ditooppista metalleja silloittavaa pyridiini-4-tiolia tai kelatoivia polypyridiini ligandeja. Yhdeksän yhdistettä syntetisoitiin sekä karakterisoitiin muun muassa röntgenkristallografian avulla. Metalli-metallikontakteja analysoitiin laskennallisella kemialla, etäisyyskriteerillä tai spektroskooppisesti. Kahdeksalla yhdisteistä, metalli-metalli kontaktien havaittiin olevan lyhyempiä kuin Bondin Van der Waals säteiden summat. Platina polymeeri havaittiin olevan myös luminesoiva sekä metallogelaattori. Fluorofiiliset vuorovaikutukset havaittiin vaikuttavan metallogelaattorin geelinmuodostamiskykyyn. Geelin mekaaniset, termiset sekä itsestään korjautuvuus ominaisuudet tutkittiin reologia menetelmällä.

Tulokset korostavat ligandin valitsemisen tärkeyttä rakenteen sekä kemiallisten ominaisuuksien räätälöinnin näkökulmasta metalli-metallikontakteja sisältävissä yhdisteissä.

Avainsanat: Metallopolymeerit, metalli-metalli kontaktit, metalli-metalli vuorovaikutus.

Author Kalle Kolari
Department of Chemistry
University of Jyväskylä
kalle.k.kolari@student.jyu.fi

Supervisors Professor Matti Haukka
Department of Chemistry
University of Jyväskylä

University Lecturer Elina Laurila
Department of Chemistry
University of Jyväskylä

Reviewers Senior research fellow Raija Oilunkaniemi
Department of Environmental and Chemical engineering
University of Oulu

University researcher Sirpa Jääskeläinen
Department of Chemistry
University of Eastern Finland

Opponent Professor Laura Rodríguez Raurell
Department of Inorganic Chemistry
University of Barcelona

PREFACE

This thesis presents work that was conducted at the University of Jyväskylä (2013-2020). Research funding was generously provided by the Magnus Ehrnrooth Foundation (2013-2016) and by the Department of Chemistry, University of Jyväskylä (2016-2018). I gratefully acknowledge the reviewers of this thesis, Senior research fellow Raija Oilunkaniemi and University researcher Sirpa Jääskeläinen, for their valuable comments regarding this study.

I am also extremely grateful to Professor Matti Haukka for introducing me the world of organometallic chemistry and x-ray crystallography. I have greatly enjoyed working on interesting projects undertaken by this group, starting from a mini-project that dates back to 2009. Thank you for your patience, sup-port, and guidance throughout this process.

In 2010, I completed my B.S. thesis while working for the project led by Univer-sity Lecturer Elina Laurila; our collaboration has continued in my thesis work, in connection with similar research topics. Thank you for sharing your knowledge and expertise on rhodium carbonyl chemistry. I have also enjoyed also our discussions of a variety of other topics.

I gratefully acknowledge Professors Kari Rissanen, Jan Lundell, and Matti Haukka for supporting my application for a Magnus Ehrnrooth private grant. Without your contributions in the form of recommendation letters, my journey might not have been possible at all.

I want to thank my colleagues, whom I regard as friends as well, for the peer support they provided and for helpful discussions when things were not going as planned. In addition to collaborating with you guys, I greatly enjoyed our coffee breaks and meetings. I really enjoyed brainstorming as well as talking about everyday things with you, the past and present members of the EMS group.

It was a great privilege to work with the staff of the Department of Chemistry. I thank each and every one of you for making working in the department ex-tremely enjoyable.

Finally, I would like to thank my family members for their endless support, which assumed many forms. My special thanks go to my closest family members—my parents, sister, and grandmothers—but I am grateful as well to all my other relatives for their continuous support during this journey.

Jyväskylä 22.5.2020
Kalle Kolari

LIST OF ORIGINAL PUBLICATIONS

I Kolari, K.; Sahamies, J.; Kalenius, E.; Novikov, A. S.; Kukushkin, V. Y.; & Haukka, M. Metallophilic interactions in polymeric group 11 thiols, *Solid State Sci.*, **2016**, *60*, 92-98.

II Kolari, K.; Laurila, E.; Chernyseva, M.; Hirva, P.; Haukka, M. Self-assembly of square planar rhodium carbonyl complexes with 4,4-di-substituted-2,2′-bipyridine ligands, **2020**,106103.

III Kolari, K.; Bulatov, E.; Tatikonda, R.; Bertula, K.; Kalenius, E.; Non-appa, Haukka, M. Self-healing, luminescent metallogelation driven by synergistic metallophilic and fluorine-fluorine interactions, **2020**, *16*, 2795-2802.

Author's contribution

The author of the thesis is the primary author and investigator for all publications included in this thesis and is responsible for the primary draft of manuscripts. The author has performed the syntheses, crystallisations, and structural characterisations with x-ray crystallography and with NMR and IR-spectroscopy of all complexes presented in publications **I-III**.

Other publication by author:

IV Lahtinen, E.; Turunen, L.; Hänninen, M. M.; Kolari, K.; Tuononen, H.M.; Haukka, M. Fabrication of Porous Hydrogenation Catalysts by a Selective Laser Sintering 3D Printing Technique. *ACS Omega*, **2019**, *4*, 7, 12012-12017.

CONTENTS

ABBREVIATIONS

ACAM	Tetraacetamidate
Biim	2,2′-biimidazole
CCDC	The Cambridge Crystallographic Data Centre
CP	Coordination polymer
DCM	Dichloromethane
DFT	Density functional theory
DPA	Di-(2-pyridyl)amide
DZP-DKH	Double zeta polarized-Douglas-Kroll-Hess basis set
IR	Infrared
LM	Ligand-to-metal
LMe	4,4′-dimethyl-2,2′-bipyridine
LNH_2	4,4′-diamino-2,2′-bipyridine
LLCT	Ligand-ligand-to-metal
EMACs	Extended metal atom chains
Me_2Biim	N,N′-dimethyl-2,2′-biimidazole
Et_2Biim	N,N′-diethyl-2,2′-biimidazole
MMLCT	Metal-metal-to-ligand charge transfer
ML	Metal-to-ligand
MLCT	Metal-to-ligand charge transfer
MOF	Metal organic framework
M06	Minnesota 06 functional
NMR	Nuclear magnetic resonanse
OPIV	Pivalic acid
SEM	Scanning electron microscopy
TEM	Transmission electron microscopy
TPP	(2,4,6-tris(pyrazolyl-1-yl)pyridine)
Trpy	2,2′:6′2′′-terpyridine
2-SPyH	Pyridine-2-thione
SpyH	Protonated pyridine-4-thiol
QTAIM	Quantum theory of atoms in molecules
VOCs	Volatile organic compounds

1 METALLOPOLYMERS

Compounds that are polymeric in nature and contain metal ions incorporated into their structure are called metal-containing polymers or metallopolymers.[1,2,3] One of the earliest examples of metallopolymers was published by Arimoto et. al. in the mid-1950s. Poly(vinylferrocene) **(1)**, the backbone of the polymeric structure, was formed via polymerisation of the ferrocene side group.[4] The schematic structure of this metallopolymer is presented in Figure **1**. Since this development, the synthesis and characterisation of metallopolymers has faced challenges. Several contributing factors, such as the lack of synthetic methods, were among the issues that affected the development of these materials, in addition to the poor solubility of metallopolymers combined with the low molecular weight of the compounds.[5] Improvements and advances of synthesis techniques such as electropolymerisation and characterisation methods (NMR and gel-permeation chromatography) in the 1990s accelerated the research on metallopolymers.[6]

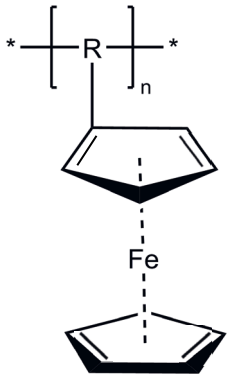

Figure 1 Schematic structure of poly(vinylferrocene) **(1)**.[4]

The metallopolymer concept, which functions as a general category for metal-containing polymers, can be divided into subclasses. Several compounds exemplify the structural variety of metallopolymers. For instance, a coordination polymer (CP), defined by IUPAC in **2013**, is a compound in which a coordination entity (a monomeric unit) extends from 1D to 3D. Metal-organic frameworks

(MOFs) can be considered as coordination polymers, since the definition of CPs applies to MOFs. Additionally, the structure of MOF should contain voids.[7] Extended metal atom chains (EMACs)[8] are compounds that contain linearly arranged metal centres connected by bridging ligands which typically are oligopyridylamides[9].

The classification of metal-containing polymers into types **I-III** was proposed by Rehahn[10] in the 1990s. In this framework, polymers are classified into types depending on the location and/or the interactions of metal ions in the polymeric backbone. In types **I** and **II**, the main bonding interactions of metal ions are covalent bonding and metal-ligand coordination. Additionally, type **I** can contain electrostatic interactions between metal ions and the polymer chain. In type **III,** metal ions are incorporated to the framework by non-covalent interactions. Type **III** metallopolymers may be called metallosupramolecular polymers, due to reversible interactions of metallic and organic components.

Defining types of interactions between metal centers and the organic polymer framework may be difficult. Hence, the location of the metal ion in the structure of the compound can instead be used to categorise materials. Type **I** has metal ions in the side group of the polymer framework, whereas in type **II** the metal ion is embedded in the main polymer backbone. The variability of structures due to the different locations of metal ions in polymeric structures yields a variety of dimensionalities for these compounds—from 1D polymers to 3D networks. In addition to the structural variety of compounds, various metals from main group or transition metals (including lanthanides and actinides) can be used to manufacture functional metallopolymers. Schematic representations of types **I-III** are presented in figure **2**. Table **1** Summarises the observed interaction types of metal centres and polymeric frameworks of types **I-III**.[11]

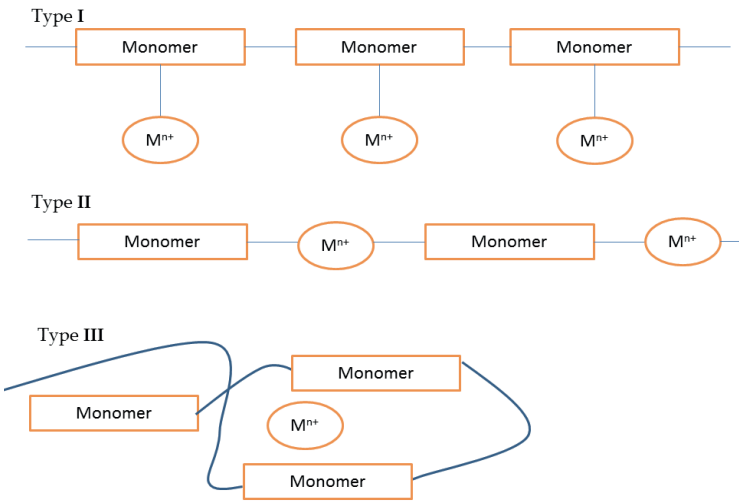

Figure 2 Schematic presentation of metallopolymer classes.

Table 1. Classification of metallopolymers to **I-III**

Type	*Ion location*	*Bonding interactions*
I	Sidechain	Electrostatic Covalent
II	Main backbone	Covalent
III	Embedded	Non-covalent

An alternative classification of these materials was proposed by Hardy et. al. In this classification polymers are divided into two main groups, with subsets based on the location of metals (type **I** and **II**) or the overall topology of metal-containing polymers (type **III** and **IV**).[12] Type **I** contain metal ions in main polymer framework, whereas in type **II** metal ions are located in side chains of polymeric backbones. Type **III** polymers are typically described as star shaped; in type **IV**, the polymeric structure is dendritic**.**[12]

Classification of metallopolymers can be also based on conductivity. In Wolf type **I**, polymers contain metals with insulating organic linkers. By contrast, in Wolf type **II**, polymers express electronic properties of metal centres and linkers. These materials can be further divided into conducting and non-conducting materials.[13]

Compounds classified as coordination polymers have been known since the 1950s.[4] Coordination polymers are materials which consist of ligands as the linking unit and metals in the form of nodes.[14] Structural variability among coordination polymers is the result of the selection of materials used to prepare compounds. Topological features (dimensionality and pore size), especially in metal-organic frameworks, is affected by many factors. In selecting the proper node—i.e. a metal with desired oxidation state—the coordination number may vary from 2 to 10 or even more. Similarly, ionic or neutral ligands with various numbers of donor atoms, the solvent used, reaction conditions, and possible counter ions all have an impact on the formed structures.[15]

1.1 Extended metal atom chains and molecular strings

Compounds wherein closely spaced metal atoms form a one-dimensional linear backbone are extended metal atom chains (EMACs)[16,17]. This type of compound

contains a minimum of three metal ions.[18,19] Metals in in these complexes are typically from d-block.[20,21] Heteronuclear[22] metal string complexes have also been reported. EMACs may be separated into classes depending on the coordination mode of ligands. In traditional metal wire compounds, ligands may bring metal atoms into close proximity by bridging[23,24] coordination mode to form extended arrays with monomeric units of varying nuclearity. Ligands of this type may vary from simple halogens[25,26] to multidentate derivatives of α-(poly)pyridylamide.[27,28] Additionally, cyclic polydentate ligands such as azoles[29–31] have been used in the synthesis of EMACs. Moreover ligands may form extended systems via supporting π -interactions, as in the case of olefin-type ligands.[32]

Direct metal-metal contact is often formed when a square-planar metal complex is self-assembled via non-covalent interactions into extended structures in solid state.[33] Typical non-covalent interactions in this process are π-interactions and hydrogen bonding, which will support formed metal-metal interactions.[34,35] For example, in a study conducted by Inoki et al., a monomeric square-planar rhodium terpyridine complex with labile acetonitrile ligand ([Rh(Trpy)(CH_3CN)](CF_3SO_3)) **(2)** (**figure 3**) was prepared.[36] In solid state, these units were packed in a linear array with non-covalent Rh-Rh interactions supported by non-covalent interactions. Additionally, Inoki et al. tuned the strength of Rh-Rh interaction by synthesizing polymeric Rh compound via reductive elimination of hydrides from square-planar Rhodium terpyridine hydride complexe in acetonitrile .

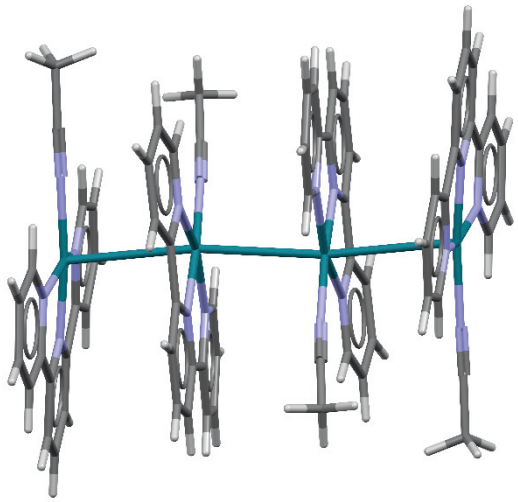

Figure 3 Representation of tetranuclear ([Rh(Trpy)(CH_3CN)](CF_3SO_3)) **(2)** published by Inoki et. al. Solvent of crystallisation and counter ion have been omitted for clarity. [36]

Chain structures with metal-metal interactions have been obtained via electrochemical polymerisation. Octahedral metal carbonyl chlorides with the general formula of [M(L)$(CO)_2Cl_2$][37,38] have been successfully polymerised as thin films in the surface of electrodes when the central metal was either osmium[39] or ruthenium[38] and ligand 2,2′-bipyridine, reported by Caix-Cecillon et. al. and Chardon-Noblat et al. In both cases, the compounds were active towards reduction of CO_2. The ruthenium compound was active in reverse water-gas shift reaction.[37–39]

1.1.1 Non-covalent metal atom chains without ligand support

One of the first one-dimensional compounds with an aligned metal atom backbone in solid state and without bridging ligands was synthesised already in the 1800s by Gustav Magnus. Deep green salt of $[Pt(NH_3)_4][PtCl_4]$ **(3)** (figure **4a**) could be regarded as one of the first coordination compounds synthesised along with Vauquelin's pink salt **(4)** (figure **4b**).[40] $[M(NH_3)_4]^{2+}$ and $[MCl_4]^{2-}$ ($M=Pt^{2+}$ or Pd^{2+}) alter to form a one-dimensional neutral polymer. Solid state structure of **3** was confirmed by x-ray crystallography in 1950s.[41] Polymeric materials with ligand-unsupported metal atom backbones may consist of purely anionic or cationic units. One of the most well-known compounds with an anionic, partially oxidised chain with metal-metal interactions is Krogmann's salt ($K_2[Pt(CN)_4X_{0.3}]$ **(5)**, figure 4**c**, where X=halogen).[42] In these types of compounds, square-planar ionic metal complexes are packed linearly, and thus an aligned metal backbone is formed. Chain structure may also consist of cationic units instead of anions. This is the case in, for example, $[Rh(MeCN)_4](BF_4)_{1.5}$ **(6)**, where square-planar cationic units of $[Rh(MeCN)_4]$ (figure **4d**) are arranged linearly with an outlying charge-balancing $(BF_4)^-$ counter ion.[43] In addition to simple monodentate ligands, chelating N[44]- and O[45]-donors containing ligands may be used for the generation of ionic square-planar complexes, which may self-assemble to form polymeric one-dimensional compounds.

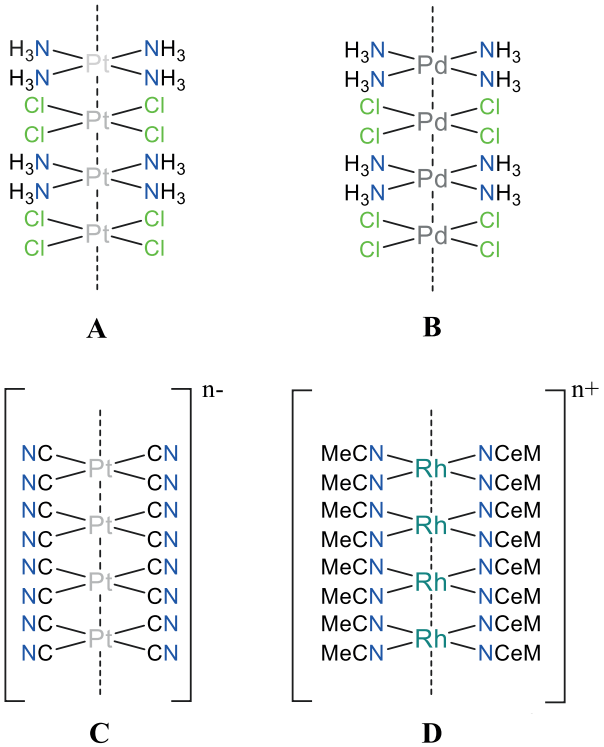

Figure 4 Schematic representations of **A)** Magnus's Green salt, $[Pt(NH_3)_4][PtCl_4]$ **(3)**[46], **B)** Vauquelin's salt, $[Pd(NH_3)_4]$ $[PdCl_4]$ **(4)**[47], **C)** Kromann's salt, $K_2[Pt(CN)_4X_{0.3}]$ (**5**)(X= halogen and counter ions omitted for clarity)[42] and **D)** $[Rh(MeCN)_4]^+$ polymer (counter ion omitted for clarity) **(6)**[43].

1.1.2 Ligand-supported metal chains

The earliest examples of extended metal atom systems where ligands bring metal atoms in close proximity to form metal backbones were published in the 20th century, and based on the utilisation of the di-(2-pyridyl)amide (DPA) ligand.[48] $[Ni_3(DPA)_4Cl_2]$ **(7)** was the first extended system, synthesised in 1968 by Hurley et. al.;[49] however, the structure[50] was not correctly solved until the 1990s. DPA ligands wrapped Ni-atoms helically to form linear Ni backbones with terminal chlorides. Additionally, solvents used for crystallisations were present (Figure **5**). Several other metals, such as Co[51], Ru[52], Rh[21], and Cu[53] yielded similar trimeric metal complexes with the general formula of $[M_3(\mu_3\text{-}DPA)_4X_2]$. It has been shown that DPA-ligand can bind metal ions in different ways, as first presented by Berry in 2004. For example, in the synthesis of $[Ru_3(DPA)_4Cl_2]$ **(8)**, DPA acted as a bridging and chelating ligand simultaneously (figure **6**).[18]

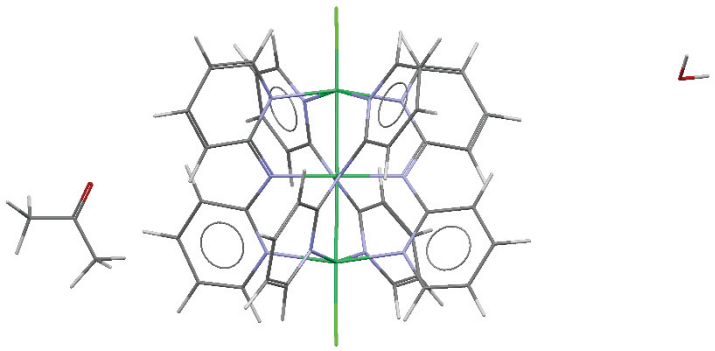

Figure 5 Crystal structure of $[Ni_3(DPA)_4Cl_2]$ **(7)** with solvents used for crystallisations.[50]

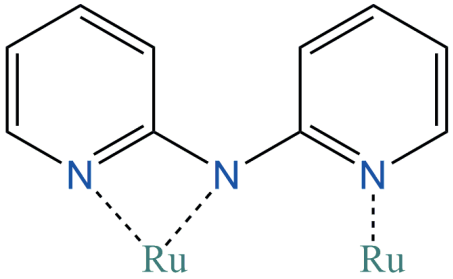

Figure 6 Partial schematic representation of $[Ru_3(DPA)_4Cl_2]$ **(8),** in which both a bridging and chelating coordination mode of DPA is present.[18]

The design of polydentate ligands has been carried out since due to the fact that the size of the ligands and the number of donor atoms in the structure limits the

length of molecular wires. To extend the length of metal backbone, the structure of the DPA ligand was modified by extending the ligand framework such that it contained more donor atoms.[17] This type of ligand is called oligo-α-pyridylamines.[9] Currently this approach has yielded molecular wires containing, for example, 11 Ni atoms by using bis[2-(1,8-naphthyridin-7-yl-amido)-1,8-naphthyridin-7-yl]amido (tentra) ligands (Figure **7**) **(9)**.[54] A similar approach has been used in the manufacture of heterometallic chains using DPA or its analogues. These heterometallic compounds may be called next generation EMACs.[16]

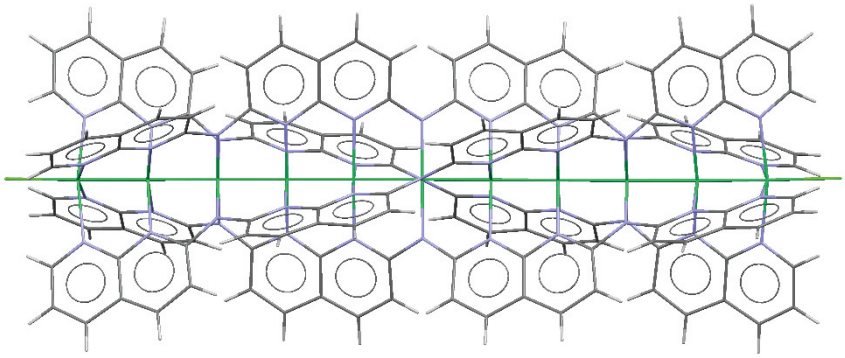

Figure 7 Crystal structure of $[Ni_{11}(TENTRA)_4Cl_2]$**(9),** without the solvent of crystallisation or counterions.[54]

Extended metal atom systems with partial ligand-support may also be generated from dinuclear units. These structures may be homo-[55] (figure **8**) or heterometallic[56] (figure **9**) in nature. For example $[Rh_2(Et_2Biim)Cl_2(CO)_4]$ **(10)** self-assembles via non-covalent interactions into homometallic chain. The $[\{Rh_2(ACAM)_4\}_3\{Pt_2(OPIV)_2(NH_3)_4\}_4](ClO_4)_8$ heterometallic chain consists of self-assembled $[Rh_2(ACAM)_4]_3$ and $[Pt_2(OPIV)_2(NH_3)_4]_4$ units **(11)**.

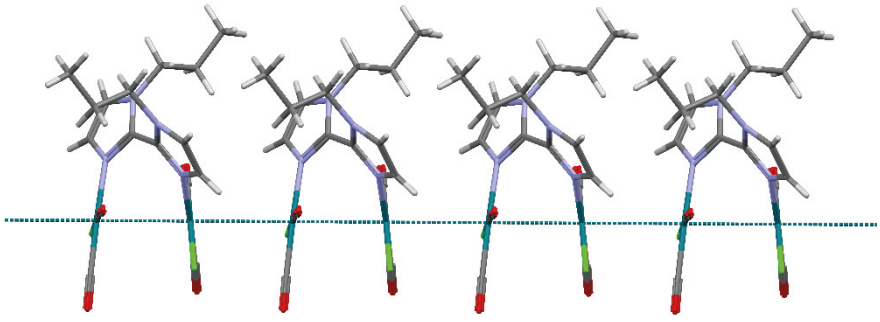

Figure 8 Extended homometallic chain of $[Rh_2(Et_2Biim)Cl_2(CO)_4]$ **(10)**.[55]

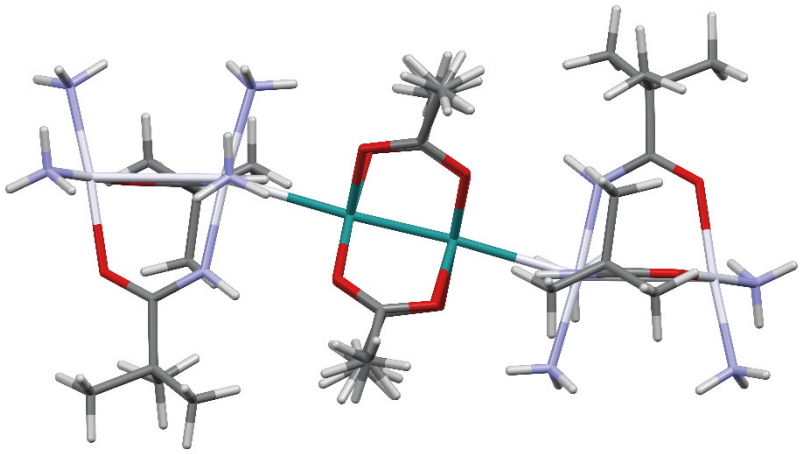

Figure 9 Heterometallic one-dimensional chain structure of $[\{Rh_2(ACAM)_4\}_3\{Pt_2(OPIV)_2(NH_3)_4\}_4](ClO_4)_8$ **(11)**. [56]

In addition to chain structures containing σ-donor ligands, there are published examples of sandwich-type compounds with π-coordinating ligands, such as aromatic and highly conjugated olefins.[57] Again the topology and length of metallic backbone is influenced by the sterical and conformational factors of the ligands and the number of π-donors (double bonds). [58]

In summary, depending of the number of donor atoms, substituents in ligands, and chosen metal, different EMACs with varying nuclearities are achieved. Nuclearities range from tri- to polynuclear compounds. As with coordination polymers, due to stability and solubility factors, the synthesis and characterisation of these compounds present challenges for research on extended metal systems.

2 METAL-METAL INTERACTIONS

Interactions of metal atoms in which the distance of two metal centres is shorter than Van der Waals radii in extended arrays[59] are affected by valence shell electron configuration. Transition metal cations with open valence d- shell configurations are typically systems where the interaction of metal centres has a noticeably or substantially covalent character.[60] Approaching pseudo-closed or closed shell configurations (d^8, d^{10}, and s^2),[61–63] the nature of bonding interactions of transition metal cations converges with attractive non-covalent interactions. Pseudo shell configuration d^8 express metal-metal interactions in square-planar complexes. This is influenced by strong field ligand which effect on the splitting of d-orbitals.[64] The most common geometries in monomeric units that will self-assemble and form direct ligand un-supported metal-metal interactions are linear[65] and square-planar.[66] Moreover, multinuclear units such as dimers may crystallise to form extended metal-metal interactions, as presented previously in figure **8**. In this thesis, the focus is pseudo- or closed shell interactions.

The origins of the research on attractive interactions of closed shell species are under discussions. The earliest suggestion about the mechanism was proposed by Hoffmann in the late 1970s, based on computations of Cu(I)-Cu(I) dimers in which hybridisation interactions of higher non-occupied (n+1)s and d_z^2 orbitals occurred.[67] Different views were developed later on. In the 1990s, computational studies conducted by Pyykkö et. al. concluded that attractive metal-metal interaction is heavily influenced by electron correlation with relativistic effects without a hybridisation component. The attractive interaction can be described in terms of dispersion interactions as well.[68] It was shown that this explanation applies especially for group 11 transition metal species with a closed shell configuration.[69]

A feature commonly observed in transition metals, in particular, is relativistic effects. The most important fact to be considered in formation of metallophilic interactions is orbital contraction. Due to relativistic effects, the radial orbit of the electron is contracted and relative orbital energies are affected. The strongest contraction is observed in s-orbitals; it lowers the relative energies of s- and also p- orbitals.[70] This results in smaller energy differences between bonding HOMO d-orbitals and non-bonding LUMO s-orbitals. Thus, relativistic effects

will impact the formation and strength of metal-metal interactions. Other factors such as orbital interactions and Pauli repulsion will also have an impact on the generation of metal-metal interactions.[71]

In short, the formation of metal-metal interactions is a complex phenomenon with several contributing factors. In general, interaction is formed when metal centres approach a sub sum of Van der Waals distance, and initially formed occupied bonding and antibonding orbitals interact with low-lying valence orbitals. This results in a stabilisation of unoccupied orbitals, which in turn stabilises the whole system. Thus attractive metallophilic attraction is formed.[64] Illustration of the valence electron structure of generic homometallic dinuclear metal-metal interaction is shown in figure **10b**. Figure **10a** represents a situation in which no metal-metal interactions are present.

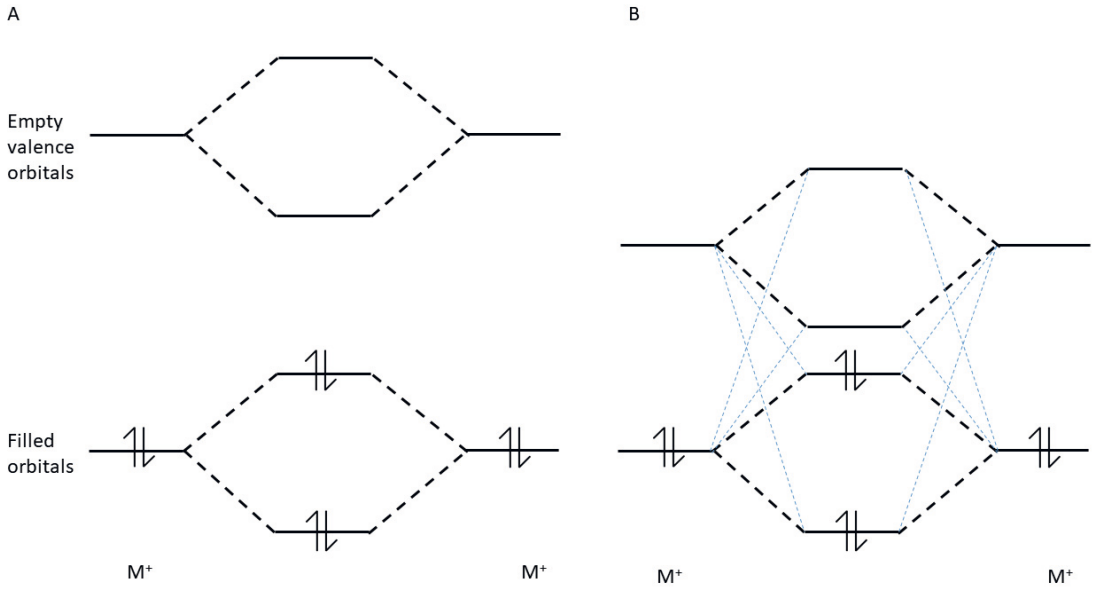

Figure 10 Schematic representations of the valence shell interactions of homometallic dinuclear metal-metal interactions. **a)** Schematic valence shell structure without metal-metal interactions. **b)** Valence shell orbital interactions when metal-metal interactions are present. Note that the relative orbital energies are not scaled.[64]

Experimental and theoretical methods are used for analysing non-covalent interactions. One of the most utilised experimental methods for solid state structures is the determination of intermolecular distance from single crystal x-ray structure. Generally, if the distance of metal centres in monomeric units in the solid state structure is sub sum of the Waals radii, metal-metal interactions may exist.[72,73] The concept of the Van der Waals radius is not straightforward, however. Radii may be defined in several ways, resulting in varying values. For instance Bondi's Van der Waals radii for Cu is stated as 1.4Å, compared to Alliger's 2.26Å.[74]

Spectroscopical methods such as uv-vis[33], Raman[75], or NMR[76] may also be utilised to confirm the presence and nature of intermetallic interactions. QTAIM has been also been used to interpret non-covalent interaction in descriptions of the electron-density topology of the systems in question.[77] Another method used to interpret actual electron density distribution is NCIPLOT, in which the identification of non-covalent interaction is based on a reduced electron-density gradient.[78]

2.1 Optical properties

Metal-metal interactions can be detected by optical experiments. For example, monomeric Pt(II) square-planar transition metal complexes, with terdentate ligands may express triplet state ligand-centred (^{3}LC), ligand-to-metal (^{3}LM), and metal-to-ligand (^{3}ML) charge transfer states. Additionally, ligand-to-ligand-charge-transfer (LLCT) may occur.[79] Polymerization of monomeric complexes *via* self-assembly into larger aggregates in co-operation with non-covalent metal-metal interaction may result in spin forbidden metal-to-metal-to-ligand charge transfer phosphorescence (MMLCT). As stated previously, MMLCT can be described as an interaction in which adjacent metal centres' d_z^2orbitals overlap, forming bonding and antibonding σ-orbitals. The energy gap between formed orbitals correlates strongly with intermetallic metal-metal separation.[80] Typically, emissions are located in the red region of the emission spectra.[81] Emission energies can be modified through the tuning of previously mentioned metal-metal interactions; this is seen, for example, in polymorphic structures.[82] For instance, a one-dimensional diamine bis(σ-acetylide) complex containing Pt-Pt interactions was published by Kang et al. in 2016. Depending on the solvent of crystallisation, either metal-π (dimethylsulfoxide or acetonitrile) or Pt-Pt interactions (dichloromethane) were achieved which affected the photophysical behaviour of the complexes. This was seen especially in solid state. According to the authors, the dimethylsulfoxide adduct expressed low-energy MLCT due to strong π- π stacking interactions around 510-800 nm. When comparing the emission properties of DCM adduct, the authors observed similar emissions of 670 and 761 nm and attributed them to MMLCT, due resulted from infinite platinum metal chain structure.[83]

2.2 Tuning optical properties by modifying metal-metal interactions

Ligand substitution has an effect on metal-metal interactions and optical properties, such as the emissions and color of the compound. The substitution effect may be divided into two aspects: electronic effects and steric effects. Electronic effects of metal-metal interactions may be examined by adding electron-

withdrawing or -donating substituents to ligand structures, as presented in work published Sluch et. al. in 2012. It was found that in [Pt(CNR)Cl_2] complexes, with R either being either an electron donor or an -acceptor substituent, electron-donating groups yielded shorter intermetallic Pt-Pt contacts and red-shifted emissions compared to compounds with electron-withdrawing substituents. Sterical effects were investigated by utilising a bulky *p*-tolyl ligand, which yielded elongated stacks of monomeric complexes without any signifying intermetallic contacs.[34]

The electronic effects of electron- withdrawing substituents may decrease the coulombic repulsion of metal centres; this leads to shorter metal-metal distances and increases the strength of metal-metal interactions, as seen in a study published in 2018. In that particular study, in Rh(I) complexes with an electron-withdrawing substituent, decorated terpyridine ligands were prepared. It was found that electron-withdrawing units may have affected the self-assembly process of monomeric units by inducing π-stacking of ligand and substituent moieties and reducing the coulombic repulsion of metal centres. Thus, intermetallic metal-metal separation was affected, and the lowest energy emission signal appeared in the red area of the VIS-spectrum.[84] Moreover, other crystal packing factors, such as counter ions[85] and secondary non-covalent interactions,[86,87] affect the formation of metal-metal contacts and the MMLCT properties in polymeric structures as well.

2.3 Copper, silver and gold metallopolymers

Metal-metal contacts of group 11 transition metals are called cuprophilic[88] (Cu), argentophilic[89] (Ag), and aurophilic[65] (Au) interactions; these are commonly termed metallophilic interactions. As mentioned previously the strength of metallophilic interaction is associated with relativistic effects. Thus, the interaction strength is said to be increased going from copper to gold.[90]

One of the first papers on a compound characterised with x-ray crystallography containing ligand-supported copper-copper interactions was published as early as the 1960s.[91] An extensive mini-review article on inter- and intramolecular interactions focusing on ligand-supported systems was presented in *Chemistry: A European Journal* in 2019. This review states that cuprophilic interactions can occur when intermetallic Cu-Cu contact is sub sum of the Van der Waals radii of 1.96 Å.[62] The value of 1.96 Å for Cu is obtained from Hu et. al. and derived from single covalent radii of the atom in question.[74] Attractive cuprophilic interaction, which counters coulombic repulsion, is argued to form by hybridisation. 4s and 4p orbitals form admixtures to 3d orbitals[92], which, in turn, transform repulsion to attraction interaction.[93]

It is stated that Cu(I) monomeric complexes aggregate via formation of cuprophilic interactions, typically with ligand-bridging metal centres.[94] This process is affected by ligands' steric and electronic factors as well as additional donor

ligands.[35] Most ligand-supported structures are polydentate nitrogen or phosphorus donor ligands.[62] There are a plethora of structures containing sulphur donor ligands, in which linear extended structures are sparce.[95] Utilising thiourea as a ligand, Taylor, Jr., et al. synthesised a dinuclear thiourea bridged compound with Cu-Cu separation of 2.839 Å, presented in figure **11**:$[Cu_2(N,N\text{-dimethylthiourea})_6][BF_4]_2$ **(12).** Similar structures have been obtained with dimethylthiourea as well.[96] Additionally a N,S donor ligand[97] and mixed-ligand approach with S-donor ligands and a halide ion[98] have been applied in the synthesis of dinuclear Cu species.

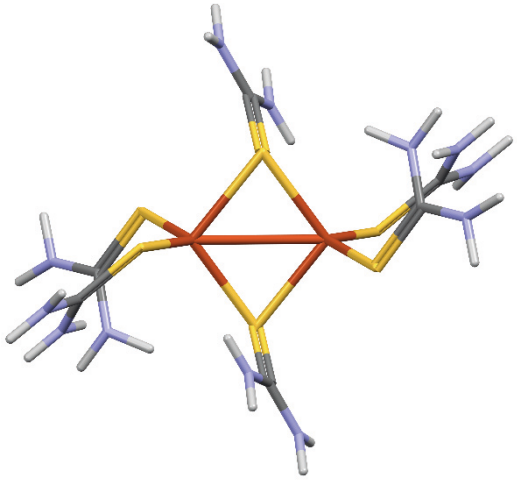

Figure 11 Dinuclear $[Cu_2(N,N\text{-dimethylthiourea})_6][BF_4]_2$ **(12)** containing metal-metal contact obtained with the utilisation of bridging ligand. Counter ions (BF_4^-) have been omitted for clarity.[96]

Ligand-unsupported structures, *i.e.*, structures without ligands in a bridging coordination mode, are infrequent. Often, secondary non-covalent interactions such as π-interactions and hydrogen bonding support copper-copper interactions.[99]

Van der Waals contact distance for silver has been estimated to be 3.44 Å by Bondi.[100] One of the latest reviews on this topic was published by Schmidbaur in 2015. Argentophilic interactions are shown to exist with various coordination geometries due to the flexible coordination geometries of silver. Assessment of argentophilicity and metal-metal interactions in general is challenging in ligand-supported structures. The review states that argentophilic interaction may be present in structures with metal contacts with sub sum of the Van der waals radii of 3.44 Å. It is stated that unsupported metal centres often yield shorter contacts than ligand-supported ones. Additionally, the effect of ligand to Ag-Ag distances is often challenging to predict; hence, assessing whether argentiphilic interaction is present is problematic. The reason why this interaction is counterintuitive is that cationic centres in close proximity should express coulombic repulsion, even if the charge distribution is localised towards ligands. As in the case of cuprophilic interactions, aggregation in ligand-unsupported silver complexes may self-

assemble into supramolecular structures *via* formation of argentophilic interactions.[101] Linear extended structures are sparse. One-dimensional structures with Ag-Ag contacts have been achieved, for example, by the utilisation of multidentate N-donor atoms containing ligands. In $[Ag_2(\mu\text{-}TPP)_2][BF_4]_2 \cdot 0.3MeNO_2$ **(13)(**figure **12.)**, the arrangement of the ligand is helical; *i.e.*, the ligand wraps Ag atoms to form a linear chain.[102,103], silver-silver intermetallic contact values vary from 2.909 Å to 3.066 Å.

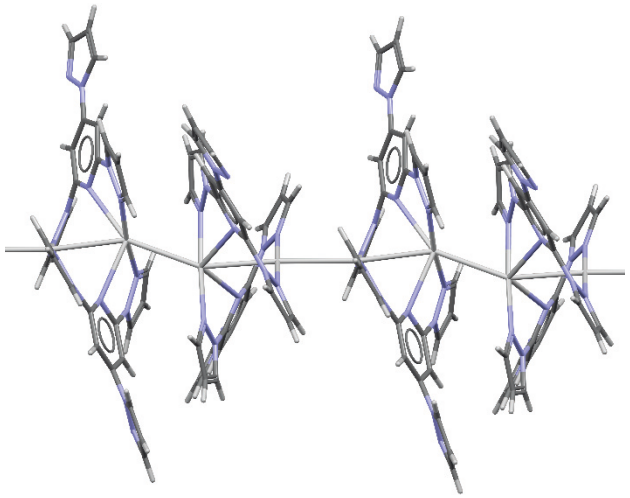

Figure 12 Continuous Ag-Ag chain in $[Ag_2(\mu\text{-}TPP)_2][BF_4]_2 \cdot 0.3MeNO_2$ **(13)**. Counter ions have been omitted for clarity.[102]

A one-dimensional chain structure with S-donor containing ligand was published in 2002 by Su et. al.; in this structure, pyridine-2-thiol was utilised as the ligand. In the structure of $([Ag(SPyH)_2]BF_4)_n$ **(14)**, silver atoms had tetrahedral coordination sphere and coordinated with the S-donor of the ligand, producing cationic polymeric structure. Intermetallic Ag-Ag separation was found to vary from 2.799 Å to 2.989 Å in solid state structures, measured at room temperature (figure **13.**)[104]

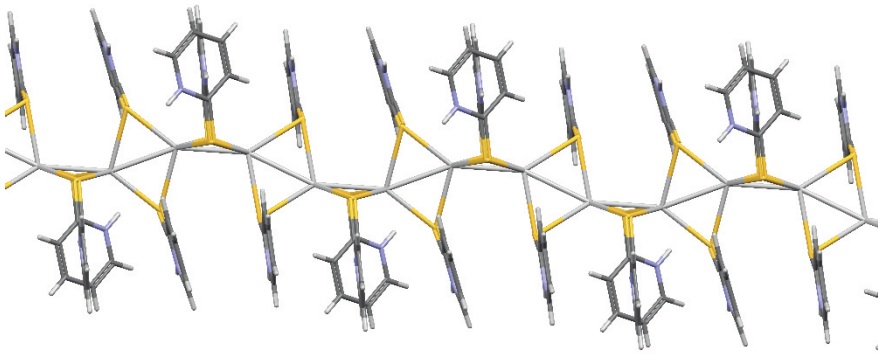

Figure 13 Continuous one-dimensional Ag polymer $([Ag(SPyH)_2]BF_4)_n$ **(14)**. Counter ions have been omitted for clarity.[104]

The literature states that if Au-Au separation in solid state structure is in the range of 2.5-3.5 Å, there is a possibility of aurophilic interactions.[105] Aurophilic interaction is regarded as a d^{10}- d^{10} dispersion[106] interaction, in which relativistic effects strengthen the interaction of ionic Au-centres.[107] This interaction strength can be comparable to a hydrogen bond.[108] It can be utilised as a tool in crystal engineering, producing 3D crystalline assemblies from one-dimensional structures.[109] It is known that secondary non-covalent interactions co-operate with aurophilic interactions in the self-assembly process.[110] $[Au(2\text{-}SPyH)_2]ClO_4^-$ **(15)** , a pentanuclear complex (figure **14**), was published in 1990. In this complex, hydrogen bonding to counter ion (ClO_4^-) and π- interactions cause steric hinderance. The hinderance prevents the formation of a continuous polymeric structure.[111]

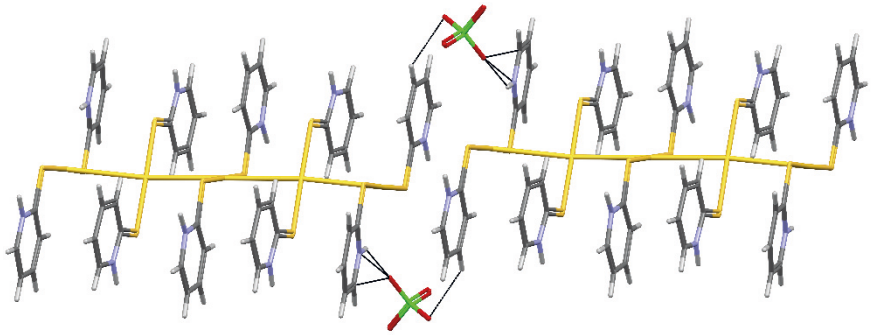

Figure 14 $[Au(2\text{-}SPyH)_2]ClO_4^-$ **(15)** complex with aurophilic interactions co-operating with secondary non-covalent interactions. Au-Au intermetallic contacts of 3.3 Å.[111]

Aurophilicity has been observed in ligand-supported as well as ligand-unsupported chain- or cluster structures.[105] Additionally, aurophilicity has been used in the fabrication of functional soft materials, metallogels.[112,86] It has been observed that there is an inverse relation between the strength of aurophilic interaction and intermetallic Au-Au separation. In 2004, Coker et. al. published a study in which ligand-unsupported $[Au(SCN)_2]^-$ structures with several counter ions and decreasing Au-Au separation yielded blue-shifted lowest energy emission signals.[113] Polymorphs with varying Au-Au separation may be distinguished by emission spectroscopy.[114]

2.4 Rhodium metallopolymers

One-dimensional polymers with direct Rh···Rh interactions are obtained via the self-assembly of mononuclear[44] square planar d^8 Rh(I) complexes or dinuclear[115,116] ligand-supported complexes. Ligand-unsupported structures typically contain π-acceptor ligands such as carbonyl[117] to stabilise the low-oxidation state and prevent oxidative addition reactions. In mononuclear complexes, square-planar geometry is often obtained by using chelating aromatic ligands, typically

contain N[84] or O[45] donor atoms, in addition to monodentate nitriles[118] and isocyanides.[119] Some examples from the literature that are related to the experimental work of this thesis are presented in the next paragraphs. (The examples were obtained via structure searches via The Cambridge Crystallographic Data Centre, CCDC.) The main focus here is on one-dimensional structures with metal-metal contact distances and possible metal-metal-metal angles, for purposes of comparison later on in the experimental part of the thesis.

Few one-dimensional rhodium polymers with 2,2′-bipyridine are found in the literature. Unsubstituted 2,2′-bipyridine yielded a neutral one-dimensional chain via reductive carbonylation of $RhCl_3$, reported by Laurila et al. A chain structure of $[Rh(bpy)(CO)_2][Rh(CO)_2Cl_2]_n$ **(16)** is presented in figure **15**; it consists of cationic $[Rh(bpy)(CO)_2]^+$ and anionic $[Rh(CO)_2Cl_2]^-$ units with Rh-Rh distance of 3.317 Å in between monomeric units. Rh-Rh distance of 3.412 Å was found amid intermolecular units. The presence of non-covalent Rh-Rh interaction was confirmed by QTAIM analysis.[44] As shown by Conifer et al., substitution of the 2,2′-bipyridine ligand may affect the charge state of monomeric unit, thus affecting the charge state of the polymeric framework. In that study, 6,6′-dihydroxy-2,2′-bipyridine produced a cationic chain structure with Rh-Rh distances varying from 3.329 Å to 3.282 Å.[120]

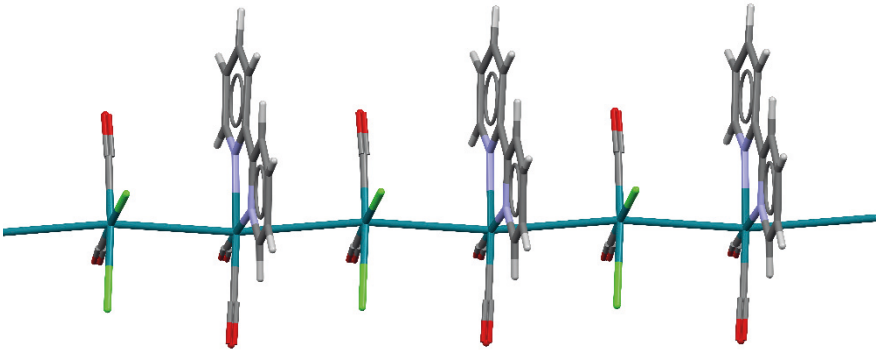

Figure 15 Neutral one-dimensional chain structure $[Rh(bpy)(CO)_2][Rh(CO)_2Cl_2]_n$ **(16)** polymer.[44]

One-dimensional rhodium bi-imidazole carbonyl compounds containing Rh-Rh interactions have been prepared with methods similar to those used for unsubstituted 2,2′-bipyridine, as presented by Laurila et. al. Reductive carbonylation of $RhCl_3$ with dimethyl-2,2′-biimidazole yielded cationic 1D stacks of $[Rh_2(Me_2Biim)(CO)_4Cl_2]^+ \cdot EtOH$ **(17)**. Rh-Rh distances was found to vary from 3.388 Å to 3.441 Å in two crystallographically independent chains. Cl^- and $[Rh(CO)_2Cl_2]^-$ balanced the charge of the polymeric chain. Introduction of additional counterions such as NO_3^- and BF_4^- produced similar chain structures with Rh-Rh distances of 3.238 Å (NO_3^-) and 3.272 Å (BF_4^-), respectively. It is concluded by the authors that the geometry of the counter ion affected the packing of the

cationic unit, causing differences between the Rh-Rh distances in the chain structures.[115] It is also possible to form one-dimensional structures from dinuclear monomeric units, as shown in a further study conducted by Laurila. The study revealed that alkyl (methyl, ethyl and propyl) substituted 2,2'-biimidazoles yielded polymers via self-assembly from dinuclear units (figure **16**) with intramolecular Rh-Rh distances ranging from 3.209 Å (methyl), to 3.147 Å (ethyl), to 3.178 Å (propyl). Intermolecular distances of 3.604 Å (methyl), 3.435 Å (ethyl), and 3.440 Å (propyl) were observed in the study. Rh-Rh-Rh angles were found to range from 163.2 ° (methyl) to 179.5 ° (propyl).[55]

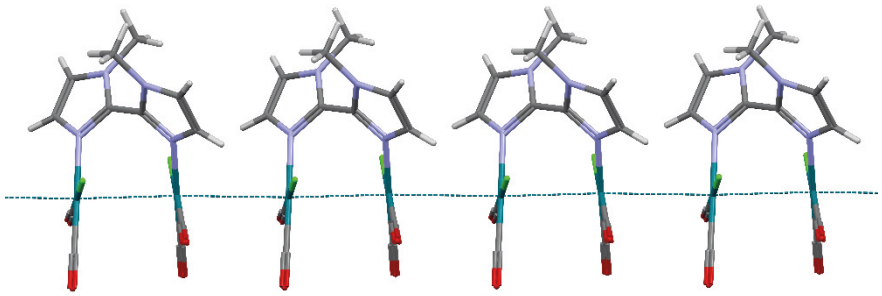

Figure 16 $[Rh_2(Me_2Biim)(CO)_4Cl_2]^+ \cdot EtOH$ **(17)** chain structure consisting of self-assembled dinuclear monomers. Solvent of crystallisations and counterions have been omitted for clarity.[55]

Computational studies showed the relation between intramolecular Rh-Rh distance and attractive metallophilic interactions via the optical behaviour of the compound. In this case, which involves the reduction of intermetallic Rh-Rh distances of $[Rh(biim)CO_2]$ and similar complexes containing substituted bi-imidazoles, it was found that attractive interaction of Rh-centers appeared as a red shift of the absorption signal. The red shift of the lowest energy-absorption signal was explained as a decrease of HOMO (metal center d_{z^2}) and LUMO (bi-imidazole orbitals) gaps in complexes containing unsubstituted bi-imidazoles.

Square-planar rhodium complexes with linear arrangement have also been achieved by using substituted or unsubstituted terdentate terpyridines containing acetonitrile[36], halide[121], or carbonyl[122] ligands. A rhodium terpyridine halide complex, with and without 4'- substituents, was reported by de Pater et al. in 2004. It was found by the authors that in rhodium complexes with unsubstituted terpyridine and chloro-ligand, with no observable contacts was found. Substitution of 4'-position with t-butyldimethylsilyl-o-carboranyl was found to affect the packing of monomeric complexes into dimeric units, with hydrophobic carborane and hydrophilic solvated chloride phases forming Rh-Rh contacts. Rh-Rh distance within the dimer was observed to be 3.150 Å.[121]

Inoki et. al. published in 2012 a dinuclear rhodium terpyridine complex with terminal acetonitrile ligands and trifluoromethanesulfonate as a counter ion. Later, the same authors pubished a compound with formula of $[Rh_4(Trpy)_4(MeCN)_4](CF_3SO_3)_4 \cdot MeCN$ **(18)** and Rh-Rh distances ranging from 3.070 Å to 3.152 Å. The Rh-Rh-Rh angle was found to be 172.2 °. The structure was found to contain the solvent of crystallisation (acetonitrile) as well as two

charge-balancing trifluoromethanesulfonate ions.[36] The solid state structure $[Rh_4(Trpy)_4(MeCN)_4](CF_3SO_3)_4 \cdot MeCN$ **(18)** is shown in figure **17**.

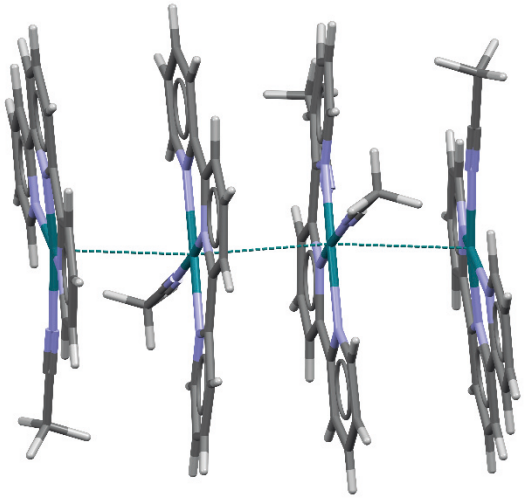

Figure 17 Solid state structure of $[Rh_4(Trpy)_4(MeCN)_4](CF_3SO_3)_4 \cdot MeCN$ **(18),** where co-crystallants have been omitted for clarity.[36]

Polymeric one-dimensional stacks $[Rh(Trpy)CO]CF_3SO_3 \cdot MeCN$ **(19)** (figure **18**), with Rh-Rh contacts in solid state, was published by Kwun-Wa Chan et al. in 2016. It was found by the authors that monomeric square-planar carbonyl units formed two crystallographically independent chains with the solvent of crystallisation and trifluoromethanesulfonate counter ions. Rh-Rh distances and angles in the solid state structure was observed to be nearly identical in both chain structures (chain 1: 3.349-3.326 Å, 160.42 °; chain 2: 3.348-3.326 Å, 160.09 °).[122]

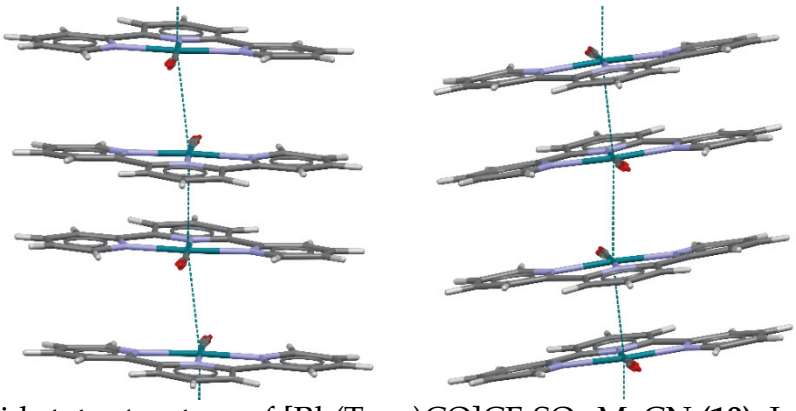

Figure 18 Solid state structure of $[Rh(Trpy)CO]CF_3SO_3 \cdot MeCN$ **(19)**. Left: chain 2; right: chain 1. The solvents used for crystallisations and counter ions have been omitted for clarity.[122]

2.5 Platinum metallopolymers

Platinum-platinum interactions have been known since the 1800s due to the discovery of Magnus green salt.[40] Magnus salts are examples of polymeric material with monodentate ligands. The crystal structure reveals that closely spaced platinum centre distances are 3.25 Å[41]; these distances allow for the formation of metal-metal interactions and aggregation into polymeric compounds.[46] The properties of green salt, such as deep green color, are altered when the metal-metal interactions are modified. Such modification can be seen as a change in intermetallic platinum-platinum distances.[41] The effect of tuning metal-metal interactions can be seen in Magnus's pink salt, which is an isomer consisting of square-planar $[Pt(NH_3)_4]$ and $[PtCl_4]$ units. Single-crystal x-ray data from pink salt are not available due to instability and the conversion of pink salt material to green salt. However, from powder x-ray crystallography, it is concluded that the intermetallic platinum-platinum separation in the solid state is 5 Å.[47]

In addition to monodentate ligands, chelating polydentate ligands are utilised to form square-planar platinum complexes, which further self-assemble into one-dimensional chain structures containing Pt-Pt contacts. For example, terpyridines have been utilised in the formation of square-planar monomeric complexes that self-assemble into structures containing dinuclear or polymeric Pt-Pt contacts.[123,124,125] One of the shortest contact distances is found in dimeric $[Pt(Trpy)Cl]ClO_4$ **(20)**, with a Pt-Pt distance of 3.269 Å; further, optical studies revealed metal-metal interaction (^{3}MMLCT) in the dimeric product.[126] A compound with a one-dimensional chain structure $[Pt(Trpy)Cl]PF_6 \cdot MeCN$ **(21)**, and continuous Pt-Pt contacts was synthesised by Zhang et al. in 2014. [Pt(Trpy)Cl] cation was self-assembled into continuous chains containing an outlying PF_6^- anion and the acetonitrile solvent of crystallisation. In this case it was found that chain structure was pseudolinear. Pt-Pt contact was found to be 3.362 Å with contact angle of 157.18 °.[82] (figure **19**). The presence of Pt-Pt interactions in both compounds was studied with TD-DFT. It was found that the increase of absorption in visible light in the acetonitrile adduct was caused by MMLCT, in which antibonding d_{z2} and the terpyridyl π-orbital energy gap was reduced; the compound expressed a red-shifted absorption signal compared with a compound without the acetonitrile solvent.

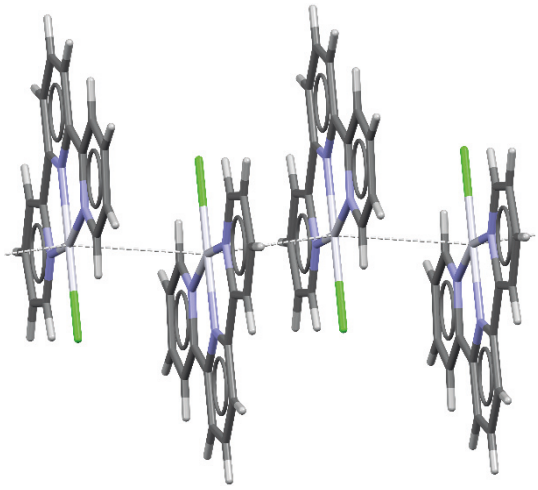

Figure 19 Chain of [Pt(Trpy)Cl]$PF_6 \cdot$MeCN **(21)**. The solvent of crystallisation and counter ion have been omitted for clarity.[82]

Janzen et. al. published the solid state structure of red [Pt(Trpy)Cl]Cl $\cdot 2H_2O$ **(22)**. The polymeric structure contained a pseudolinear Pt-Pt chain with a typical 'head-to-tail' arrangement of chlorido ligand and terpyridine ligand (figure **20**). In this case, the crystal packing is affected by the formation of hydrogen bonding between the solvent of crystallisation and the outlying counter ion, Cl^-. Pt-Pt distances were shown to be 3.328 Å and 3.444Å[124]. Additionally, an orange polymorph existed without Pt-Pt contacts. Hence compounds containing Pt-Pt distances in either dinuclear or polynuclear arrays affect the color of the compound in question. Color change is related to intermetallic distances and thus interactions of metal centres in solid state structures.

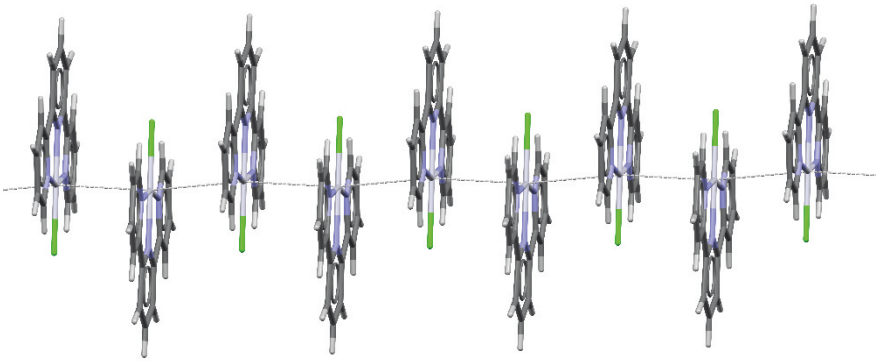

Figure 20 'Head-to-tail' chain structure of [Pt(Trpy)Cl]Cl $\cdot 2H_2O$ **(22)**, which is a red crystalline material and a polymorphic structure containing continuous Pt-Pt interactions. The solvent of crystallisation and counter ion have been omitted for clarity.[124]

2.6 Applications

Compounds with metal-metal backbone express intriguing properties due to the metal-metal interactions. Properties are influenced by modification of these metal-metal interactions in the backbone. Potential properties such as conductivity[127], magnetism[128], photoluminescence[65], and catalytic activity[129] can be utilised in molecular electronics[130] and vapochromic sensors.[131] In addition, compounds with metal-metal contacts have shown to have biological activity vis-à-vis cancer cells. These are typically dinuclear Rh,Re and Ru compounds with rather strong bonding interactions.[132]

Structurally extended metal atom chains are analogous to electric wire. The core consisting of closely spaced metal atoms is surrounded by insulating ligands, which guide the direction of possible conduction.[133] Tuning the conductive properties is performed by modifying the interactions of metal ions of the backbone via axial ligands and the selection of transition metals. Kai-Neng Shih et al. showcased the effect of ligands on conductivity through the tuning of d-electron coupling in $[Ru_3(DPA)_4X_2]$ complexes, where x corresponds to thiocyanate or cyanate terminal ligands. It was shown that single-molecule conductivity clearly increased when terminal thiocyanates were changed to cyanate ligands. This finding was reached through calculations of the result of a stronger ligand field effect, which affected the relative energies of frontier molecular orbitals and the strengths of axial-ligand–dependent metal-metal interactions.[20] It is established that bond orders of metal centres indicate the degree of delocalisation of electrons and the strength of electron transport in the direction of the M-M backbone. This was shown, for example, in a study conducted by Ting et. al., where oligo-α-pyridylamine complexes of Co, Ni, and Cr ($[M_xL_4(NCS)_2]$ where x=3-7) with different bond orders ranging from 0 to 1.5 were synthesised and the conductivity was measured. Conductivity was found to increase when the bond order decreased from 1.5 in the Cr-containing complex to 0.5 with a Co backbone and 0 with a Ni-core.[134]

In a way that is similar to these conduction properties, compounds with closely spaced metal atoms in linear arrays can express photophysical properties such as luminescence. In the literature, there are examples of structures that range from smaller discrete ligand-supported dinuclear[135] units to extended ligand-unsupported polymers.[136] Typical metals in homometallic compounds are from d-block, and in the heterometallic case d- and f-block metals have been used to form functional emitting material.[137] The tuning of emissive properties in solid state has been accomplished by modifying the coordinating ligands. In a study by Sluch et. al., the emission energy of platinum aryl isocyanide complexes was found to shift according to substituent changes in the aryl fragment of the ligand. Adding methyl substituents resulted in red shift, and electron- acceptor groups resulted in a opposite shift of the lowest energy-emission signal.[34]

It has been shown that extended systems with metal backbone are able to participate in catalytic reactions, such as hydroformylation and the reverse water-gas shift reaction, among others. $[Ru(CO)_4]_n$ was shown to catalyse a one-pot reverse water-gas shift reaction, coupled with hydroformylation, in a study by

Laurila et. al. According to this study, the Ru catalyst did not retain an extended framework; it thus acted as a precursor complex in catalysis.[138]

These complexes are typically stimuli-responsive optical materials (VOCs and mechanical stress, for example), which change the photophysical behaviour and color of the compounds. For example, a change in the photophysical properties of polymeric Pt(II) complexes containing metal-metal interactions arises from changes in interactions of metal centres. This can be seen as a bathochromic shift of the lowest energy signal that is affected by the strength of metal-metal interactions. Thus, it is possible to perform a differentiation, in the aggregation state, of Pt complexes with metallophilic interactions.[139] Similar photophysical behaviour has been observed in other polymeric compounds containing metal-metal interactions or bonds. Mochida and Tominaga, for example, reported square planar Rh(I) isocyanide complexes with bulky counter ions that expressed similar photophysical behaviour, which was affected by the aggregation of monomeric units.[119]

3 RESULTS AND DISCUSSION

3.1 Aims of the work

The focus of this thesis was the development and fine-tuning of synthetical procedures to obtain linear and one-dimensional polymeric compounds containing a sub sum of Bondi's Van der Waals radii intermetallic contacts. Two approaches were utilised. In the first approach, a bridging ligand was used to bring metal centres into close proximity and allow the formation of metal-metal interactions. The second approach utilised the self-assembly of square planar units via non-covalent interactions, such as hydrogen bonding and π- and fluorine interactions, to enable close packing of monomeric units to form metal-metal contacts in polymeric structure.

In the first paper, the aim was to produce polymers with metal-metal interactions via the self-assembly of bridging pyridine-4-thiol and group 11 transition metals. Pyridine-4-thiol was selected due to its ditopic nature as well as its polarisability. One-dimensional and continuous compounds were of special interest, because, according to the CSD, such structures are scarce.

In the second paper, the effect of 4,4'-disubstitution of 2,2'-bipyridine with an electron-donating and poor-hydrogen bonding methyl substituent for solid state structures, versus a hydrogen-bonding amine substituent, were investigated. Additionally, crystallisation conditions impact on the self-assembly process was of interest, as was the formation of intermetallic metal-metal contacts in rhodium carbonyl polymers. Previous research on this topic utilising 2,2'-bipyridine presented polymeric structures with only 6,6'-disubstituted groups. The effect of non-covalent interaction on the self-assembly of polymeric structures was thus investigated.

Finally, in the third publication, the goal was to synthesise luminescent polymeric materials with Pt-Pt contacts. The aim was to synthesise square-planar monomeric units that would self-assemble, in co-operation with non-covalent interactions, into infinite one-dimensional structures. Fluorinated terpyridine was chosen as a ligand to promote the formation of square-planar geometry as well as fluorine-fluorine interactions.

3.2 Metal-metal contacts in polymeric copper, silver and gold thiols

Pyridine-4-thiol was chosen as a ligand due to its ditopic and tautomeric nature as well as its anionic (figure **21**) form. It contains exocyclic sulphur and endocyclic nitrogen donors. Anionic form of pyridine-4-thiol was employed to control the charge state of obtained compounds. This was performed by modification of reaction conditions. The S-donor was particularly of interest due to the softness of the donor and its potential bridging coordination mode with Cu(I) and Ag(I) metals. Soft group 11 transition metals were utilised as metals because of the known formation of metallophilic interactions.

There are one-dimensional structures containing pyridine-2-thiol as a ligand; thus, a similar pyridine-4-thiol was used as the ligand. As a ligand, pyridine-4-thiol has been previously utilised with several metals (Cu, Ag, Rh and Ru), with the charge state varying from neutral to anionic. Additionally, oxidation that forms disulphide bonds occurs. The main structure types are cages and clusters, and cyclic and dimer structures have also been known to occur.

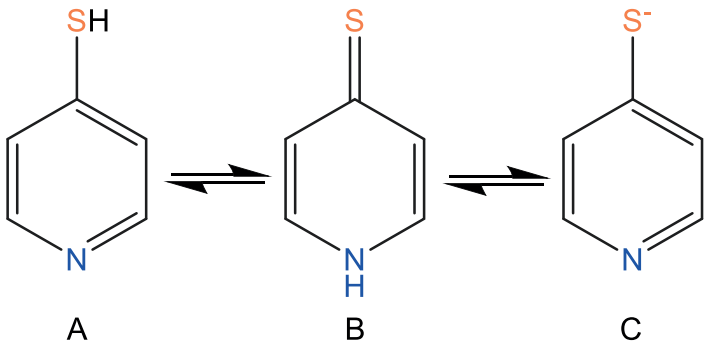

Figure 21 Schematic presentation of pyridine-4-thiol and its forms. A and B are tautomeric stuctures and C deprotonated form.[147]

Three polymeric compounds were prepared: $[Cu_2(SpyH)_4]^{2+}{}_n$ with a $ZnCl_4^{2-}$ anion **(23)**, $[Ag_2(SpyH)_2(Spy)_2]_n$ **(24)**, and $[Au(SpyH)_2]_n^+$ with a Cl^- counter ion **(25)**. In general the syntheses of these polymeric compounds with metal oxidation of (I) can be described as follows: the ligand and metal salt are dissolved separately in chosen solvents. The solution containing the ligand is combined with the metal salt solution dropwise, with vigorous stirring. The silver polymer is obtained as a crystalline material through evaporation of the reaction solvent (**24**). In the case of copper polymer **(23)**, product form crystalline material when counterion ($ZnCl_4^{2-}$) is formed via solvent diffusion of $ZnCl_2$ containing solution and reaction mixture. Similarly, Au polymer form crystals via solvent diffusion method by layering the metal salt and ligand solutions **(25)**.

The reaction conditions had an influence on the charge state of the formed polymeric compounds. In the case of compounds $[Cu_2(SpyH)_4]^{2+}{}_n$ **(23)** and $[Au(SpyH)_2]_n{}^+$ **(25),** cationic polymers were produced without any addition potassium hydroxide. Addition of potassium hydroxide to the reaction mixture produced a neutral polymer $[Ag_2(SpyH)_2(Spy)_2]_n$ **(24)**, due to the partial deprotonation of pyridine-4-thiol ligands that yielded anionic moieties.

The oxidation state of (I) in $[Cu_2(SpyH)_4]^{2+}{}_n$ **(23)** was obtained via an *in situ* reaction of $Cu(II)Cl_2$ and pyridine-4-thiol. The oxidation of pyridine-4-thiol yielded 4,4′-dipyridyldisulfide, and Cu(II) was reduced to Cu(I) ions. This method was utilised due to the low solubility of Cu(I)Cl salt with respect to various organic solvents. The yield of $[Cu_2(SpyH)_4]^{2+}{}_n$ **(23)** was found to be at 44%. The solid state structure of **23** is presented in figure **22**. In the obtained structure, the metal centres were coordinated with bridging pyridine-4-thiol. Intrametallic Cu ⋯ Cu (**23**) separation was measured at 2.6241 (6) Å - 2.6283(6) Å. In comparison with the example studied in literature item **12**, the obtained metal-metal distance is clearly contracted (in item **12**, the Cu-Cu distance was found to be 2.839 Å). The polymeric chain in compound **23** is cationic. The ligand is tautomerised via the migration of the proton from S- to the N-donor. Compensating for the charge of cationic polymer, the ratio of monoanions and Cu centres was found to be 1:1. The $ZnCl_4^{2-}$ anion was found to be hydrogen-bonded to the dangling pyridine-4-thiol ligand and the solvent of crystallisation.

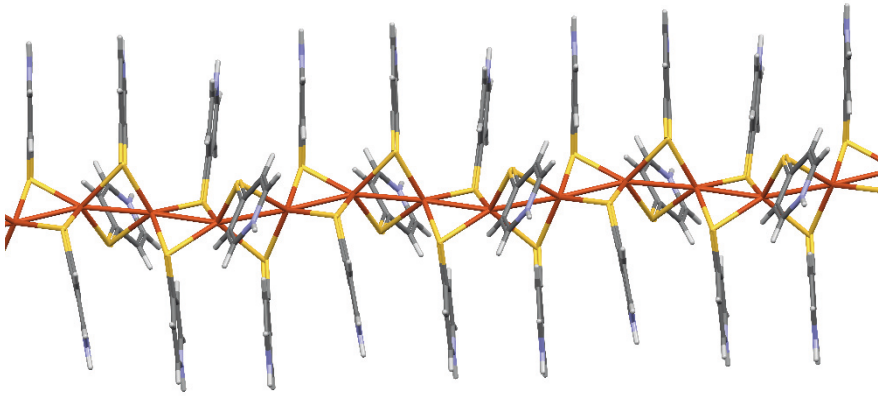

Figure 22 The solid state structure of $[Cu_2(SpyH)_4]_n{}^{2+}$ **(23)**. Solvent of crystallisation and counter ion $ZnCl_4^{2-}$ have been omitted for clarity.

The MS-QTOF CID experiment confirmed the polymeric nature of the compound, showing fragments of $Cu+Cu_n(Spy)_n$ in which n ranges from 3 to 6. The spectrum is presented in figure **23**.

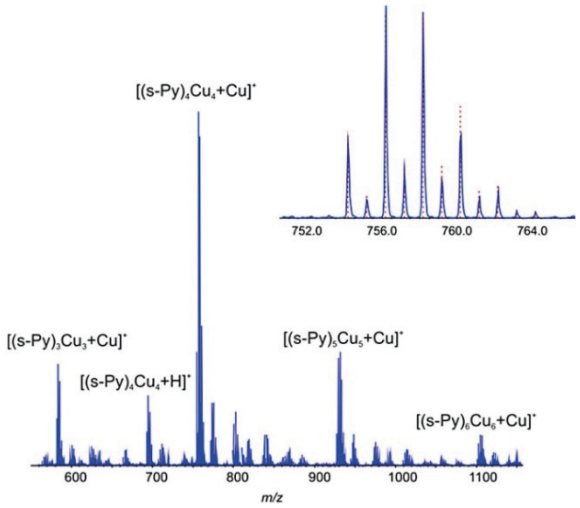

Figure 23 MS-QTOF CID spectrum for compound **23** where the polymeric nature of the structure is seen as increasing fragment sizes. Reproduced with permission of Elsevier Masson SAS.

Compound **24** contains a neutral polymeric isostructural solid state structure (figure **24**) versus compound **23**'s chain structure, which is the result of a reaction condition modification with a strong mineral base. Every other ligand in the solid state structure is deprotonated and thus anionic, balancing the charge of the metal centres. The absence of a charge-countering ion due to partial ligand deprotonation in compound **2** enables more efficient packing, *i.e.* a linear polymeric chain instead of a pseudolinear structure as in compound **23**. Ag···Ag contacts were found to be 3.1939(2) Å- 3.1940(2) Å. As stated in section 2.3, when metal-metal separation is less than 3.44 Å, there are potentially metallophilic interactions. In compound **14**, with a similar structure and containing pyridine-2-thiol, Ag-Ag distance was found to vary from 2.799 Å to 2.989 Å. No solvent of crystallisation was present in the solid state structure.

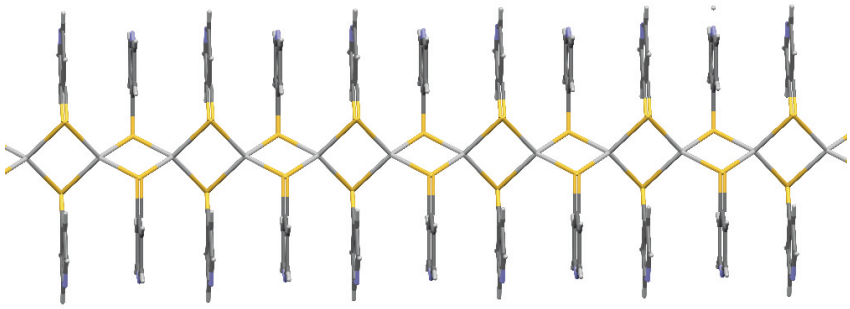

Figure 24 Structure of $[Ag_2(SpyH)_2(Spy)_2]_n$ **24**. Every other nitrogen ion is deprotonated in the structure, yielding neutral metallopolymers.

The bridging coordination mode of pyridine-4-thiol ligand is not present in the solid state structure of compound **25** (figure **25**); this is result from oxidation state of Au**(I)**. Au**(I)** complexes follow 14 electron rule and is 2-coordinate in contrast

to Cu**(I)** and Ag**(I).** Cationic $[Au(SpyH)_2]^+$ forms a one-dimensional linear stack with charge-balancing chloride ions. The contact distance of Au was found to be 3.4277(2) Å. Examples of structure (**15**) in the literature containing pyridine-2-thiol had Au-Au contacts of 3.3 Å and were tetranuclear in nature. The monomeric unit was characterised via a positive polarisation MS-QTOF experiment (figure **26**). In all, the structure's secondary bonding interactions, such as π-stacking, support the polymeric structure and metal-metal contacts.

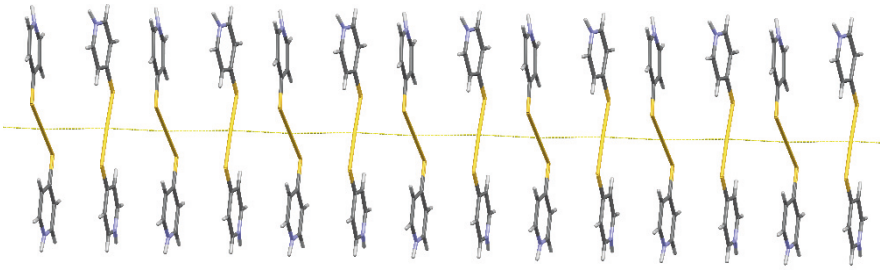

Figure 25 Chain structure of $[Au(SpyH)_2]_n^+$ **25** with Au-Au contacts. Counter ions have been omitted for clarity.

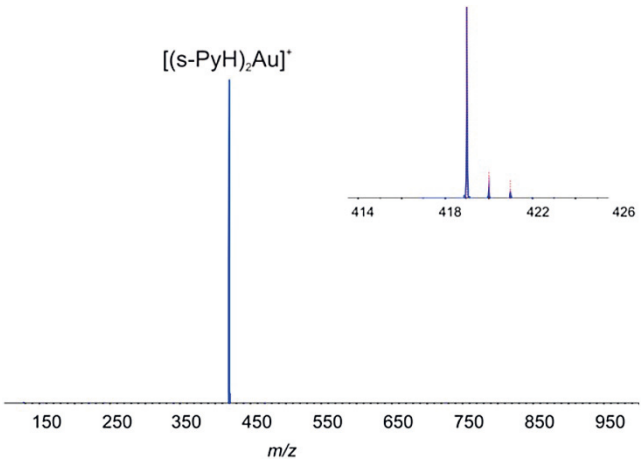

Figure 26 MS-QTOF positive polarisation exact mass spectrum for compound **25**. Reproduced with permission of ELSEVIER.

All structures contained aligned metal centres with contact distances below the sum of Van der Waals radii. This usually is a good indication of metal-metal interactions in ligand-unsupported structures. In the case of polymeric structures where the ligand brings metal atoms in close proximity, assessing the possibility of metal-metal interaction using only intermetallic distance is challenging. Hence additional experimental measurements, such as measurements of conductivity, and theoretical tools from computational chemistry are needed.

Computational chemistry was utilised to gain information about metal-metal interactions and electron-density distribution in polymeric systems. Models for the calculation were obtained from experimental solid state structures. Computations were performed by DFT with the M06 functional.[140] Basis sets for

all atoms were set as DZP-DKH.[141–143] Electron-density topology analyses were performed via the QTAIM[144] method. Bond critical points were found in structures **23** and **25**; such points have been used as an indication of metal-metal interactions between metal centres in polymeric structures. No BCPs were found in structure **24**, even though the distance of Ag centres is below the sum of Van der Waals radii. These results showcase the challenges of relying on bond length criteria (sub sum of Bondi's Van der Waals radii), the impact of bridging coordinating ligand on metallophilicity, and QTAIM analysis for characterisation of the presence of metal-metal interactions. Computations suggested that there are no interactions between Ag centres in compound **24**, despite the Ag-Ag distance begin a sub sum of Bondi's Van der Waals radii. This can be regarded as a good example of contradictory results from computational chemistry versus the analysis of solid state structure and distance criteria, when it comes to the possibility of metal-metal interactions.

In copper-based polymers, the metal-metal contacts have a considerably covalent nature, given the |G(r)|/V(r) parameter derived from computational results. This parameter is ratio of potential energy density and kinetic energy density. Using this formulation, non-covalent interactions(r)|/V(r)>1 and for considerable covalent character in bonding interactions(r)|/V(r)< 1. Metal-metal contacts in compound **25** are typical interactions of a non-covalent nature, where |G(r)|/V(r) equals to 1. These findings are confirmed by the interaction energies of the metal-metal contacts in compounds **23** versus **25**, those energies having been derived via two different approaches (Espinosa and Vener). The interaction energies of the metal-metal contacts in compounds **23** and **25** are in good correlation with the computational data: 5.7-10.7 kcal/mol in compound **23** and 3.0-3.5 kcal/mol in compound **25**.[145,146]

3.3 Rhodium-Rhodium contacts of self-assembled of square planar rhodium carbonyl complexes

The effects of 4,4′-disubstitution in 2,2′-bipyridine on the self-assembly and formation of metal-metal contacts in square-planar rhodium bipyridine carbonyl polymers were investigated. Substituents were chosen according to hydrogen-bonding ability and electronic effect. Rhodium bipyridine carbonyl compounds were synthesised in accordance with procedures outlined in the literature: namely, with one-pot reductive carbonylation of $RhCl_3 \cdot xH_2O$ with varying reaction times and cooling rates. Slow cooling of the reaction vessel produced crystalline material from the products. The ligands used in this project were 4,4′-dimethyl-2,2′-bipyridine **(LMe)** and 4,4-diamino-2,2′-bipyridine **(LNH_2)**.

Polymeric structures with close metal-metal contacts were obtained in three products consisting of either altering cationic ($[Rh(L)(CO)_2]^+$) and anionic ($[Rh(CO)_2Cl_2]^-$) or purely cationic complexes: neutral $([Rh(LMe)(CO)_2][Rh(CO)_2Cl_2])_n$ **(26)**, trinuclear chain

([Rh(LMe)$(CO)_2$][Rh$(CO)_2Cl_2$][Rh(LMe)$(CO)_2]_n$)([Rh$(CO)_2(Cl)_2]$)$_n$) **(27)**, and cationic stacks ([Rh$(LNH_2)CO_2$] [Rh$(CO)_2Cl_2]$)$_n$·EtOH **(28)**. Additionally, a product containing metal-π contacts in a cationic polymeric structure of ([Rh$(LNH_2)(CO)_2]$)$_n$([Rh$(CO)_2Cl_2]$)$_n$ **(29)** was achieved.

The solid state structure of compound **26** (figure **27**) shows a packing of square-planar units into one-dimensional stacks. Two crystallographically independent chains are present due to differences in the packing of stacks. Chain **A** is packed more efficiently than chain **B**; this is seen in difference between Rh-Rh distances and Rh ⋯ Rh ⋯ Rh angles in 1D stacks. In chain **A**, Rh-Rh contacts are 3.3581(2) – 3.4038(2) Å and Rh ⋯ Rh ⋯ Rh angle 169.98(1) °. Differences in packing efficiency are seen in the elongation of Rh-Rh distances; for chain **B**, these distances are 3.3692(2) – 3.4172(2) Å. Simultaneously, the Rh ⋯ Rh ⋯ Rh angle is decreased to 166.03(1). Close Rh-Rh contacts implicates potential metal-metal interactions in this structure. A one-dimensional rhodium chain[44] has been previously published utilising unsubstituted 2,2′-bipyridine. This chain was presented in the introductory section as compound **16**. The Rh-Rh distances in compound **16** vary from 3.317 Å to 3.412 Å; compared to compound **26**'s metal-metal separations, these measurements are very similar. The Rh ⋯ Rh ⋯ Rh angle of **16** was observed to be 170.93 °, which is closer to the Rh-Rh angles in chain **A**. The deviation of the Rh-Rh angle in chain **B** as compared with the value of **16** is due to less efficient crystal packing.

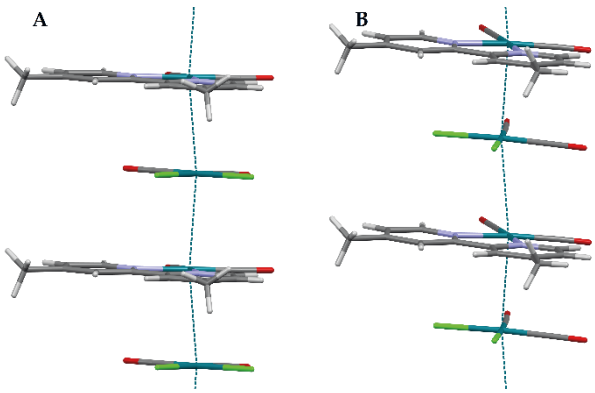

Figure 27 Solid state structure of compound **26** with two crystallographically independent chains.

Compound **27** (figure **28**) consists of trinuclear units which pack to form a chain structure. Intermetallic Rh-Rh contacts in trinuclear unit range from Rh ⋯ Rh ⋯ Rh 3.2299(12) to Rh ⋯ Rh ⋯ Rh 3.2798(11) Å, and intermetallic Rh ⋯ Rh distance was found to be 3.9690(13) Å. Additionally, counter ion [Rh$(CO)_2Cl_2]^-$ formed a linearly assembled stack adjacent to the trinuclear chain with a Rh ⋯ Rh contact of 3.6198(17) Å. The Rh-Rh angles of the intrametallic metal centres ranged from 162.36(4) to 166.97(4) °. Further, adjacent trinuclear cationic units were tilted with respect to each other, having an Rh ⋯ Rh ⋯ Rh angle of 149.44(4) °. The interactions of trinuclear units and linearly assembled

counter ions are weak. As in compound **26**, the close contacts of Rh1, Rh2, and Rh3 in the trinuclear units enable potential metal-metal interactions of metal centres. In this case, the Rh-Rh contacts are contracted slightly compared to the example discussed in literature item **16.** Compared with compound **16**, the angle of the intermetallic metal centres is increased, whereas, due to the tilt of cationic units, the angles of the metal centres are decreased.

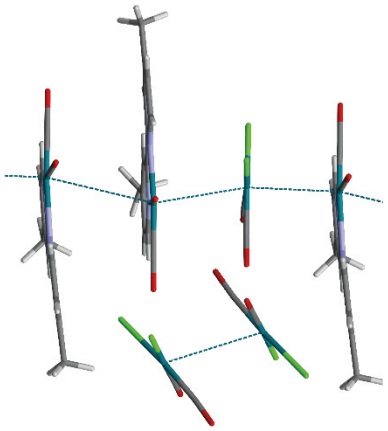

Figure 28 Chain structure of compound **27** with counter ions stacking with each other adjacent to the polymeric chain.

The cationic polymer structure of compound **28** (figure **29**) contained Rh ⋯ Rh contacts with a distance of 3.5216(10) Å with Rh ⋯ Rh ⋯ Rh angle of 155.76(3). Counter ions were located adjacent to the chain structure. Compared to compound **26**, the Rh-Rh distances are elongated, and the monomeric units were packed less efficiently. This was seen in the decrease of the Rh ⋯ Rh ⋯ Rh angle, since the value of this angle was found to be 155.76(3) °. Metal-metal contacts in the polymeric framework were due to the formation of hydrogen bonding of the amino substituent to the solvent of crystallisation, with donor-acceptor distances from 2.80(2) to 2.83(3) Å. This strong interaction affected the self-assembly process by directing anionic units further away from the cationic centres, enabling the formation of metal-metal contacts and potential metal-metal interactions. It is expected that these possible metal-metal interactions will be weak, due to the elongated Rh-Rh distances.

Metal-metal contacts in the polymeric structure are typically supported by secondary bonding interactions. This situation was found to apply in all of the cases where metal-metal contacts were present.

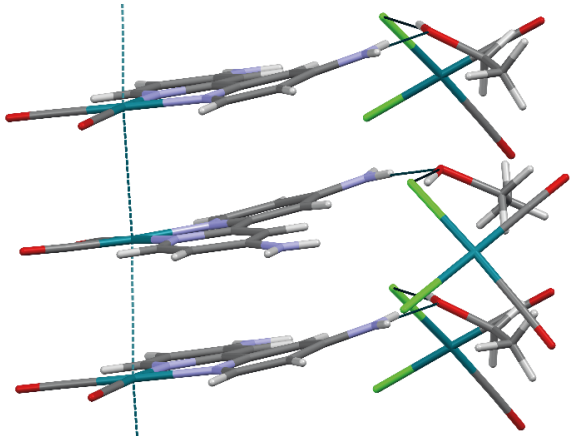

Figure 29 One-dimensional chain structure of compound **28** containing metal-metal contacts due to hydrogen bonding of the amino substituent to the solvent of crystallisation.

A cationic polymeric structure with metal-π contacts was obtained when hydrogen bonding of the amino substituents to the solvent of crystallisation was not present, as seen in compound **29** (figure **30**). Here, only hydrogen bonding to the counter ion located adjacent to the polymeric chain was observed. Hydrogen-bonding distances were found to vary from 3.272(2) Å to 3.669(3) Å. These dominating directional bonding interactions affected self-assembly via sterical effects, hindering close packing of the metal centres. Thus the monomeric units self-assembled into a chain structure *via* metal-π interactions. Interaction distances of metal-π contacts were found to vary from 3.392(2) Å to 3.601(2) Å.

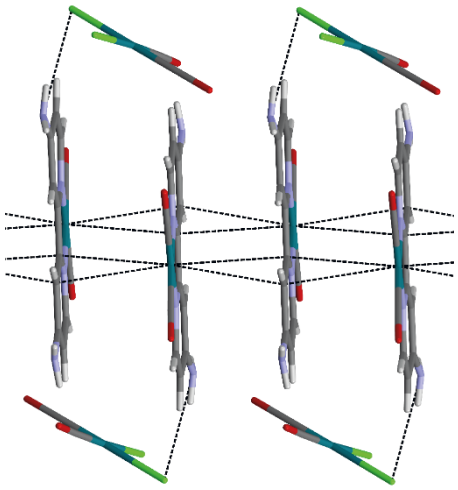

Figure 30 Chain structure of compound **29**, with metal-π interactions forming a cationic polymer.

To conclude, as seen from the structures **26** and **27-29**, the self-assembly of square-planar rhodium carbonyl monomers may be influenced by the selection of substituents. If a poor hydrogen-bonding substituent is chosen, it is more likely

to obtain structures with metal-metal contacts containing cationic and anionic counterparts in the polymeric framework. If a good hydrogen-bonding substituent is part of the ligand structure, a competition between hydrogen bonding and other non-covalent interactions, such as metal-metal interactions, will affect self-assembly. Here, it is challenging to predict outcomes, but it seems that cationic polymers will be produced. In any case, it is difficult to control the self-assembly so that metal-metal contacts will form. The strength of the potential metal-metal interactions thereby formed is also difficult to assess based only on intermetallic distances.

3.4 Pt-Pt contacts of square-planar platinum perfluoroterpyridine complexes

The formation metal-metal contacts in the self-assembly of square-planar platinum chloride based complexes with perfluorinated and alkylated terpyridines was investigated. Platinum was chosen due to optimal square planar geometry with d^8-configuration, luminescent properties expressed complexes of platinum, and the potential for formation of metal-metal interactions. Two compounds were synthesised: compound **30** containing a perfluorinated alkyl chain, and compound **31** with the alkyl chain as a substituent.

Both compounds crystallised as yellow needles. Single crystal x-ray diffraction revealed that compounds **30** and **31** contain square planar dimeric units with platinum-platinum contacts. For **30** (figure **31**), Pt-Pt distance is 3.4096(5) Å; for **31** (figure **32**), it is 3.3031(2) Å. π-interactions are supporting non-covalent Pt···Pt contacts. The charge of the monomeric units is compensated for with solvated chloride-ion in both structures. In comparison with examples in the literature of similar assemblies, the Pt-Pt contacts of **31** are close to the intermetallic distances of **21** (Pt-Pt distance of 3.362 Å), in which the presence of Pt-Pt interactions was confimed by DFT calculations. The Pt-Pt distances of compound **30** are comparable with those of compound **22**, presented in the introductory part of this thesis.

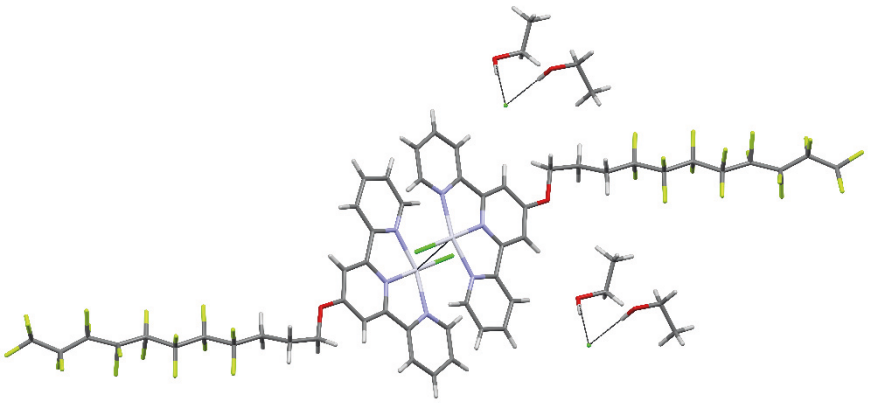

Figure 31 Solid state structure of compound **30**. Disordered fluorine-atoms have been omitted for clarity.

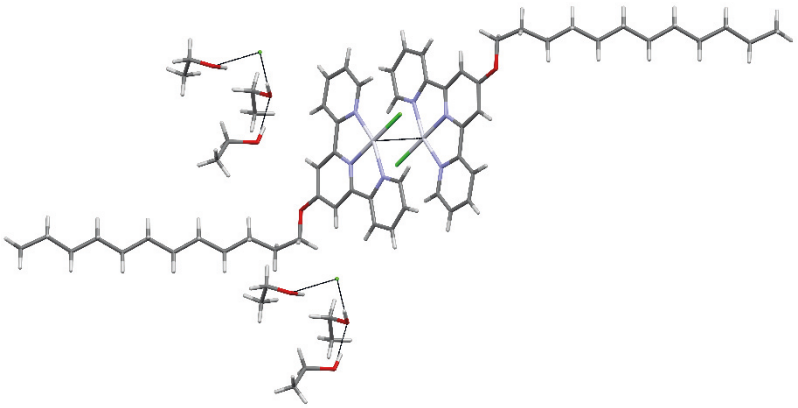

Figure 32 Structure of compound **31.**

Dinuclear units formed polymeric structures via metal-π- contacts with adjacent units' terpyridine moieties. The packing of polymeric chains formed fluorous (compound **30**) or hydrophobic (compound **31**) phases due to the formation of non-covalent interactions of sidechains. Additionally, channels filled with solvated counter ions formed (figure **33**). Crystalline yellow material transformed into red amorphous powder, as was confirmed by powder x-ray crystallography. This was a consequence of ethanol evaporation from the crystal structure. No definite structure for red powder was determined. However, there are reported cases of platinum terpyridine compounds in which an isomorphic structure correlates with different arrangement of platinum-platinum contacts and colour.[123,124]

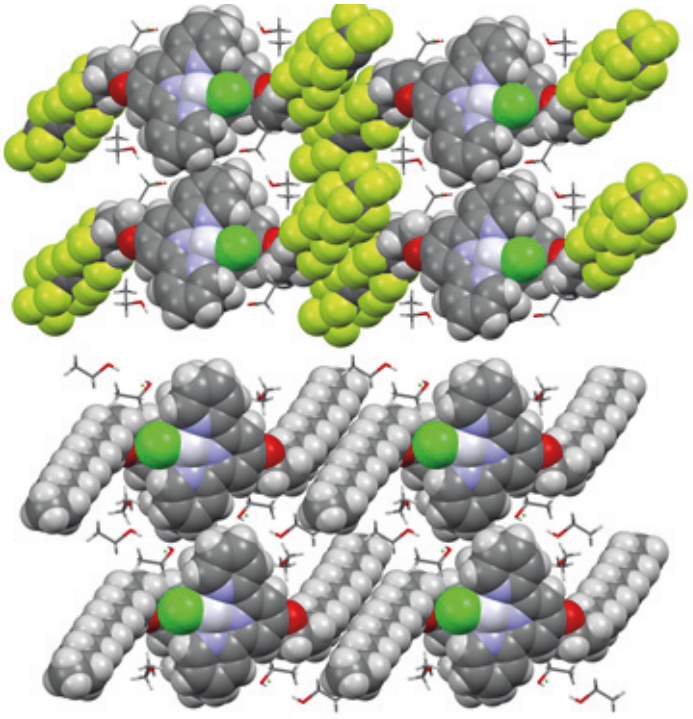

Figure 33 Top: packing of compound **30;** bottom**:** packing of compound **31**. Solvent accessible channels are filled with the solvent of crystallisation—namely, ethanol. Reproduced with permission from the Royal Society of Chemistry.

In order to gain more insight into the intramolecular metal-metal interactions, optical studies were performed. Both compounds **30** and **31** were found to express intriguing photophysical properties in the solid (**30** and **31**) and gel (**30**) states. Solid state measurement of reflectance (figure **34b**) of the transformation from yellow crystalline material to air-dried red amorphous powder (figure **34a**) revealed a red shift from λ≈515 nm to λ≈530 nm in both compounds **30** and **31**. Additionally, an even stronger red shift was observed with the vacuum-dried red material. A yet more drastic shift was observed in the reflectance of compound **30**. Similarly, a red shift of emissions (figure **34c**) in the transformation from yellow crystals to red amorphous powder was observed. It is known that the formation of metal-metal interactions alters photophysical behaviour. This may be seen as a change of MLCT to MMLCT bands. In the case of compound **30**, the photophysical behaviour, *i.e.* red shift reflectance, may be accounted for by MMLCT bands.

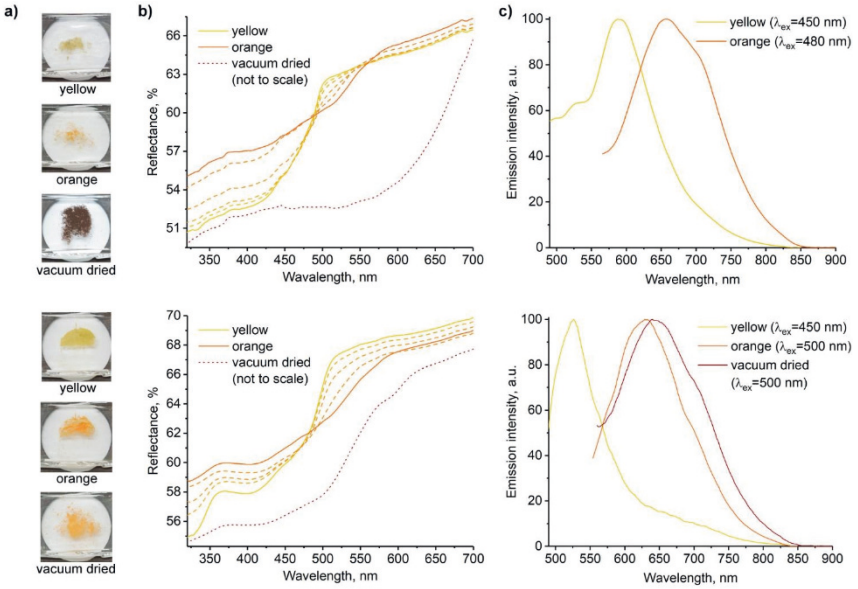

Figure 34 Top: compound **30;** bottom: compound **31**. **a)** Images of compounds in solid state forms; **b)** reflectance spectra; and **c)** normalized emission spectra. Reproduced with permission from the Royal Society of Chemistry.

It was found that compound **30** acted as a metallogelator in polar organic solvents. DMSO in higher weight/volume % concentrations than 0.6. 1 w/v% gel was found to produce a gel to sol (figure **35**) transformation (from red gel to yellow solution) at 69 °C. Compound **31**, by contrast, formed an unstable gel in ethanol with 1.5 w/v%. This difference in gel stabilities indicated that the main driving force of gelation can be the formation of these fluorine-fluorine interactions in cooperation with other non-covalent interactions such as metallophilic attraction, versus the formation of hydrophobic interactions.

The absorption spectrum (figure **35**, solid lines) of 0.6 w/v% gel was expressed as a λ_{abs}=500 nm band at 25 °C, whose intensity decreased with increasing temperatures. Correspondingly, in the emission spectra (figure **34**, dashed lines), the lowest energy-emission band of λ_{em}=640 nm blue shifted upon heating to 25 °C, and reached a value of λ_{em}=600 nm. Thus, both the absorption and the emission behaviour correlate well with results from the solid state measurements. Hence, the bands at λ_{abs}=500nm and λ_{em}=600 nm are due to MMLCT, which is, in turn, dependent on temperature and the aggregation of complexes. In short, absorption and emission spectroscopy is useful method for analysing the potential presence of metal-metal interactions. To conclude, results indicate presence of metal-metal interactions.

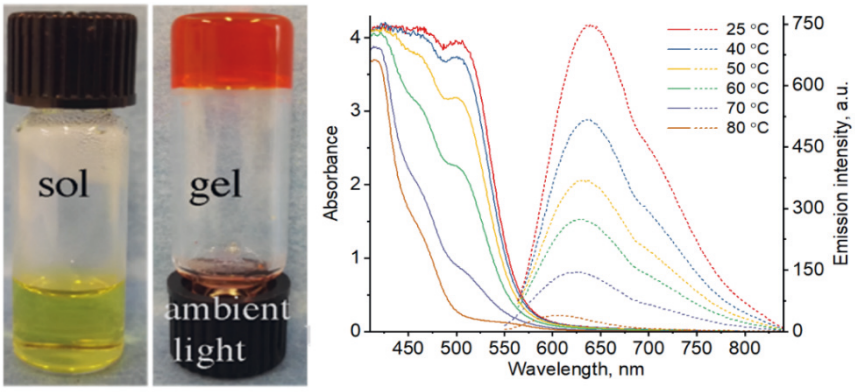

Figure 35 Left: images of solution and 0.6 w/v% gel from compound **30**. Right: absorption (solid lines) and emission spectra (dashed lines) of 0.6 w/v% gel from compound **30**. Reproduced with permission from the Royal Society of Chemistry.

To further elaborate the impact of fluorophilic interactions to gelation of compound **30**, variable temperature ^{19}F NMR of 1 w/v% gel and IR spectroscopy of 1 w/v% gel, 0.4 w/v% solution as well as solid forms were performed. ^{19}F NMR revealed changes in fluorophilic interactions upon heating gel sample from 30 ° C up to 90 ° C which was seen as chemical shift value changes ranging from 0.15 ppm to 1.61 ppm. Additionally signal appearance turned from broad and featureless (30 ° C) to sharp (90 ° C). Moreover, comparison of chemical shift values of dilute and concentrated solution revealed similar fluorine environments. This suggests that in gel state, the observed ^{19}F signals are from moieties which are not incorporated in supramolecular gel structure.
The presence and strength of fluorophilic interactions was estimated with IR spectroscopy experiments which revealed that strength of interactions decrease gradually from solid (1144 cm^{-1}) to gel (1148 cm^{-1}) and solution (1153 cm^{-1}).
The colour of the gel obtained from compound **30** corresponded to that of the solid amorphous powder. Thus absorption and emission studies were conducted with the intention of analysis on platinum-platinum interactions in the gel state as well.

Surface studies with electron microscopy (SEM and TEM) were also performed to get more insight into the morphological features of the supramolecularly arranged fibres. SEM studies of aerogel obtained from compound **30** in DMSO by a freeze-drying method revealed helical fibres with right- and left-

handedness (figure **36**). Both types of handedness are present due to the achiral gelator. TEM (figure **37**) imaging of 1 w/v% gel showed that these fibres formed interconnected fibril structures.

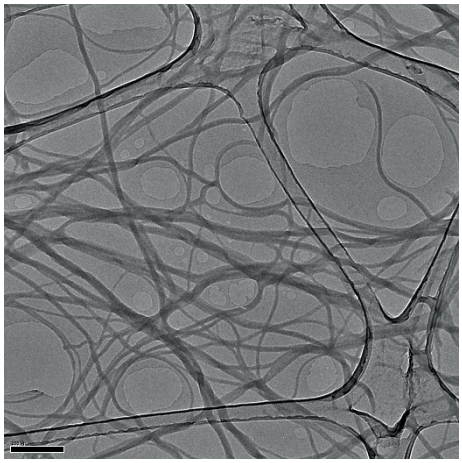

Figure 36 SEM image of 1 w/v% gel obtained from compound **30** in DMSO. Reproduced with permission from the Royal Society of Chemistry.

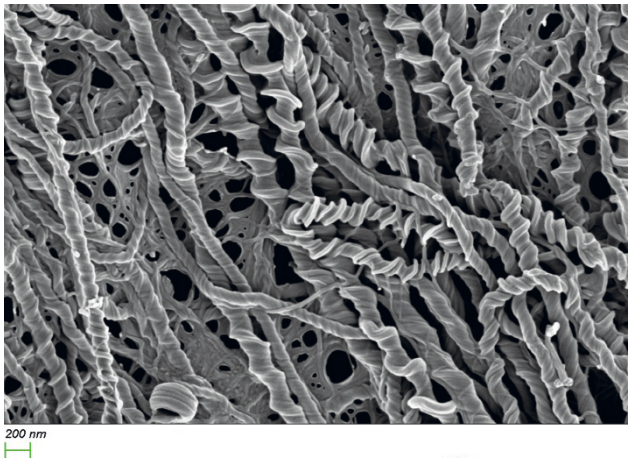

Figure 37 TEM image of 1 w/v% gel showing interconnected fibrils. Reproduced with permission from the Royal Society of Chemistry.

The rheological (figure **38**), *i.e.* mechanical, properties of the 1 w/v% gel prepared from compound **30** in DMSO were also investigated. These measurements concluded that compound **30** indeed formed gel material with DMSO (figure **38a**). The presence of junctioned networks was confirmed by the frequency sweep method together with the SEM results. A sweep strain experiment was performed to determine the critical-strain value, that is, the point at which gel struc-

ture breaks (figure **38b**). The rapid-self-healing property of the material was confirmed by the step-strain method (figure **38b**). Robustness and thermoreversibility (figure **38d**) were confirmed by a temperature sweep cycle experiment.

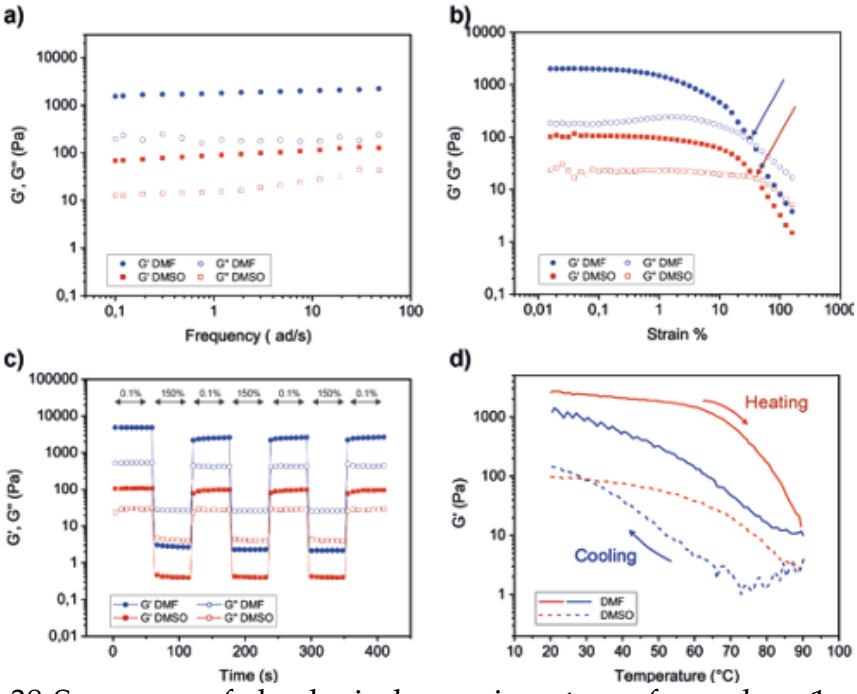

Figure 38 Summary of rheological experiments performed on 1 w/v% gel derived from DMSO. a) frequency sweep, b) strain sweep, c) step-strain and d) temperature sweep experiments. Reproduced with permission from the Royal Society of Chemistry.

SUMMARY AND CONCLUSIONS

In this thesis, the synthesis and structural characterisations of metallopolymers (compounds **23-28** and **30-31**) containing close metal-metal contacts were investigated. Computational studies (QTAIM) of **23-25** provided information about the bonding interactions in closely spaced metal centres in the polymeric structure. In addition to solid state studies, gas phase mass spectrometry (collision induced dissociation spectrum) was utilised to determine the polymeric nature of compound **23** as well as accurate masses for compounds **25**, **30,** and **31**. The coordination mode of carbonyl ligands and the presence of moisture in the samples were investigated with IR spectroscopy in the case of compounds **26** and **27**. The reflectivity of the solid state samples of **30** and **31**, coupled with absorption and emission spectroscopy of obtained gel from compound **30** in DMSO, was utilised to obtain information about non-covalent Pt-Pt interactions in these states. Electron microscopy, in addition to rheological measures of gel material obtained with compound **30,** afforded insight into the fiber structure and mechanical properties of the material in question.

The purpose of this study was to synthesise metallopolymers with close metal-metal contacts in solid-state structures containing group 11, Rh, and Pt transition metals. In each project, close meta-metal contacts were achieved. In copper and gold thiols as well as platinum terpyridine chloride complexes, the existence of metal-metal interactions was proved, whether computationally (**23**, **25**) or spectroscopically (**30** and **31**). Spectroscopy was found to be a useful method for the revealing of metal-metal interactions in platinum terpyridine chloride complexes in solid and gel states.

Regarding the remaining compounds, the presence of metal-metal interactions is speculative. According to the solid state structure, intermetallic separations are a sub sum of Van der waals radii, suggesting metal-metal interactions. Other methods should be applied to confirm the existence of these non-covalent interactions, as was done in the case of polymeric pyridine-4-thiols. Computations suggested that no metal-metal interactions were present in compound **24**, which is very similar in structure to **23** and features a sub sum of Van der waals radii**.** These results highlight the challenge of relying on only the solid state characterisation and the bond length criteria for detection of the presence of metal-metal interactions. Thus in the case of rhodium bipyridine carbonyl polymers, it is assumed that potential metal-metal interactions are present.

As the study demonstrates, rational ligand choice for the synthesis and tuning of compounds containing metal-metal contacts is crucial. The importance of the choice of ligands for synthesis purposes is especially apparent in polymeric metal thiols. The utilisation of ligands with ditopic and tautomeric properties in addition to a soft bridging donor atom is justified. The bridging coordination mode is particularly important in the synthesis of copper and silver thiols. As with the group 11 thiols, the use of fluorinated terpyridine ligands to prepare metal-metal contact containing platinum based polymers is an example of rational ligand choice. The formation of secondary non-covalent fluorine-fluorine interactions of ligand substituent yielded Pt-Pt contacts in the solid state struc-

ture, even though interaction is dinuclear in single crystal form. However spectroscopical studies of these complexes (especially **30)** suggested potential polynuclear metal-metal contacts and interactions in bulk powder and gel state.

The tuning of metal-metal contact distances, potential metal-metal interactions, and the overall structure of metallopolymers is affected by ligand structure. This is seen in the synthesis of rhodium bipyridine carbonyl polymers. Small changes in ligand substituent properties, such as the replacement of non-hydrogen-bonding by hydrogen-bonding substituents, will have an impact on the overall structure (cation-anion versus cationic stacks) and metal-metal contact distances in the polymer. In this case, the tuning of metal-metal contacts is achieved by affecting the formation of potential secondary non-covalent interactions. In the absence of a hydrogen-bonding substituent, cation-anion arrangements with metal-metal contacts are observed. If the substituent is replaced with a hydrogen-bonding one, cationic stacks with metal-metal contacts and hydrogen bonding to the solvent of crystallisation were observed. Without hydrogen bonding to the solvent of crystallisation, no metal-metal contacts were observed.

Overall, the thesis has demonstrated the importance of rational ligand choice and design for the synthesis and tuning of metal-metal contacts containing late transition metal polymers. It has been shown that from a synthesis point of view, properties of metals such as available coordination geometries and oxidation states have to be considered carefully—in order for products containing metal-metal contacts to be obtained. Additionally, the ligand substituent influence on competing secondary non-covalent interactions has to take into concideration. This was shown especially in the case of self-assembly process in rhodium bipyridine carbonyl polymers. Moreover, it was demonstrated that the utilisation of self-assembly strategies for the construction of compounds with metal contacts is highly influenced by the competition among individual non-covalent interactions. Hence, rational ligand choice and design, with a view towards minimising competing secondary non-covalent interactions in the self-assembly process, could provide one path towards the creation of functional polymeric materials with metal contacts.

REFERENCES

1. Eloi, J. C., Chabanne, L., Whittell, G. R. & Manners, I. Metallopolymers with emerging applications. *Mater. Today* **11**, 28–36 (2008).
2. Whittell, G. R. & Manners, I. Metallopolymers: New multifunctional materials. *Advanced Materials* **19**, 3439–3468 (2007).
3. Wang, Y., Astruc, D. & Abd-El-Aziz, A. S. Metallopolymers for advanced sustainable applications. *Chem. Soc. Rev.* **48**, 558–636 (2019).
4. Arimoto, F. S. & Haven, A. C. Derivatives of Dicyclopentadienyliron1. *J. Am. Chem. Soc.* **77**, 6295–6297 (1955).
5. Williams, K. A., Boydston, A. J. & Bielawski, C. W. Main-chain organometallic polymers: synthetic strategies, applications, and perspectives. *Chem. Soc. Rev.* **36**, 729–744 (2007).
6. Nguyen, P., Gómez-Elipe, P. & Manners, L. Organometallic polymers with transition metals in the main chain. *Chem. Rev.* **99**, 1515–1548 (1999).
7. Batten, S. R., Champness, N. R., Chen, X-M., Garcia-Martinez, J., Kitagawa, S., Öhrström, L., O'Keefe, M., Paik Suh, M., Reedijk, J. Terminology of metal–organic frameworks and coordination polymers (IUPAC Recommendations 2013). *Pure Appl. Chem.* **85**, 1715–1724 (2013).
8. Berry, J. F., Cotton, F. A., Fewox, C. S., Lu, T., Murillo, C. A., Wang, X. Extended metal atom chains (EMACs) of five chromium or cobalt atoms: Symmetrical or unsymmetrical? *J. Chem. Soc. Dalt. Trans.* **4**, 2297–2302 (2004).
9. Peng, S. M., Wang, C-C., Jang, T-L., Chen, Y-H., Li, F-Y., Mou, C-Y., Leung, M-K. One-dimensional metal string complexes. *J. Magn. Magn. Mater.* **209**, 80–83 (2000).
10. Rehahn, M. Organic/inorganic hybrid polymers. *Acta Polym.* **49**, 201–224 (1998).
11. Winter, A. & Schubert, U. S. Synthesis and characterization of metallo-supramolecular polymers. *Chem. Soc. Rev.* **45**, 5311–5357 (2016).
12. Hardy, C. G., Zhang, J., Yan, Y., Ren, L. & Tang, C. Metallopolymers with transition metals in the side-chain by living and controlled polymerization techniques. *Prog. Polym. Sci.* **39**, 1742–1796 (2014).
13. Stanley, J. M. & Holliday, B. J. Luminescent lanthanide-containing metallopolymers. *Coordination Chemistry Reviews* **256**, 1520–1530 (2012).
14. Dutta, B., Das, D., Datta, J., Chandra, A., Jana, S., Sinra, C., Pratim Ray, P., Hedayetullah Mir, M. Synthesis of a Zn(II)-based 1D zigzag coordination polymer for the fabrication of optoelectronic devices with remarkably high photosensitivity. *Inorg. Chem. Front.* **6**, 1245–1252 (2019).
15. Kitagawa, S., Kitaura, R. & Noro, S. I. Functional porous coordination polymers. *Angewandte Chemie - International Edition* **43**, 2334–2375 (2004).
16. Hua, S.-A., Cheng, M.-C., Chen, C. & Peng, S.-M. From Homonuclear Metal String Complexes to Heteronuclear Metal String Complexes. *Eur. J. Inorg. Chem.* **2015**, 2510–2523 (2015).
17. Po-Chun Liu, I., Chen, C. & Peng, S.-M. The Road to Molecular Metal Wires: The Past and Recent Advances of Metal String ComplexesThe Road to Molecular Metal Wires: The Past and Recent Advances of Metal String

Complexes. *Bull. Japan Soc. Coord. Chem.* **59**, 3–10 (2012).

18. Berry, J. F., Cotton, F. A. & Murillo, C. A. Mono-, di-, and tri-ruthenium complexes with the ligand 2,2′-dipyridylamide (dpa): Insights into the formation of extended metal atom chains. *Inorganica Chim. Acta* **357**, 3847–3853 (2004).
19. Cortijo, M., Bulicanu, V., Pedersen, K. S., Rouzieres, M., Bendix, J., Clerac, R., Hillard, E. A. Rational Self-Assembly of Tricobalt Extended Metal Atom Chains and $[MF_6]^{2-}$ Building Blocks into One-Dimensional Coordination Polymers. *Eur. J. Inorg. Chem.* **2018**, 320–325 (2018).
20. Shih, K. N., Huang, M-J., Lu, H-C., Fu, M-D., Kuo, C-K., Huang, G-C., Lee, G-H., Chen, C-H., Peng, S-M. On the tuning of electric conductance of extended metal atom chains via axial ligands for $[Ru_3(\mu_3\text{-dpa})_4(X)_2]^{0/+}$ (X = NCS^-, CN^-). *Chem. Commun.* **46**, 1338–1340 (2010).
21. Huang, G. C., Liu, I. P-C., Kuo, J-H., Huang, Y-L., Yeh, C-Y., Leem G-H., Peng, S-M. Further investigations of linear trirhodium complexes: Experimental and theoretical studies of $[Rh_3(dpa)_4Cl_2]$ and $[Rh_3(dpa)_4Cl_2](BF_4)$ [dpa = bis(2-pyridyl)amido anion]. *J. Chem. Soc. Dalt. Trans.* **3**, 2623–2629 (2009).
22. Cheng, M. C., Mai, C. L., Yeh, C. Y., Lee, G. H. & Peng, S. M. Facile synthesis of heterotrimetallic metal-string complex $[NiCoRh(dpa)_4Cl_2]$ through direct metal replacement. *Chem. Commun.* **49**, 7938–7940 (2013).
23. Liu, I. P. C., Chen, C-F., Hua, S-A.,Chen, C-H., Wang, H-T., Lee, G-H., Peng, Shie-Ming Clear evidence of electron delocalization: Synthesis, structure, magnetism, EPR and DFT calculation of the asymmetric hexanickel string complex containing a single mixed-valence $(Ni_2)^{3+}$ unit. *J. Chem. Soc. Dalt. Trans.* 3571–3573 (2009).
24. Yeh, C. Y., Chiang, Y. L., Lee, G. H. & Peng, S. M. Unsymmetrical linear pentanuclear nickel string complexes: $[Ni_5(tpda)_4(H_2O)(BF_4)](BF_4)_2$ and $[Ni_5(tpda)_4(SO_3CF_3)_2](SO_3CF_3)$. *Inorg. Chem.* **41**, 4096–4098 (2002).
25. Zhu, Y., Yu, T., Hao, P., Shen, J. & Fu, Y. Halogen-Dependent Thermochromic Properties in Three Methyl-Viologen/Haloargentate Charge Transfer (CT) Salts. *J. Clust. Sci.* **27**, 1283–1291 (2016).
26. Scott, B., Willett, R., Saccani, A., Sandrolini, F. & Ramakrishna, B. L. A study of pseudo 1-D copper(I) halide systems exhibiting anomalous copper(II) character: physical characterization of (paraquat) Cu_2X_4 (X = Cl, Br, I). *Inorganica Chim. Acta* **248**, 73–80 (1996).
27. Wang, W., Zhao, D., Zhao, M-J., Li, H., Liu, S., Ismayilov, R. H., Lee, G-H., Peng, S-M. Linear hexanuclear nickel complexes with rich electrochemical features and facility to reduction. *J. Mol. Struct.* **1130**, 748–752 (2017).
28. Berry, J. F., Cotton, F. A., Lu, T., Murillo, C. A., Roberts, B. K., Wang, X. Molecular and electronic structures by design: Tuning symmetrical and unsymmetrical linear trichromium chains. *J. Am. Chem. Soc.* **126**, 7082–7096 (2004).
29. Tejel, C., Ciriano, M. A., López, J. A., Lahoz, F. J. & Oro, L. A. Rhodium and Iridium Pyrazolato Blues. *Angew. Chemie Int. Ed.* **37**, 1542–1545 (1998).
30. Ardizzoia, G. A., LaMonica, G., Maspero, A., Moret, M. & Masciocchi, N. Pyrazolato Metal Complexes: Synthesis, Characterization and X-ray

Crystal Structures of Polynuclear Organometallic Re–Mn Derivatives. *Eur. J. Inorg. Chem.* **2000**, 181–187 (2000).

31. Ehlert, M. K., Rettig, S. J., Storr, A., Thompson, R. C. & Trotter, J. Metal pyrazolate polymers. Part 1. Synthesis, structure, and magnetic properties of the $[Cu(pz)_2]x$ polymer . *Can. J. Chem.* **67**, 1970–1974 (1989).
32. Horiuchi, S., Tachibana, Y., Yamashita, M., Yamamoto, K., Masai, K., Takase, K., Matsutani, T., Kawamata, S., Kurashige, Y., Yanai, T., Murahashi, T. Multinuclear metal-binding ability of a carotene. *Nat. Commun.* **6**, 6742 (2015).
33. Wong, V. C. H., Po, C., Leung, S. Y-L., Chan, A. K-W., Yang, S., Zhu, B., Cui, X., Yam, V. W-W. Formation of 1D Infinite Chains Directed by Metal-Metal and/or π- π Stacking Interactions of Water-Soluble Platinum(II) 2,6-Bis(benzimidazol-2′-yl)pyridine Double Complex Salts. *J. Am. Chem. Soc.* **140**, 657–666 (2018).
34. Sluch, I. M., Miranda, A. J., Elbjeirami, O., Omary, M. A. & Slaughter, L. M. Interplay of metallophilic interactions, π-π Stacking, and ligand substituent effects in the structures and luminescence properties of neutral Pt(II) and Pd(II) aryl isocyanide complexes. *Inorg. Chem.* **51**, 10728–10746 (2012).
35. Doshi, A., Sundraraman, A., Venkatasubbaiah, K., Zakharov, L. N., Rheingold, A. L., Myahkostupov, M., Piotrowiak, P., Jäkle, F. Pentafluorophenyl Copper–Pyridine Complexes: Synthesis, Supramolecular Structures via Cuprophilic and π-Stacking Interactions, and Solid-State Luminescence. *Organometallics* **31**, 1546–1558 (2012).
36. Inoki, D., Matsumoto, T., Nakai, H. & Ogo, S. Experimental study of reductive elimination of H 2 from rhodium hydride species. *Organometallics* **31**, 2996–3001 (2012).
37. Caix-Cecillon, C., Chardon-Noblat, S., Deronzier, A., Haukka, M., Pakkanen, T. A., Ziessel, R., Zsoldos, D. Electrochemical formation and spectroelectrochemical characterization of organometallic $[Ru(L)(CO)_2]_n$ polymers; L = disubstituted-2,2′-bipyridine. *J. Electroanal. Chem.* **466**, 187–196 (1999).
38. Chardon-Noblat, S., Da Costa, P., Deronzier, A., Haukka, M., Pakkanen, T. A., Ziessel, R. Electropolymerization of $[Ru(bpy)(CO)_2Cl_2]$ (bpy = 2,2′-bipyridine: A revisited trans versus cis(Cl) isomeric influence study. *J. Electroanal. Chem.* **490**, 62–69 (2000).
39. Chardon-Noblat, S., Deronzier, A., Hartl, F., Van Slageren, J. & Mahabiersing, T. A Novel Organometallic Polymer of Osmium(0), $[Os(2,2'\text{-bipyridine})(CO)_2]_n$: Its Electrosynthesis and Electrocatalytic Properties Towards CO_2 Reduction. *Eur. J. Inorg. Chem.* **2001**, 613–617 (2001).
40. Kauffman, G. Gustav Magnus and his Green Salt. *Platin. Met. Rev.* **20**, 21–24 (1976).
41. Atoji, M., Richardson, J. W. & Rundle, R. E. On the Crystal Structures of the Magnus Salts, $Pt(NH_3)_4PtCl_4$. *J. Am. Chem. Soc.* **79**, 3017–3020 (1957).
42. Krogmann, K. Planar Complexes Containing Metal-Metal Bonds. *Angew. Chemie Int. Ed. English* **8**, 35–42 (1969).
43. Prater, M. E., Pence, L. E., Clerac, R., Finniss, G. M., Campana, C., Auban-Senzier, P., Jerome, D., Canadell, E., Dunbar, K. R. A remarkable family of

rhodium acetonitrile compounds spanning three oxidation states and with nuclearities ranging from mononuclear and dinuclear to one-dimensional chains. *J. Am. Chem. Soc.* **121**, 8005–8016 (1999).

44. Laurila, E., Oresmaa, L., Hassinen, J., Hirva, P. & Haukka, M. Neutral one-dimensional metal chains consisting of alternating anionic and cationic rhodium complexes. *Dalt. Trans.* **42**, 395–398 (2013).
45. Mitsumi, M., Ohtake, S., Kakuno, Y., Komatsu, Y., Ozawa, Y., Toriumi, K., Yasuda, N., Azuma, N., Miyazaki, Y. Multifunctional one-dimensional rhodium(I)-semiquinonato complex: Substituent effects on crystal structures and solid-state properties. *Inorg. Chem.* **53**, 11710–11720 (2014).
46. Bremi, J., Fontana, M., Caseri, W. & Smith, P. Polymeric quasi-one-dimensional platinum compounds. *Macromol. Symp.* **235**, 80–88 (2006).
47. Bremi, J., Brovelli, D., Caseri, W., Hähner, G., Smith, P., Tervoort, T. From Vauquelin's and Magnus' salts to gels, uniaxially oriented films, and fibers: Synthesis, characterization, and properties of tetrakis(1-aminoalkane)metal(II) tetrachlorometalates(II). *Chem. Mater.* **11**, 977–994 (1999).
48. Schweitzer, B., Daniel, C. & Gourlaouen, C. Metal–metal bonding in 1st, 2nd and 3rd row transition metal complexes: a topological analysis. *J. Mol. Model.* **23**, 21–25 (2017).
49. Hurley, T. J. & Robinson, M. A. Nickel(II)-2,2′-dipyridylamine system. I. Synthesis and stereochemistry of the complexes. *Inorg. Chem.* **7**, 33–38 (1968).
50. Aduldecha, S. & Hathaway, B. Crystal structure and electronic properties of tetrakis[μ_3-bis(2-pyridyl)amido]dichlorotrinickel(II)-water-acetone (1/0.23/0.5). *J. Chem. Soc. Dalt. Trans.* 993–998 (1991).
51. Cotton, F. A., Murillo, C. A. & Wang, X. Can crystal structure determine molecular structure? For $Co_3(dpa)_4Cl_2$, yes. *J. Chem. Soc. - Dalt. Trans.* **3**, 3327–3328 (1999).
52. Niskanen, M., Hirva, P. & Haukka, M. Metal-metal interactions in linear tri-, penta-, hepta-, and nona-nuclear ruthenium string complexes. *J. Mol. Model.* **18**, 1961–1968 (2012).
53. Berry, J. F., Cotton, F. A., Daniels, L. M., Murillo, C. A. & Wang, X. Oxidation of $Ni_3(dpa)_4Cl_2$ and $Cu_3(dpa)_4Cl_2$: Nickel-nickel bonding interaction, but no copper-copper bonds. *Inorg. Chem.* **42**, 2418–2427 (2003).
54. Ismayilov, R. H., Wang, W-Z., Lee, G-H., Yeh, C-Y., Hua, S-A., Song, Y., Rohmer, M-M., Benard, M., Peng, S-M. Two linear undecanickel mixed-valence complexes: Increasing the size and the scope of the electronic properties of nickel metal strings. *Angew. Chemie - Int. Ed.* **50**, 2045–2048 (2011).
55. Laurila, E., Tatikonda, R., Oresmaa, L., Hirva, P. & Haukka, M. Metallophilic interactions in stacked dinuclear rhodium 2,2′-biimidazole carbonyl complexes. *CrystEngComm* **14**, 8401–8408 (2012).
56. Yamada, T., Ebihara, M. & Uemura, K. Heterometallic one-dimensional chain with tetradeca metal repetition constructed by amidate bridged dirhodium and pivalate bridged diplatinum complexes influenced by hydrogen bonding. *Dalt. Trans.* **45**, 12322–12328 (2016).

57. Murahashi, T., Mochizuki, E., Kai, Y. & Kurosawa, H. Organometallic Sandwich Chains Made of Conjugated Polyenes and Metal−Metal Chains. *J. Am. Chem. Soc.* **121**, 10660–10661 (1999).
58. Yamane, M., Yamashita, M., Yamamoto, K. & Murahashi, T. Contiguous multiple π-coordination of π-conjugated polyenes: bonding nature and charge delocalization behaviour of polyene–(palladium chain) sandwich clusters. *Phys. Chem. Chem. Phys.* **20**, 4287–4296 (2018).
59. Pyykkö, P. Relativistic Effects in Structural Chemistry. *Chem. Rev.* **88**, 563–594 (1988).
60. Xiong, X.-G. & Pyykkö, P. Unbridged Au(II)–Au(II) bonds are theoretically allowed. *Chem. Commun.* **49**, 2103–2105 (2013).
61. Gussenhoven, E. M., Olmstead, M. M. & Balch, A. L. Amine involvement in the self-association of planar complexes of the type, cis-$Ir(CO)_2$ Cl(primary amine). *J. Organomet. Chem.* 17–24 (2019).
62. Harisomayajula, N. V. S., Makovetskyi, S. & Tsai, Y.-C. Cuprophilic Interactions in and between Molecular Entities. *Chem. – A Eur. J.* **25**, 8936–8954 (2019).
63. Wesendrup, R. & Schwerdtfeger, P. Extremely Strong s^2 – s^2 Closed-Shell Interactions. *Angew. Chemie Int. Ed.* **39**, 907–910 (2000).
64. Doerrer, L. H. Steric and electronic effects in metallophilic double salts. *Dalt. Trans.* **39**, 3543–3553 (2010).
65. Głodek, M., Pawlędzio, S., Makal, A. & Plażuk, D. Cover Feature: The Impact of Crystal Packing and Aurophilic Interactions on the Luminescence Properties in Polymorphs and Solvate of Aroylacetylide–Gold(I) Complexes. *Chem. – A Eur. J.* **25**, 13045–13045 (2019).
66. Palmans, R., MacQueen, D. B., Pierpont, C. G. & Frank, A. J. Synthesis and Characterization of Bis(2,2′-bipyridyl)platinum(I): A Novel Microtubular Linear-Chain Complex. *J. Am. Chem. Soc.* **118**, 12647–12653 (1996).
67. Mehrotra, P. K. & Hoffmann, R. Cu(I)-Cu(I) Interactions. Bonding Relationships in d10-d10 Systems. *Inorg. Chem.* **17**, 2187–2189 (1978).
68. Pyykkö, P. Relativistic Effects in Chemistry: More Common Than You Thought. *Annu. Rev. Phys. Chem.* **63**, 45–64 (2012).
69. Pyykkö, P. & Zhao, Y. Ab initio Calculations on the $(ClAuPH_3)_2$ Dimer with Relativistic Pseudopotential: Is the "Aurophilic Attraction" a Correlation Effect? *Angew. Chemie Int. Ed. English* **30**, 604–605 (1991).
70. Thayer, J. S. Relativistic Effects and the Chemistry of the Heaviest Main-Group Elements. *J. Chem. Educ.* **82**, 1721 (2005).
71. Brands, M. B., Nitsch, J. & Guerra, C. F. Relevance of Orbital Interactions and Pauli Repulsion in the Metal-Metal Bond of Coinage Metals. *Inorg. Chem.* **57**, 2603–2608 (2018).
72. Liu, J.-F. F., Min, X., Lv, J-Y., Pan, F-X., Pan, Q-J., Sun, Z-M. Ligand-Controlled Syntheses of Copper(I) Complexes with Metal–Metal Interactions: Crystal Structure and Relativistic Density Functional Theory Investigation. *Inorg. Chem.* **53**, 11068–11074 (2014).
73. Huang, S., Yang, B., Zhong, J., Zhang, H. A theoretical investigation on the metal-metal interaction in a series of pyrazolate bridged platinum(II) complexes. *Synth. Met.* **205**, 222–227 (2015).

74. Hu, S-Z., Zhou, Z-H., Robertson, B. E. Consistent approaches to van der Waals radii for the metallic elements. *Z. Kristallogr.* **224**, 375-383 (2009).
75. Colis, J. C. F., Staples, R., Tripp, C., Labrecque, D. & Patterson, H. Metallophilic interactions in closed-shell d 10 metal-metal dicyanide bonded luminescent systems Eu[Ag xAu 1-x$(CN)_2]_3$ and their tunability for excited state energy transfer. *J. Phys. Chem. B* **109**, 102–109 (2005).
76. Perras, F. A. & Bryce, D. L. Direct Characterization of Metal–Metal Bonds between Nuclei with Strong Quadrupolar Interactions via NMR Spectroscopy. *J. Phys. Chem. Lett.* **5**, 4049–4054 (2014).
77. Novikov, A. S. Strong metallophilic interactions in nickel coordination compounds. *Inorganica Chim. Acta* **483**, 21–25 (2018).
78. Johnson, E. R., Keinan, S., Mori-Sanchez, P., Contreras-Garcia, J., Cohen, A. J., Yang, W. Revealing Noncovalent Interactions. *J. Am. Chem. Soc.* **132**, 6498–6506 (2010).
79. Díez, Á., Fornies, J., Larraz, C., Lalindem E., Lopez, J. A., Martin, A., Moreno, M. T., Sicilia, V. Structural and Luminescence Studies on π···π and Pt···Pt Interactions in Mixed Chloro-Isocyanide Cyclometalated Platinum(II) Complexes. *Inorg. Chem.* **49**, 3239–3251 (2010).
80. Chakraborty, A., Yarnell, J. E., Sommer, R. D., Roy, S. & Castellano, F. N. Excited-State Processes of Cyclometalated Platinum(II) Charge-Transfer Dimers Bridged by Hydroxypyridines. *Inorg. Chem.* **57**, 1298–1310 (2018).
81. Zhu, Y., Luo, K., Zhao, L., Ni, H. & Li, Q. Binuclear platinum(II) complexes based on 2-mercaptobenzothiazole 2-mercaptobenzimidazole and 2-hydroxpyridine as brigding ligands: Red and near-infrared luminescence originated from MMLCT transition. *Dye. Pigment.* **145**, 144–151 (2017).
82. Zhang, R., Liang, Z., Han, A., Wu, H., Du, P., Lai, W., Cao, R. Structural, spectroscopic and theoretical studies of a vapochromic platinum(II) terpyridyl complex. *CrystEngComm* **16**, 5531–5542 (2014).
83. Kang, J., Zhang, X., Zhou, H., Gai, X., Jiam T., Xu, L., Zhang, J., Li, Y., Ni, J. 1-D 'platinum Wire' Stacking Structure Built of Platinum(II) Diimine Bis(σ-acetylide) Units with Luminescence in the NIR Region. *Inorg. Chem.* **55**, 10208–10217 (2016).
84. Chan, A. K. W., Ng, M., Low, K. H. & Yam, V. W. W. Versatile Control of Directed Supramolecular Assembly via Subtle Changes of the Rhodium(I) Pincer Building Blocks. *J. Am. Chem. Soc.* **140**, 8321–8329 (2018).
85. Yam, V. W.-W., Chan, K. H.-Y., Wong, K. M.-C. & Zhu, N. Luminescent Platinum(II) Terpyridyl Complexes: Effect of Counter Ions on Solvent-Induced Aggregation and Color Changes. *Chem. – A Eur. J.* **11**, 4535–4543 (2005).
86. Chen, J., Zhang, Z., Wang, C., Gao, Z., Wang, F. Cooperative self-assembly and gelation of organogold(I) complexes: Via hydrogen bonding and aurophilic Au···Au interactions. *Chem. Commun.* **53**, 11552–11555 (2017).
87. Yu, C., Wong, K. M.-C., Chan, K. H.-Y. & Yam, V. W.-W. Polymer-Induced Self-Assembly of Alkynylplatinum(II) Terpyridyl Complexes by Metal···Metal/π···π Interactions. *Angew. Chemie Int. Ed.* **44**, 791–794 (2005).
88. Claveria-Cadiz, F., Arratia-Perez, R., Guajardo-Maturana, R. & Muñoz-Castro, A. Survey of short and long cuprophilic d10-d10 contacts for

tetranuclear copper clusters. Understanding of bonding and ligand role from a planar superatom perspective. *New J. Chem.* **42**, 8874–8881 (2018).
89. Lamming, G., Kolokotroni, J., Harrison, T., Penfold, T. J., Clegg, W., Waddell, P. G., Probert, M. R., Houlton, A. Structural Diversity and Argentophilic Interactions in One-Dimensional Silver-Based Coordination Polymers. *Cryst. Growth Des.* **17**, 5753–5763 (2017).
90. O'Grady, E. & Kaltsoyannis, N. Does metallophilicity increase or decrease down group 11? Computational investigations of $[Cl\text{-}M\text{-}PH_3]_2$(M = Cu, Ag, Au, [111]). *Phys. Chem. Chem. Phys.* **2**, 680–687 (2004).
91. Brown, I. D. & Dunitz, J. D. The crystal structure of diazoaminobenzene copper(I). *Acta Crystallogr.* **14**, 480–485 (1961).
92. Merz, K. M. & Hoffmann, R. d10-d10 Interactions: multinuclear copper(I) complexes. *Inorg. Chem.* **27**, 2120–2127 (1988).
93. Etaiw, S. E. din H. & El-bendary, M. M. The Influence of Copper-Copper Interaction on the Structure and Applications of a Metal-Organic Framework Based on Cyanide and 3-Chloropyridine. *J. Inorg. Organomet. Polym. Mater.* **23**, 510–518 (2013).
94. Zheng, S.-L., Messerschmidt, M. & Coppens, P. An Unstable Ligand-Unsupported CuI Dimer Stabilized in a Supramolecular Framework. *Angew. Chemie Int. Ed.* **44**, 4614–4617 (2005).
95. Johnson, K. & Steed, J. W. Effects of non-molecular forces on molecular structure in tris(thiourea)-copper(I). *J. Chem. Soc. - Dalt. Trans.* 2601–2602 (1998).
96. Taylor, I. F., Weininger, M. S. & Amma, E. L. Preparation, crystal structure, and bonding in the dimers of tris(thiourea) coppers(I) tetrafluoroborate and tris(s-dimethylthiourea) copper(I) tetrafluoroborate. *Inorg. Chem.* **13**, 2835–2842 (1974).
97. Harkins, S. B. & Peters, J. C. Amido-Bridged Cu_2N_2 Diamond Cores that Minimize Structural Reorganization and Facilitate Reversible Redox Behavior between a Cu(1)Cu(1) and a Class III Delocalized Cu(1.5)Cu(1.5) Species. *J. Am. Chem. Soc.* **126**, 2885–2893 (2004).
98. Bertil Noren;Åke Oskarsson. Bond length variation in tetrahydrothiophene solvates of the coinage metals. *Acta Chem. Scand.* **41a**, 12–17 (1986).
99. Carvajal, M. A., Alvarez, S. & Novoa, J. J. The Nature of Intermolecular CuI···CuI Interactions: A Combined Theoretical and Structural Database Analysis. *Chem. – A Eur. J.* **10**, 2117–2132 (2004).
100. Bondi, A. Van der waals volumes and radii. *J. Phys. Chem.* **68**, 441–451 (1964).
101. Schmidbaur, H. & Schier, A. Argentophilic interactions. *Angew. Chemie - Int. Ed.* **54**, 746–784 (2015).
102. Capel Berdiell, I., Warriner, S. L. & Halcrow, M. A. Silver(I) complexes of bis- and tris-(pyrazolyl)azine derivatives – dimers, coordination polymers and a pentametallic assembly. *Dalt. Trans.* **47**, 5269–5278 (2018).
103. Hou, L. & Li, D. A novel photoluminescent Ag-terpyridyl complex: One-dimensional linear metal string with double-helical structure. *Inorg. Chem. Commun.* **8**, 128–130 (2005).
104. Su, W., Hong, M., Weng, J., Liang, Y., Zhao, Y., Cao, R., Zhou, Z., Chan, A.

S. C. Tunable polymerization of silver complexes with organosulfur ligand: counterions effect, solvent- and temperature-dependence in the formation of silver(I)-thiolate(and/or thione) complexes. *Inorganica Chim. Acta* **331**, 8–15 (2002).

105. Schmidbaur, H. & Schier, A. Aurophilic interactions as a subject of current research: An up-date. *Chem. Soc. Rev.* **41**, 370–412 (2012).
106. Muñiz, J., Wang, C. & Pyykkö, P. Aurophilicity: The effect of the neutral ligand l on [{ClAuL}2] systems. *Chem. - A Eur. J.* **17**, 368–377 (2011).
107. Baron, M., Tubaro, C., Biffis, A., Basato, M., Graiff, C., Poater, A., Cavallo, L., Armaroli, N., Accorsi, G. Blue-Emitting Dinuclear N-heterocyclic Dicarbene Gold(I) Complex Featuring a Nearly Unit Quantum Yield. *Inorg. Chem.* **51**, 1778–1784 (2012).
108. Imoto, H., Nishiyama, S., Yumura, T., Watase, S., Matsukawa, K., Naka, K. Control of aurophilic interaction: Conformations and electronic structures of one-dimensional supramolecular architectures. *Dalt. Trans.* **46**, 8077–8082 (2017).
109. Katz, M. J., Sakai, K. & Leznoff, D. B. The use of aurophilic and other metal–metal interactions as crystal engineering design elements to increase structural dimensionality. *Chem. Soc. Rev.* **37**, 1884–1895 (2008).
110. Hapka, M., Dranka, M., Orlowska, K., Chalasinski, G., Szczesniak, M. M., Zachara, J. Noncovalent interactions determine the conformation of aurophilic complexes with 2-mercapto-4-methyl-5-thiazoleacetic acid ligands. *Dalt. Trans.* **44**, 13641–13650 (2015).
111. Usón, R., Laguna, A., Laguna, M., Jimenez, J., Gomez, M. P., Sainz, A., Jones, P. G. Gold complexes with heterocyclic thiones as ligands. X-Ray structure determination of $[Au(C_5H_5NS)_2]ClO_4$. *J. Chem. Soc. Dalt. Trans.* 3457–3463 (1990).
112. Lima, J. & Rodríguez, L. Supramolecular Gold Metallogelators: The Key Role of Metallophilic Interactions. *Inorganics* **3**, 1–18 (2014).
113. Coker, N. L., Krause Bauer, J. A. & Elder, R. C. Emission Energy Correlates with Inverse of Gold−Gold Distance for Various $[Au(SCN)_2]^-$ Salts. *J. Am. Chem. Soc.* **126**, 12–13 (2004).
114. Balch, A. L. Polymorphism and luminescent behavior of linear, two-coordinate gold(I) complexes. *Gold Bull.* **37**, 45–50 (2004).
115. Laurila, E., Oresmaa, L., Niskanen, M., Hirva, P. & Haukka, M. Metal-metal interactions in stacked mononuclear and dinuclear rhodium 2,2′-biimidazole carbonyl complexes. *Cryst. Growth Des.* **10**, 3775–3786 (2010).
116. Laurila, E., Tatikonda, R., Oresmaa, L., Hirva, P. & Haukka, M. Metallophilic interactions in stacked dinuclear rhodium 2,2′-biimidazole carbonyl complexes. *CrystEngComm* **14**, 8401–8408 (2012).
117. Hirva, P., Haukka, M., Jakonen, M. & Pakkanen, T. A. Growth of the metal framework in linear ruthenium and osmium carbonyls. *Inorganica Chim. Acta* **359**, 853–862 (2006).
118. Mann, K. R., Lewis, N. S., Williams, R. M., Gordon, J. G. & Gray, H. B. Further Studies of Metal-Metal Bonded Oligomers of Rhodium(I) Isocyanide Complexes. Crystal Structure Analysis of $[Rh_2(CNPh)_8](BPh_4)_2$ *Inorg. Chem.* **17**, 828–834 (1978).

119. Tominaga, T. & Mochida, T. Multifunctional Ionic Liquids from Rhodium(I) Isocyanide Complexes: Thermochromic, Fluorescence, and Chemochromic Properties Based on Rh−Rh Interaction and Oxidative Addition. *Chem. - A Eur. J.* **24**, 6239–6247 (2018).
120. Conifer, C. M., Taylor, R. A., Law, D. J., Sunley, G. J., White, A. J. P., Britovsek, G. J. P. First metal complexes of 6,6′-dihydroxy-2,2′-bipyridine: from molecular wires to applications in carbonylation catalysis. *Dalt. Trans.* **40**, 1031–1033 (2011).
121. De Pater, B. C., Fruhauf, H-W., Vrieze, K., de Gelder, R., Baerends, E. J., McCormack, D., Lutz, M., Spek, A. L., Hartl, F. Strongly nucleophilic RhI centre in square-planar complexes with terdentate (κ3) 2,2′:6′,2″-terpyridine ligands: Crystallographic, electrochemical and density functional theoretical studies. *Eur. J. Inorg. Chem.* 1675–1686 (2004).
122. Chan, A. K. W., Wu, D., Wong, K. M. C. & Yam, V. W. W. Rhodium(I) Complexes of Tridentate N-Donor Ligands and Their Supramolecular Assembly Studies. *Inorg. Chem.* **55**, 3685–3691 (2016).
123. Angle, C. S., DiPasquale, A. G., Rheingold, A. L. & Doerrer, L. H. Red and yellow solvates of chloro(2,2′:6′,2″-terpyridine) -platinum(II) chloride and Pt···Pt interactions. *Acta Crystallogr. Sect. C Cryst. Struct. Commun.* **62**, 340–342 (2006).
124. Janzen, D. E. & Mann, K. R. Red and orange polymorphs of [Pt(terpy)Cl]Cl ·2H2O. *J. Chem. Crystallogr.* **43**, 292–298 (2013).
125. Yip, H.-K., Cheng, L.-K., Cheung, K.-K. & Che, C.-M. Luminescent platinum(II) complexes. Electronic spectroscopy of platinum(II) complexes of 2,2′:6′,2″-terpyridine (terpy) and p-substituted phenylterpyridines and crystal structure of [Pt(terpy)CI][CF_3SO_3]. *J. Chem. Soc. Dalt. Trans.* 2933–2938 (1993).
126. Bailey, J. A., Hill, M. G., Marsh, R. E., Miskowski, V. M., Schaefer, W. P., Gray, H. B. Electronic Spectroscopy of Chloro(terpyridine)platinum(II). *Inorg. Chem.* **34**, 4591–4599 (1995).
127. Femoni, C., Kaswalder, F., Iapalucci, M. C., Longoni, G. & Zacchini, S. Infinite molecular {[Pt3n(CO)6n]$^{2-}$} ∞ conductor wires by self-assembly of [Pt3n(CO)6n]$^{2-}$ (n = 5-8) cluster dianions formally resembling CO-sheathed three-platinum cables. *Eur. J. Inorg. Chem.* **6**, 1483–1486 (2007).
128. Wang, C.-C., Lo, W-C., Chou, C-C., Lee, G-H., Chen, J-M., Peng, S-M. Synthesis, Crystal Structures, and Magnetic Properties of a Series of Linear Pentanickel(II) Complexes: [$Ni_5(\mu_5\text{-tpda})_4X_2$] (X =$Cl^-$, CN^- , N^{3-} , NCS^-) and [$Ni_5(\mu_5\text{-tpda})_4(CH_3CN)_2]^-(PF_6)_2$ (tpda^{2-} = the Tripyridyldiamido Dianion). *Inorg. Chem.* **37**, 4059–4065 (2002).
129. Li, Z., Han, Y., Gao, Z., Fu, T. & Wang, F. Non-covalent molecular tweezer/guest complexation with Pt(II) Pt(II) metal-metal interactions: Toward intelligent photocatalytic materials. *Mater. Chem. Front.* **2**, 76–80 (2018).
130. Caseri, W. Derivatives of Magnus' green salt from intractable materials to solution-processed transistors. *Platin. Met. Rev.* **48**, 91–100 (2004).
131. Wadas, T. J., Wang, Q-M., Kim, Y-J., Flaschenreim, C., Blanton, T. N., Eisenberg, R. Vapochromism and its structural basis in a luminescent Pt(II)

terpyridine-nicotinamide complex. *J. Am. Chem. Soc.* **126**, 16841–16849 (2004).
132. Chifotides, H. T. & Dunbar, K. R. Interactions of metal - Metal-bonded antitumor active complexes with DNA fragments and DNA. *Acc. Chem. Res.* **38**, 146–156 (2005).
133. Tsai, T. W., Huang, Q. R., Peng, S. M. & Jin, B. Y. Smallest electrical wire based on extended metal-atom chains. *J. Phys. Chem. C* **114**, 3641–3644 (2010).
134. Ting, T. C., Hsu, L-Y. Huang, M-J., Horng, E-C., Lu, H-C., Hsu, C-H., Jiang, C-H., Jin, B-Y., Peng, S-M., Chen, C-h. Energy-Level Alignment for Single-Molecule Conductance of Extended Metal-Atom Chains. *Angew. Chemie - Int. Ed.* **54**, 15734–15738 (2015).
135. Brown-Xu, S. E., Kelley, M. S. J., Fransted, K. A., Chakraborty, A., Schatz, G. C., Castellano, F. N., Chen, L. X. Tunable Excited-State Properties and Dynamics as a Function of Pt-Pt Distance in Pyrazolate-Bridged Pt(II) Dimers. *J. Phys. Chem. A* **120**, 543–550 (2016).
136. Büchner, R., Cunningham, C. T., Field, J. S., Haines, R. J., McMillin, D. R., Summerton, G. C. Luminescence properties of salts of the [Pt(4′Ph-terpy)Cl]$^{+}$ chromophore: Crystal structure of the red form of [Pt(4′Ph-terpy)Cl]BF_4 (4′Ph-terpy = 4′-phenyl-2,2′: 6′,2″-terpyridine). *J. Chem. Soc. - Dalt. Trans.* 711–717 (1999).
137. Mahapatra, T. S., Singh, H., Maity, A., Dey, A., Pramanik, S. K., Suresh, E., Das, A. White-light-emitting lanthanide and lanthanide-iridium doped supramolecular gels: modular luminescence and stimuli-responsive behaviour. *J. Mater. Chem. C* **6**, 9756–9766 (2018).
138. Kontkanen, M. L., Oresmaa, L., Moreno, M. A., Jänis, J., Laurila, E., Haukka, M. One-dimensional metal atom chain $[Ru(CO)_4]_n$ as a catalyst precursor-Hydroformylation of 1-hexene using carbon dioxide as a reactant. *Appl. Catal. A Gen.* **365**, 130–134 (2009).
139. Yoshida, M. & Kato, M. Regulation of metal–metal interactions and chromic phenomena of multi-decker platinum complexes having π-systems. *Coordination Chemistry Reviews* **355**, 101–115 (2018).
140. Zhao, Y. & Chen, F. Empirical likelihood inference for censored median regression model via nonparametric kernel estimation. *J. Multivar. Anal.* **99**, 215–231 (2008).
141. Barros, C. L., de Oliveira, P. J. P., Jorge, F. E., Canal Neto, A. & Campos, M. Gaussian basis set of double zeta quality for atoms Rb through Xe: application in non-relativistic and relativistic calculations of atomic and molecular properties. *Mol. Phys.* **108**, 1965–1972 (2010).
142. Canal Neto, A. & Jorge, F. E. All-electron double zeta basis sets for the most fifth-row atoms: Application in DFT spectroscopic constant calculations. *Chem. Phys. Lett.* **582**, 158–162 (2013).
143. Jorge, F. E., Canal Neto, A., Camiletti, G. G. & Machado, S. F. Contracted Gaussian basis sets for Douglas–Kroll–Hess calculations: Estimating scalar relativistic effects of some atomic and molecular properties. *J. Chem. Phys.* **130**, 64108 (2009).
144. Bader, R. F. W. Atoms in Molecules. *Acc. Chem. Res.* **18**, 9–15 (1985).

145. Vener, M. V, Egorova, A. N., Churakov, A. V & Tsirelson, V. G. Intermolecular hydrogen bond energies in crystals evaluated using electron density properties: DFT computations with periodic boundary conditions. *J. Comput. Chem.* **33**, 2303–2309 (2012).
146. Espinosa, E., Molins, E. & Lecomte, C. Hydrogen bond strengths revealed by topological analyses of experimentally observed electron densities. *Chem. Phys. Lett.* **285**, 170–173 (1998).
147. Anjali, K. S., Vittal, J. J., Dean, P. A. W. Syntheses, characterization and thermal properties of $[M(Spy)_2(SpyH)_2]$(M=Cd and Hg; Spy^-=pyridine-4-thiolate; SpyH=pyridinium-4-thiolate)) and $[M(SpyH)_4](ClO_4)_2$ (M=Zn, Cd and Hg). *inorg. Chim. Acta.* **351**, 79-88 (2003)

ORIGINAL PAPERS

I

METALLOPHILIC INTERACTIONS IN POLYMERIC GROUP 11 THIOLS

by

Kalle Kolari, Joona Sahamies, Elina Kalenius, Alexander S. Novikov, Vadim Yu. Kukushkin, & Matti Haukka, 2016

Solid State Sci., **2016**, *60*, 92–98

Solid State Sciences 60 (2016) 92–98

Contents lists available at ScienceDirect

Solid State Sciences

journal homepage: www.elsevier.com/locate/ssscie

Metallophilic interactions in polymeric group 11 thiols

Kalle Kolari [a], Joona Sahamies [a], Elina Kalenius [a], Alexander S. Novikov [b], Vadim Yu. Kukushkin [b], Matti Haukka [a, *]

[a] University of Jyvaskyla, Department of Chemistry, P.O Box 35, FI-40014, University of Jyvaskyla, Finland
[b] Institute of Chemistry, Saint Petersburg State University, Universitetskaya Nab. 7/9, 199034 Saint Petersburg, Russian Federation

ARTICLE INFO

Article history:
Received 8 March 2016
Received in revised form
2 August 2016
Accepted 7 August 2016
Available online 15 August 2016

Keywords:
Cu
Ag
Au
4-pyridinethiol
Metallophilic interactions

ABSTRACT

Three polymeric group 11 transition metal polymers featuring metallophilic interactions were obtained directly via self-assembly of metal ions and 4-pyridinethiol ligands. In the cationic $[Cu_2(S\text{-}pyH)_4]^{2+}_n$ with $[ZnCl_4]^{2-}_n$ counterion (**1**) and in the neutral $[Ag(S\text{-}py)\ (S\text{-}pyH)]_n$ (**2**) 4-pyridinethiol (S-pyH) and its deprotonated form (S-py) are coordinated through the sulfur atom. Both ligands are acting as bridging ligands linking the metal centers together. In the solid state, the gold(I) polymer $[Au(S\text{-}pyH)_2]Cl$ (**3**) consists of the repeating cationic $[Au(S\text{-}pyH)_2]^+$ units held together by aurophilic interactions. Compound **1** is a zig-zag chain, whereas the metal chains in the structures of **2** and **3** are linear. The protonation level of the thiol ligand had an impact on the crystallization of polymers. Both nature of the metal center and reaction conditions affected the polymerization. QTAIM analysis confirmed direct metal-metal contacts only in polymers **1** and **3**. In polymer **2**, no theoretical evidence of argentophilic contacts was obtained even though the Ag···Ag distance was found to be less than sum of the Bondi's van der Waals radius of silver.

1. Introduction

Metallopolymers is a class of compounds that covers a wide range of metal containing polymeric systems [1]. The structures vary from mainly organic polymers with metal centers in the main or side chain, to systems with direct covalent metal-metal bonds [2a,b,c,d], and non-covalent metallophilic assemblies of metal species [2e,f,g,h]. The motivation for preparation of metallopolymers lie in their versatile properties, such as conductivity [2i] and photophysical properties [3] as well as their magnetic [4] and catalytic [5] behavior. These properties determined applications of metallopolymers such as photovoltaic cells, catalysts and light emitting devices [1–5].

In most cases, the key properties arise from the interactions between metal centers [6a,b,c]. These interactions can be achieved by linking metal centers together with a suitable (usually conjugated) ligands and building coordination polymers [6d]. Another approach is to exploit direct metal-metal contacts. These contacts can either be covalent metal-metal bonds or non-covalent metallophilic contacts [6e]. Polymeric transition metal systems that have only covalent metal-metal bonds between the repeating units are relatively rare [2b,d]. More commonly, metal-metal contacts are further supported by suitable multidentate ligands that can force metal centers close to each other. Multidentate nitrogen ligands are widely used supporters [6f, g,h,2h]. However, metals can also be brought together by single atom bridges. Simple bridging ligands such as halides, pseudo halides or sulfur containing ligands can be used in this type of systems [7]. In metal thiols and closely related coordination compounds, the soft sulfur atom is readily available for coordination and capable to act as bridging atom through its free electron pairs [8a-d]. Usually, thiol ligands can be relatively easily modified to adjust their electronic and steric properties. Because of this adjustability, thiols are excellent components for coordination chemistry [8e-i]. Heterocyclic thiols provide particularly versatile group of thiol ligands [9–12].

The 4-pyridine thiol is one of the commonly used heterocyclic thiol ligand. It can exist in different tautomeric forms, thiol (**A**), thione (**B**) and zwitterionic (**C**) forms (Fig. 1).

Removal of the NH proton from 4-pyridinethiol opens up a possibility to use both of softer sulfur and harder nitrogen for coordination. Therefore, pyridinethiols have drawn attention as potential ambidentate ligands [13] exhibiting interesting spectroscopic [14a] and electrochemical [14b] behavior. Due to exocyclic sulfur and heterocyclic nitrogen donor, pyridine thiols

* Corresponding author.
E-mail address: matti.o.haukka@jyu.fi (M. Haukka).

http://dx.doi.org/10.1016/j.solidstatesciences.2016.08.005
1293-2558/

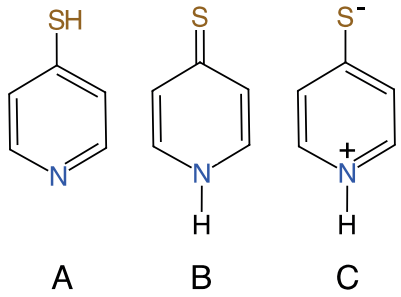

Fig. 1. Schematic representation of tautomeric forms of 4-pyridinethiol.

have also been successfully exploited as ditopic ligands [15] for oligomeric and polymeric metal systems. Polynuclear species combining different metals by thiols have been used for example in catalytic [16a], pharmaceutical [16b], biochemical [16c], luminescent [16d], and magnetic [16e] materials and also as precursors for silver chalconides [16f]. One of the potential applications of thiols is to use them as supporting single-atom linking ligands in metallophilic polymers.

Metallophilicity can be described as attraction between closed shell or pseudo closed shell d^{10} or d^8 transition metal cations [17a]. Strength of a metallophilic interaction is typically comparable to hydrogen bonds and it is clearly stronger than van der Waals interactions [17a]. Metallophilic interactions have been widely studied by the means of spectroscopic techniques [17a,6c], computational chemistry [17b-e] and structural studies [17f,g]. Metallophilicity is considered to be mainly a dispersion force with electron correlation effects [18]. Structurally metallophilicity can favor formation of various extended polynuclear structures including dimers, 1D chains, 2D sheets, 3D networks or molecular aggregates [19].

In this paper, we describe generation of linear and pseudolinear group 11 metallopolymers supported by sulfur coordinated 4-pyridinethiols. The primary goal was generation of novel metallophilic interactions due to application of the thiols that serve as molecular staples bringing together two metal atoms. The impact of the metal center and reaction conditions to the formation of polymers and their solid state structures are also briefly discussed.

2. Materials and methods

2.1. General remarks

Reagents were used as received. Acetonitrile and methanol were HPLC grade. Purity of ethanol and dichlromethane were 99.5%. NMR spectra were recorded with a Bruker 500 MHz NMR with BBFO probe under ambient conditions. Mass spectra were measured on an ABSciex QSTAR Elite ESI-Q-TOF MS.

2.2. X-ray structure determinations

The crystals of $[Cu_2(S\text{-}pyH)_4]_n$ $[ZnCl_4]_n$ (**1**), [Ag(S-py) (S-pyH)]$_n$ (**2**), and $[Au(S\text{-}pyH)_2]Cl$ (**3**) were immersed in cryo-oil, mounted in a MiTeGen loop and measured at 120–170 K. The X-ray diffraction data were collected on an Agilent Technologies Supernova or an Bruker AXS KappaApex diffractometers using Cu Kα (λ = 1.54184 Å) or Mo Kα radiation (λ = 0.70173 Å). The CrysAlisPro [20] or Denzo/Scalepack [21] program packages were used for cell refinements and data reductions. The structures were solved by charge flipping method using the SUPERFLIP [22] program or by direct methods using SHELXS-2014 [23] program. An empirical absorption correction based on equivalent reflections (CrysAlisPro [20] or SADABS [24]) was applied to all data. Structural refinements were carried out using SHELXL-2014 [23] with the Olex2 [25] and SHELXLE [26] graphical user interfaces. In **1**, the NH and OH hydrogen atoms were located from the difference Fourier map but constrained to ride on their parent atoms, with U_{iso} = 1.5 U_{eq} (parent atom). In **3**, the NH hydrogens were located from the difference Fourier map and refined isotropically. All other hydrogens were positioned geometrically and constrained to ride on their parent atoms, with C–H = 0.98–1.00 Å, N–H = 0.88 Å, and U_{iso} = 1.2–1.5 Ueq (parent atom). The crystallographic details are summarized in Table 1.

Table 1
Crystal data for **1**–**3**.

	1	**2**	**3**
empirical formula	$C_{22}H_{26}Cl_4Cu_2N_4O_1S_4Zn$	$C_{10}H_9AgN_2S_2$	$C_{10}H_{10}AuClN_2S_2$
Fw	824.96	329.18	454.74
temp (K)	123 (2)	170 (2)	120 (2)
λ(Å)	1.54184	0.71073	1.54184
cryst syst	Monoclinic	Orthorhombic	Monoclinic
space group	$P2_1/n$	Ibam	$P2_1/c$
a (Å)	10.0163 (3)	12.1624 (6)	16.9203 (6)
b (Å)	10.0845 (3)	13.7874 (10)	11.3649 (5)
c (Å)	29.8809 (13)	6.3879 (4)	6.7730 (3)
α (deg)	90	90	90
β (deg)	95.051 (3)	90	99.647 (4)
γ (deg)	90	90	90
V (Å^3)	3006.54 (19)	1071.17 (12)	1284.02 (10)
Z	4	4	4
ρ_{calc} (Mg/m^3)	1.823	2.041	2.352
μ(Mo Kα) (mm^{-1})	8.656	2.234	26.271
No. reflns.	12623	7680	5014
Unique reflns.	6128	849	2585
GOOF (F^2)	1.022	1.126	1.072
R_{int}	0.0926	0.0640	0.0961
R1[a] ($I \geq 2\sigma$)	0.0347	0.0253	0.0381
w*R*2[b] ($I \geq 2\sigma$)	0.0878	0.0615	0.0918
Largest diff. peak and hole eÅ^{-3}	0.589/-0.633	0.457/−0.517	1.811/−1.340

[a] $R1 = \Sigma||F_o| - |F_c||/\Sigma|F_o|$.
[b] $wR2 = [\Sigma[w\ (F_o2 - F_c2)2]/\Sigma[w\ (F_o2)2]]1/2$.

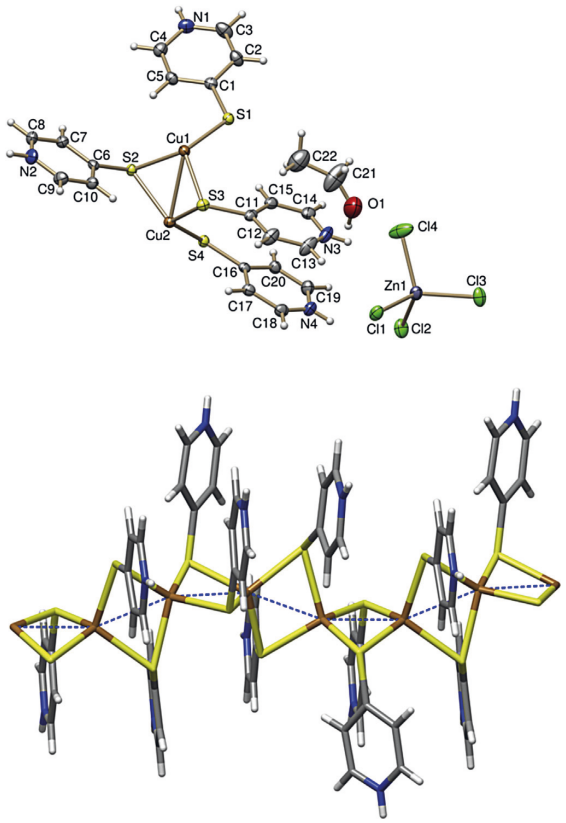

Fig. 2. Top: The asymmetric unit of $[Cu_2(S\text{-}pyH)_4]_n\,[ZnCl_4]_n$. The thermal ellipsoids are drawn at the 50% probability level. Bottom: The chain structure of **1**. The solvent of crystallization and the courter anions have been omitted for clarity. Color codes for atoms in the figure are: H (white), C (gray), N (blue), O (red), Cl (green), S (yellow), Cu (Orange), and Zn (violet). (For interpretation of the references to colour in this figure legend, the reader is referred to the web version of this article.)

2.3. Mass spectrometry

Mass spectrometry experiments were performed on ABSciex QSTAR Elite ESI-Q-TOF mass spectrometer equipped with an API 200 TurboIonSpray ESI source from AB Sciex (former MDS Sciex) in Concord, Ontario (Canada). The samples for the MS measurements were prepared either by dilution in MeCN (**1**, 12.9 μM) or MeOH (**3**, concentration unknown due to low solubility). The samples were injected into the ESI source with a flow rate of 5 μl/min. The parameters were optimized to get maximum abundance of the ions under study. Room-temperature nitrogen was used as nebulization. The measurement and data handling was accomplished with Analyst® QS 2.0 Software. Mass spectra were externally calibrated by ESI Tuning mix (Agilent Technologies). The compositions of the ions were verified by comparing experimental *m/z* values and isotopic patterns with the theoretically calculated. In CID experiments, low resolution isolation in quadrupole Q1 was performed and the isolated ions were activated by CE-values from 10 to 40. nitrogen was used as a collision gas in the Q2 quadrupole (5.0 psi) and the product ions were detected by TOF scans.

2.4. Computational details

The single point calculations for model clusters has been carried out at the DFT level of theory using the M06 functional [27] (this functional describes reasonably weak dispersion forces and non-covalent interactions) with the help of the Gaussian-09 [28] program package. The experimental X-ray geometries were used as starting points. The calculations were carried out using DZP-DKH basis sets [29] for all atoms. No symmetry operations have been applied. The topological analysis of the electron density distribution with the help of the atoms in molecules (QTAIM) method developed by Bader [30] has been performed by using the Multiwfn program (version 3.3.4) [31]. The Cartesian atomic coordinates of the used model structures presented in the supporting material.

2.5. Syntheses

The aim of this study was to study possibilities to obtain metallopolymers that contain metallophilic contacts via self-assembly of metal-ions and the ligand. Thus, reactions were not optimized for maximum yields and purities. According to the ^{1}HNMR (Figs. 1 and 2 in ESI), the crude products of **1** and **3** contained unreacted 4-pyridylthiol, 4,4'-dipyridyldisulfide, and 4-pyridylsulfide as the main impurities. ^{1}H NMR spectra also revealed presence of residual solvents in the crude product. ^{1}H NMR spectrum of product **3** shows second order ^{1}H coupling and differ from previously reported chemical shifts due to solvent effects. Because of decomposition of **3** in DMSO the ^{1}H NMR was measured in 4-d MeOH. The silver polymer **2** was insoluble in most common solvents and no ^{1}H NMR spectrum in solution could be obtained. ATR-IR analysis was performed for polymer **2** (Fig. 4 in ESI).

2.6. $[Cu_2(S\text{-}pyH)_4]_n\,[ZnCl_4]_n$ (**1**)

A solution of $CuCl_2\cdot 2H_2O$ (0.06 mmol, 10 mg) in MeCN/EtOH mixture (3:1 ratio, 3 mL) was added to a solution of 4-pyridinethiol (0.3 mmol, 33 mg) in 3 mL of same solvent mixture. The reaction

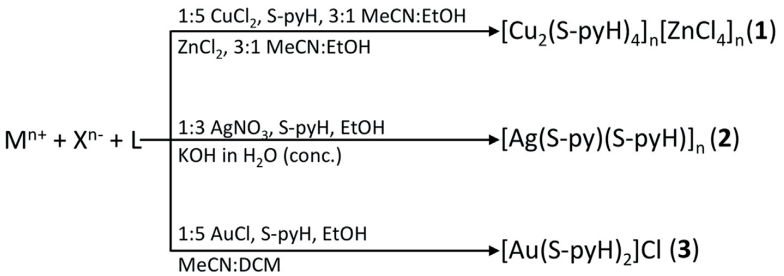

Scheme 1. Synthetic routes to **1**–**3**.

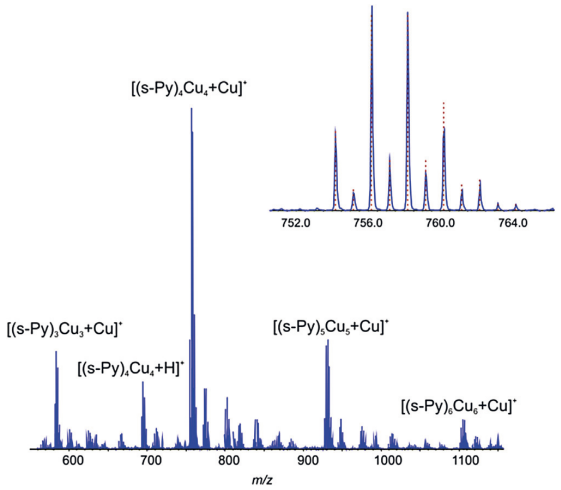

Fig. 3. The ESI-QTOF MS spectrum of **1** in MeCN. Inset showing the comparison between experimental and theoretical (red dotted lines) isotopic distribution for the $[(S\text{-}Py)_4Cu_4 + Cu]^+$ ($C_{20}H_{16}N_4S_4Cu_5^+$). (For interpretation of the references to colour in this figure legend, the reader is referred to the web version of this article.)

mixture was stirred for 5 min. Additional 5 mL of solvent mixture was added to the reaction flask cautiously without mixing until two distinct layers of solutions was formed. $ZnCl_2$ (0.12 mmol, 16 mg) was dissolved in 9 mL of 3:1 solvent mixture of acetonitrile/ethanol. Solution containing zinc chloride was then carefully added to the reaction mixture and the flask was closed with a rubber septa and the solution was left to stand at room temperature. X-ray quality yellow orange crystals were obtained within three days directly from the reaction mixture. Crystals were filtered and washed 3 times with 1 mL of 3:1 acetonitrile/ethanol mixture and dried under vacuum overnight. The crude solid product of complex **1** contained residues crystallization solvents EtOH, MeCN, and water. Several crystals of **1** were analyzed by single-crystal X-ray diffraction and in these structures the ratio of solvents of crystallization varied depending on the drying time. The best structure solution was obtained from a crystal that incorporated only disordered EtOH. The sample used for the elemental analysis, in turn, contained only MeCN. That was confirmed by ^{1}H NMR. The yield of **1** was 44% (20.4 mg). ^{1}H NMR (MeOD): 8.54 (d, 2H, $J = 6.6$ Hz), 8.62 (d, 2H, $J = 6.4$ Hz). Elemental analyses calc. for $[Cu_2(S\text{-}pyH)_4]_n^{2+}$ $[ZnCl_4]_n^{2-}$ · 0.5 MeCN C: 31.55%, H: 2.71% and N: 7.88% found C: 31.35%, H: 2.88% and N: 7.55%.

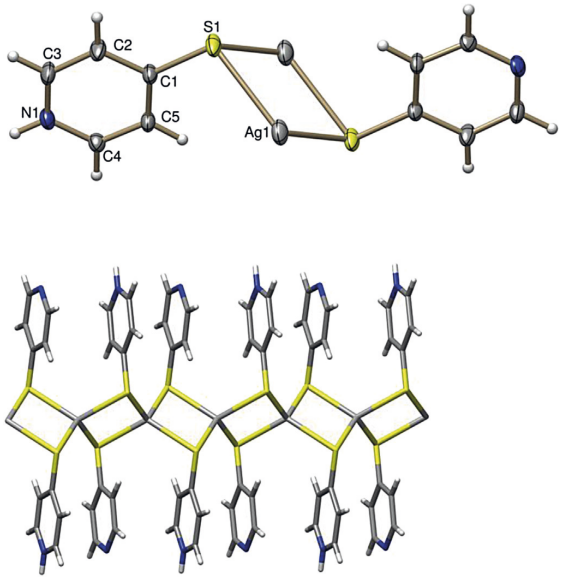

Fig. 4. Top: The repeating unit of **2**. The thermal ellipsoids are drawn at the 50% probability level. Bottom: The polymeric chain structure of **2**. Color codes for atoms in the figure are: H (white), C (gray), N (blue), S (yellow), and Ag (gray). (For interpretation of the references to colour in this figure legend, the reader is referred to the web version of this article.)

2.7. *[Ag(S-py) (S-pyH)]$_n$* (**2**)

$AgNO_3$ (0.09 mmol, 15 mg) was dissolved separately in 3 mL of acetonitrile and 4-pyridinethiol (0.3 mmol, 33 mg) in 5 mL of ethanol. Concentrated KOH solution was prepared by weighing 0.538 g of KOH in 5 mL of water. Concentrated KOH solution (4 mL) was added into ligand solution to make the solution clearly basic. The Ag containing solution was then added rapidly to the basic ligand solution and the mixture was stirred overnight at room temperature. During this time the color of the reaction mixture turned from colorless to orange yellow. Small amount of precipitate formed during stirring was removed by filtering and the filtrate was left standing in a vessel closed with septa. The crystalline yellow orange product was obtained from the filtrate at room temperature within a week. The yield of **2** was 83% (24.6 mg). Elemental analyses calculated for $[Ag(S\text{-}py)\ (S\text{-}pyH)]_n$ C: 36.48%, H: 2.76% and N 8.51% found C: 36.45%, H: 2.97% and N 8.64%.

2.8. *[Au(S-pyH)$_2$]Cl* (**3**)

The organic ligand, 4-pyridinethiol (0.09 mmol, 10 mg), was introduced in 8 mL of dichloromethane and stirred for 1 h until it was completely dissolved. AuCl (0.02 mmol, 5 mg) was dissolved in 2 mL of acetonitrile and the metal solution was carefully layered onto the ligand solution after which the reaction vial was closed with septa. X-ray quality yellow crystals were formed within two weeks. Crystals were filtered, washed three times with 2 mL of acetonitrile and dried under vacuum overnight. The crude product of **3** contained always traces of water even if the X-ray structure did not contain water of crystallization. NMR spectrum of compound **2** confirms presence of water in the sample. The product was not stable enough to be heated in vacuum. The yield of the product **3** was 30% (2.7 mg). ^{1}H NMR (MeOD) 8.03 (d, 4H, $J = 7.1$ Hz), 7.97 (d, 4H, $J = 7.1$ Hz). MS + TOF 418.99 *m/z*. Elemental analyses calculated for $[Au(S\text{-}pyH)_2]Cl\cdot H_2O$ C: 25.41%, H: 2.56% and N: 5.93% found C: 25.66%, H: 2.24% and N: 5.94%.

3. Results and discussion

The general syntheses routes to compounds **1**–**3** are summarized in Scheme 1. Complexes $[Cu_2(S\text{-}pyH)_4]_n$ $[ZnCl_4]_n$ (**1**) and $[Ag(S\text{-}py)\ (S\text{-}pyH)]_n$ (**2**) were prepared by dissolving metal salt and ligand separately in different solvents and then adding the metal complex solution into the solutions of the ligand (Scheme 1). The crystalline $[Au(S\text{-}pyH)_2]Cl$ (**3**) was obtained by the layering metal containing acetonitrile solution onto the dichloromethane solution of the ligand. In the case of the Au complex, the product was obtained when the solutions were slowly mixed.

In the synthesis of silver system, **2**, additional KOH was needed

Table 2
Experimental and theoretical *m/z* values and mass accuracies for ions observed in mass spectra for **1** and **3**.

Sample	Ion	Composition	m/z_{exp}	m/z_{theor}	Mass accuracy (*m/z*)
1	$[(S\text{-}Py)_3Cu_3 + Cu]^+$	$C_{15}H_{12}N_3S_3Cu_4$	583.7365	583.7353	−0.001
	$[(S\text{-}Py)_4Cu_4 + H]^+$	$C_{20}H_{17}N_4S_4Cu_4$	694.7445	694.7495	0.005
	$[(S\text{-}Py)_4Cu_4 + Cu]^+$	$C_{20}H_{16}N_4S_4Cu_5$	758.6782	758.6694	−0.009
	$[(S\text{-}Py)_5Cu_5 + Cu]^+$	$C_{25}H_{20}N_5S_5Cu_6$	931.6010	931.6055	0.005
	$[(S\text{-}Py)_6Cu_6 + Cu]^+$	$C_{30}H_{24}N_6S_6Cu_7$	1104.5379	1104.5416	0.004
3	$[(S\text{-}PyH)_2Au]^+$	$C_{10}H_{10}N_2S_2Au$	418.9944	418.9945	0.0001

for deprotonation of 4-pyridinethiol ligand. The positive charges of the metal centers were balanced by the deprotonated S-py$^-$ligands. To obtain crystalline neutral polymer, half of the thiol ligands had to be deprotonated. With copper (**1**) and gold (**3**), high quality crystals of the cationic products could be obtained without any deprotonation of the ligands. In these cases the positive charges of the metals were balanced by counter anions $[ZnCl_4]^{2-}$ (**1**) and Cl^- (**3**).

3.1. Cationic copper polymer $[Cu_2(S\text{-}pyH)_4]_n^{2+}$ (*1*)

Several counterions including PF_6^-, trifluoromethanesulfonate and lithium tetrakis (pentafluorophenyl)borate ethyl etherate were tested for crystallization of positively charged polymeric $[Cu_2(S\text{-}pyH)_4]_n^{2+}$ (**1**) but high quality crystals were obtained only by using $[ZnCl_4]^{2-}$ anion. Similar dinuclear Cu structure with chloride ion balancing the charge of the complex has been previously reported [32] but polymeric chain has remained unknown until now. In the polymeric structure of **1,** the copper(I) centers are linked together by two S-coordinated 4-pyridinethiol ligands (S-pyH) (Fig. 2). The structure also incorporates slightly disordered ethanol of crystallization, which is hydrogen bonded to the nitrogen of the S-pyH ligand (N2···O1^i: 2.994 (5) Å, i = x−1/2,−y + 1/2,z−1/2). The sulfur atoms are arranged tetrahedrally around the copper atoms in the polymeric chain. These sulfur bridges pull metal centers closely together forming a 1D polymeric zig-zag chain (Fig. 2) with direct metal-metal contacts. The distances between the copper atoms are nearly identical throughout the chain varying from 2.6241 (6) Å to 2.6283 (6) Å. Weak π-π interactions between the pyridine rings support the chain structure further. Short metal-metal distances between copper atoms indicate relatively strong cuprophilic interactions. The $[ZnCl_4]^{2-}$ anion is interacting with the cationic polymer primarily through hydrogen bonds between the NH hydrogens of the S-PyH ligand and chlorides of the anionic zinc complex (N3···Cl4: 3.147 (3) Å, N3···Cl1: 3.286 (3), N4···Cl2: 3.373 (3) Å, N2···Cl4^i: 3.201 (3) Å, i = x−1/2,−y + 1/2,z−1/2).

The polymeric character of **1** can also be seen from the mass spectrometric study. The ESI-TOF mass spectrum of **1** (Fig. 3) shows distribution of polymeric singly charged ions $[(S\text{-}Py)_nCu_n + Cu]^+$, $[(S\text{-}Py)_nCu_n + H]^+$, and $[(S\text{-}Py)_nCu_n + NH_4]^+$ (n = 3–6). The base peak of the spectrum is $[(S\text{-}py)_4Cu_5]^+$ at *m/z* 758.68, which agrees well with the theoretical value of *m/z* 758.67 (for detailed analysis of mass accuracies see Table 2) and shows a nice fit to calculated isotopic distribution pattern. This ion also displays a structure related dissociation pattern in a CID (collision induced dissociation) experiment, in which the polymer fragments through consecutive eliminations of S-Py and (S-Py)Cu units (ESI, Fig. S3).

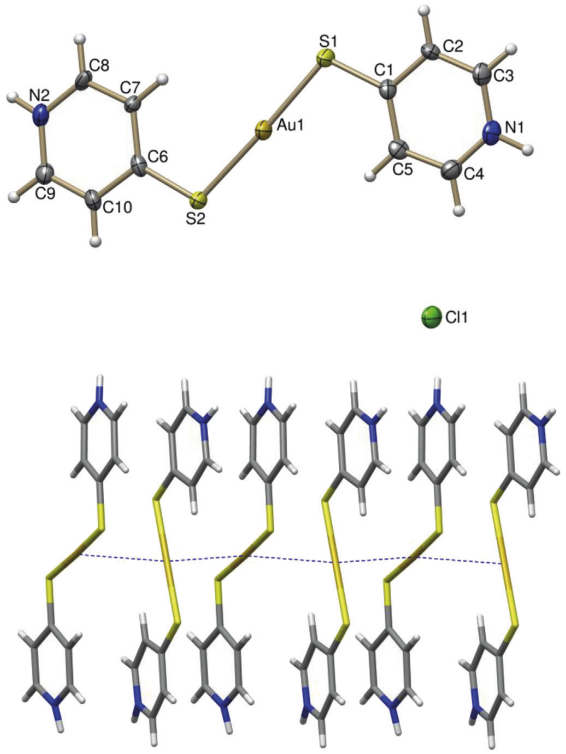

Fig. 5. Top: The molecular unit of **3**. The thermal ellipsoids are drawn at the 50% probability level. Bottom: The chain structure of **3**. The counterions were omitted for clarity.

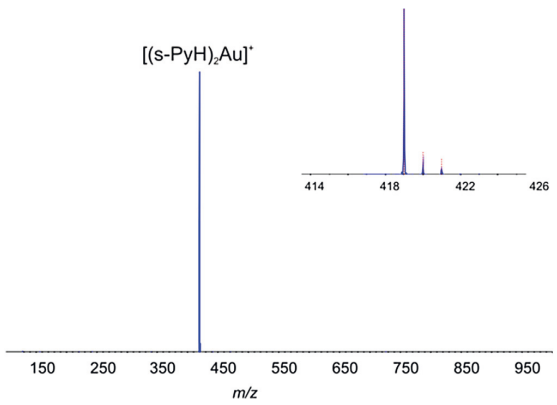

Fig. 6. The ESI-QTOF MS spectrum of **3** in MeOH. Inset showing the comparison between experimental and calculated (red dotted lines) isotopic distribution for the $[(S\text{-}PyH)_2Au]^+$ ($C_{10}H_{10}AuN_2S_2^+$) ion. (For interpretation of the references to colour in this figure legend, the reader is referred to the web version of this article.)

Table 3
Values of the density of all electrons – ρ(**r**), Laplacian of electron density – $\nabla^2\rho(\mathbf{r})$, energy density – H_b, potential energy density – V(**r**), and Lagrangian kinetic energy – G(**r**) (Hartree) at the bond critical points (3, −1) (BCPs), corresponding to the non-covalent M···M interactions in (**1**) and (**3**) as well as energies of these interactions E_{int} (kcal/mol), defined by two approaches.

Polymer	ρ(r)	$\nabla^2\rho(r)$	H_b	V(r)	G(r)	E_{int}[a]	E_{int}[b]
Cu(I) (**1**)	0.034	0.034–0.038	−0.012	−0.033 to −0.034	0.021–0.022	10.35–10.67	5.65–5.92
Au(I) (**3**)	0.016	0.044	0.000	−0.011	0.011	3.45	2.96

[a] $E_{int} = -V(\mathbf{r})/2$ [33].
[b] $E_{int} = 0.429G(\mathbf{r})$ [34].

3.2. Neutral silver polymer [Ag(S-py) (S-pyH)]$_n$ (**2**)

The polymeric $[Ag(S\text{-}py)(S\text{-}pyH)]_n$ (**2**) was crystallized in an orthorhombic space group Ibam. The asymmetric unit consists of one S-PyH or S-py$^-$ ligand coordinated to a silver center via sulfur atoms. This give a repeating unit with two Ag atoms and one S-pyH and one S-py ligands (Fig. 4). In other words, every second pyridyl ring in the chain is deprotonated compensating the charge of the silver centers. As in the case of copper polymer **1**, the thiol ligands act as molecular staples bringing metal centers to close proximity. The silver-silver distances are practically identical throughout the chain varying from 3.1939 (2) Å to 3.1940 (2) Å (Ag1···Ag1^{i}, Ag1···Ag1^{ii}, i = −x + 1,−y,−z, ii = −x + 1,−y,−z + 1). The Ag–Ag distances are clearly shorter than the sum of Bondi's van der Waals radii of silver atoms (3.44 Å) bond. Just like in the case of the copper polymer, the chain structure is again further supported by weak π-π interactions between the pyridyl rings. By contrast to the copper polymer, the Ag polymer is linear and the Ag···Ag···Ag angle is 180°. The sulfur ligands are again tetrahedrally arranged around the metal atoms in the polymeric structure. The neighboring chains are connected via hydrogen bonds between the protonated and deprotonated pyridyl nitrogens (N1···N1^{iii}: 2.675 (4) Å, iii = x + 1,−y + 1,z).

3.3. Cationic non-covalent polymer $[Au(S\text{-}pyH)_2]^+_n$ (**3**)

The structure of **3** has been reported earlier [33]. However, the current structure is based on higher quality data and therefore includes also the hydrogen atoms that were previously not detected. Because of the restricted coordination geometry of Au(I), the structure of the Au polymer $[Au(S\text{-}pyH)_2]_nCl$ (**3**) differs from the Cu and Ag structures described above. The Au(I) favors linear coordination geometry and therefore, S-pyHs are not bridging but acting as terminal ligands (Fig. 5). In the crystal structure of **3**, the cationic $[Au(S\text{-}pyH)_2]^+$ units are stacked together forming a linear chains with weak aurophilic contacts (Au···Au^{i}: 3.4277 (2) Å, i = x, −y + 1/2, z + 1/2, Fig. 5). The chain structure is further supported by weak π-π-interactions between the pyridyl rings. Despite the aurophilic and π-π interactions the chains of gold atoms are not perfectly linear (Au^{i}···Au···Au^{ii}: 162.21 (2)°, i = x, −y + 1/2, z + 1/2, ii = x, −y + 1/2, z−1/2). The asymmetric unit of **3** (Fig. 5) consist of two neutral S-pyH ligated to the Au center via the sulfur atom. The positive charge is compensated by the Cl$^-$ anion, which is hydrogen bonded to the NH hydrogens of the pyridyl rings (N2···Cl1^{iii}: 3.054 (5) Å, N1···Cl1^{iv}: 3.057 (6) Å, iii = −x + 1, y−1/2, −z + 1/2, −z, iv = −x, −y + 1, −z). The cationic nature of the gold complex is evident also according to positive polarization ESI-MS mass spectra, which display $[Au(S\text{-}pyH)_2]^+$ ion at *m/z* 419 as a single peak (Fig. 6).

3.4. Computational results

Computational QTAIM analysis [30] of the crystal structures suggested presence of the non-covalent M···M interactions only in Cu(I) (1) and Au(I) (3) polymers. The computational results are summarized in Table 3.

The QTAIM analysis of (**1**) confirmed the presence of nine bond critical points (BCPs) (3, −1) for Cu···Cu contacts in the copper polymer and the presence of four BCPs for Au···Au contacts in the gold chain (**3**), indicating attractive interactions between the metal centers. Surprisingly, no BCPs for Ag···Ag contacts could be found in Ag(I) polymer (**2**). In the case of **3**, low electron density, positive value of the Laplacian, and zero energy density at BCPs indicate typical non-covalent interactions, whereas in **1**, Cu···Cu metallophilic interactions already posses a noticeable degree covalent component (relatively high ρ(**r**), noticeably negative H_b value, $-G(\mathbf{r})/V(\mathbf{r}) < 1$ at the appropriate BCPs). We also estimated the interactions energies of the metal-metal contacts according to the procedures proposed by Espinosa et al. [34] and Vener et al. [35] The energies are in line with the QTAIM parameters indicating weak interactions in gold polymers (3.0–3.5 kcal/mol) and relatively stronger contacts in copper polymer (5.7–10.7 kcal/mol).

4. Summary

The 4-pyridinethiol was found to support linear chain structures of Cu(I) and Ag(I) and to serve as useful bridging ligand bringing metal centers to close proximity. Owing the restricted coordination geometry of Au(I), 4-pyridinethiol does not favor bridging coordination with gold. Instead, the cationic gold(I) complexes were stacked together forming non-covalent metallopolymer with weak aurophilic contacts. According to the QTAIM analysis, metal-metal interactions appear only in the Cu(I) and Au(I) polymers. No bond critical points were observed in the Ag(I) polymer despite the fact that the Ag···Ag distance is shorter than the sum of Bondi's van der Waals radii. One of the main advantages of 4-pyridinethiol ligand is possibility to change its protonation level by removal of the NH hydrogen. This allows adjusting the charge of the ligand that can be used to compensate the positive charge of metal centers. This, in turn, allows design of neutral or charged metallopolymers.

Acknowledgment

Financial support provided by the Magnus Ehrnrooth foundation (K.M) and Academy of Finland (M.H project no 139571, E.K project no's 284562 and 278743) as well as COST Action CM1302 are gratefully acknowledged. A.S.N is grateful to Russian Foundation for Basic Research for support (project No. 16-33-60063).

Appendix A. Supplementary data

Supplementary data related to this article can be found at http://dx.doi.org/10.1016/j.solidstatesciences.2016.08.005.

References

[1] a) J.-C. Eloi, L. Chabanne, G.R. Whittel, I. Manners, Mater. Today 22 (4) (2008) 28;
b) G.R. Whittel, M.D. Hager, U.S. Schubert, I. Manners, Nat. Mater. 10 (2011)

176;
c) G.R. Whittell, I. Manners, Adv. Mater. 19 (2007) 3439.
[2] a) S. Chardon-Noblat, P. Da Costa, A. Deronizer, M. Haukka, T.A. Pakkanen, R. Ziessel, J. Electroanal. Chem. 490 (2000) 62;
b) W.R. Hastings, M.C. Baird, Inorg. Chem. 25 (1986) 2913;
c) P. Hirva, M. Haukka, M. Jakonen, T.A. Pakkanen, Inorg. Chim. Acta 359 (2006) 853;
d) S. Chardon-Noblat, A. Deronizer, F. Hartl, J.V. Slageren, T. Mahabiersing, Eur. J. Inorg. Chem. (2001) 613;
e) E. Laurila, L. Oresmaa, M. Niskanen, P. Hirva, M. Haukka, Cryst. Growth Des. 10 (8) (2010) 3775;
f) E. Laurila, R. Tatikonda, P. Hirva, M. Haukka, CrystEngComm. 14 (2012) 8401;
g) E. Laurila, L. Oresmaa, J. Hassinen, P. Hirva, M. Haukka, Dalton Trans. 42 (2013) 395;
h) L. Koskinen, S. Jääskeläinen, L. Oresmaa, M. Haukka, CrystEngComm. 14 (2012) 3509;
i) B.J. Holliday, T.B. Stanford, T.M. Swager, Chem. Mater. 18 (2006) 5649.
[3] D. Knapton, S.J. Rowan, C. Weder, Macromolecules 39 (2006) 651.
[4] T.-L. Choi, K.-H. Lee, W.-J. Joo, S. Lee, T.-W. Lee, M.Y. Chae, J. Am. Chem. Soc. 129 (2007) 9842.
[5] N. Masciocchi, M. Moret, P. Cairati, F. Ragaini, A. Sironi, J. Chem. Soc. Chem. Commun. (1994) 189.
[6] a) Y. Zhou, X. Zhang, W. Chen, H. Qiu, J. Organomet. Chem. 693 (2008) 205;
b) Y.-Q. Jiao, G.-W. Lu, K. Zhao, Y. Chen, J.-H. Lan, C.-J. Shao, A.-J. Wang, P. Zhang, W.-S. Zhang, G.-G. Zhou, Q. Yang, M. Wang, J. Mol. Struct. 957 (2010) 1;
c) C.-M. Che, S.-W. Lai, Coord. Chem. Rev. 249 (2005) 1296;
d) C.-T. Chen, K.S. Suslick, Coord. Chem. Rev. 128 (1993) 293;
e) L.H. Doerrer, Dalton Trans. 39 (2010) 3543;
f) R.H. Ismayilov, W.-Z. Wang, G.-H. Lee, C.-Y. Yeh, S.-A. Hua, Y. Song, M.-M. Rohmer, M. Benard, S.-M. Peng, Angew. Chem. Int. Ed. 50 (2011) 2045;
g) J.-T. Sheu, C.-C. Lin, I. Chao, C.-C. Wang, S.-M. Peng, Chem. Commun. 3 (1996) 315;
h) E.-C. Yang, M.-C. Cheng, M.-S. Tsai, S.-M. Peng, J. Chem. Soc. Chem. Commun. (1994) 2377.
[7] a) H. Hartl, Angew. Chem. Int. Ed. 26 (1987) 927;
b) S.-E.-D.H. Etaiw, D.M. Abd El-Aziz, M.S. Ibrahim, I.A.S. Badr El-din, Polyhedron (2009) 1001;
c) L.F. Dahl, C.H. Wei, Inorg. Chem. 9 (1970) 1878.
[8] a) I.F. Taylor, M.S. Weininger, E.L. Amma, Inorg. Chem. 13 (1974) 2835;
b) E. Block, M. Gernon, H. Kang, G. Ofori-Okai, J. Zubieta, Inorg. Chem. 30 (1991) 1736;
c) A.A. Isab, S. Nawaz, M. Saleem, M. Altaf, M. Monim-ul-Mehboob, S. Ahmad, H.S. Evans, Polyhedron 29 (2010) 1251;
d) W. Su, M. Hong, J. Weng, Y. Liang, Y. Zhao, R. Cao, Z. Zhou, A.S.C. Chan, Inorg. Chim. Acta 331 (2002) 8;
e) J.-K. Cheng, Y.-G. Yao, J. Zhang, Z.-J. Li, Z.-W. Cai, X.-Y. Zhang, Z.-N. Chen, Y.-B. Chen, Y. Kang, Y.-Y. Qin, Y.-H. Wen, J. Am. Chem. Soc. 126 (25) (2004) 7796;
f) E. Jalilian, S. Lidin, J. Solid State Chem. 183 (2010) 2656;
g) H. Wang, R. Zhong, X.-Q. Guo, X.-Y. Feng, X.-F. Hou, Eur. J. Inorg. Chem. (2010) 174;
h) Y.-F. Han, Y.-J. Lin, W.-G. Jia, G.-X. Jin, J. Organomet. Chem. (2009) 2077;
i) S. Qin, Y. Ke, S. Lu, J. Li, X. Pei, X. Wu, W. Du, J. Mol. Struct. 689 (2004) 75.
[9] Z.-M. Hao, H.-P. Liu, H.-H. Han, W.-T. Wang, X.-M. Zhang, Inorg. Chem. Commun. 12 (2009) 375.
[10] K.S. Anjali, J.J. Vittal, P.A.W. Dean, Inorg. Chim. Acta 351 (2003) 79.
[11] H. Wang, R. Zhong, X.-G. Guo, X.-Y. Feng, X.-F. Hou, Eur. J. Inorg. Chem. 174 (2010).
[12] K.E. Neo, H.V. Huynh, L.L. Koh, W. Henderson, T.S.A. Hor, Dalton Trans. (2007) 5701.
[13] J. Wang, Y.-H. Zhang, H.-X. Li, Z.-J. Lin, M.-L. Tong, Cryst. Growth. Des. 7 (11) (2007) 2352.
[14] a) W. Paw, R.J. Lachicotte, R. Eisenberg, Inorg. Chem. 37 (16) (1998) 4139;
b) M. El-khateeb, K. Shawakfeh, M. Al-Btoosh, H. Görls, W. Weigand, Polyhedron 16 (1997) 3641.
[15] B.I. Kharisov, P.E. Martinez, V.M. Jimenez-Perez, O.V. Kharissova, B.N.M. Martinez, N. Perez, J. Coord. Chem. 63 (1) (2010) 1.
[16] a) S.-Q. Bai, L. Jiang, J.-L. Zuo, T.S.A. Hor, Dalton Trans. 42 (2013) 11319;
b) D.H. Brown, W.E. Smith, Chem. Soc. Rev. 9 (1980) 217;
c) C. Hinnen, K. Niki, J. Electroanal. Chem. 264 (1989) 157;
d) Y.-K. He, Z.-B. Han, Y. Ma, X.-D. Zhang, Inorg. Chem. Commun. 10 (2007) 829;
e) A.B. Lago, R. Carballo, O. Fabelo, N. Fernandez-Hermida, F. Lloret, E.M. Vazquez-Lopez, Cryst. Eng. Commun. 15 (2013) 10550;
f) G.K. Kole, K.V. Vivekananda, M. Kumar, R. Ganguly, S. Dey, V.K. Jain, Cryst. Eng. Commun. 17 (2015) 4367.
[17] a) J. El-Bahraoui, J. Mol. Struct. 493 (1999) 249;
b) M.M. Alam, E. Fromager, Chem. Phys. Lett. 554 (2012) 37;
c) H.L. Hermann, G. Boche, P. Schwerdtfeger, Chem. Eur. J. 7 (2001) 5333;
d) B. Assadollahzadeh, P. Schwerdtfeger, Chem. Phys. Lett. 462 (2008) 222;
e) F.A. Cotton, X. Feng, D.J. Timmons, Inorg. Chem. 37 (1998) 4066;
f) D.E. Harwell, M.D. Mortimer, C.B. Knobler, F.A.L. Anet, M.F. Hawthorne, J. Am. Chem. Soc. 118 (1996) 2679;
g) P.D. Harvey, Coord. Chem. Rev. 153 (1996) 175.
[18] M.M. Alam, E. Fromager, Chem. Phys. Lett. 554 (2012) 37.
[19] C.-M. Che, S.-W. Lai, Coord. Chem. Rev. 249 (2005) 1296.
[20] Agilent, CrysAlisPro, Agilent Technologies Inc, Yarnton, Oxfordshire, England, 2013.
[21] Z. Otwinowski, W. Minor, Processing of X-Ray diffraction data collected in oscillation mode, in: C.W. Carter, J. Sweet (Eds.), Methods in Enzymology, Volume 276, Macromolecular Crystallography, Part AAcademic Press, New York, 1997, pp. 307–326.
[22] L. Palatinus, G. Chapuis, J. Appl. Cryst. 40 (2007) 786–790.
[23] G.M. Sheldrick, Acta Cryst. A64 (2008) 112–122.
[24] G.M. Sheldrick, SADABS - Bruker AXS Scaling and Absorption Correction, Bruker AXS, Inc., Madison, Wisconsin, USA, 2012.
[25] O.V. Dolomanov, L.J. Bourhis, R.J. Gildea, J.A.K. Howard, H. Puschmann, J. Appl. Cryst. 42 (2009) 339–341.
[26] C.B. Hübschle, G.M. Sheldrick, B. Dittrich, J. Appl. Cryst. 44 (2011) 1281–1284.
[27] Y. Zhao, D.G. Truhlar, Theor. Chem. Acc. 120 (2008) 215.
[28] M.J. Frisch, G.W. Trucks, H.B. Schlegel, G.E. Scuseria, M.A. Robb, J.R. Cheeseman, G. Scalmani, V. Barone, B. Mennucci, G.A. Petersson, H. Nakatsuji, M. Caricato, X. Li, H.P. Hratchian, A.F. Izmaylov, J. Bloino, G. Zheng, J.L. Sonnenberg, M. Hada, M. Ehara, K. Toyota, R. Fukuda, J. Hasegawa, M. Ishida, T. Nakajima, Y. Honda, O. Kitao, H. Nakai, T. Vreven, J.A. Montgomery Jr., J.E. Peralta, F. Ogliaro, M. Bearpark, J.J. Heyd, E. Brothers, K.N. Kudin, V.N. Staroverov, T. Keith, R. Kobayashi, J. Normand, K. Raghavachari, A. Rendell, J.C. Burant, S.S. Iyengar, J. Tomasi, M. Cossi, N. Rega, J.M. Millam, M. Klene, J.E. Knox, J.B. Cross, V. Bakken, C. Adamo, J. Jaramillo, R. Gomperts, R.E. Stratmann, O. Yazyev, A.J. Austin, R. Cammi, C. Pomelli, J.W. Ochterski, R.L. Martin, K. Morokuma, V.G. Zakrzewski, G.A. Voth, P. Salvador, J.J. Dannenberg, S. Dapprich, A.D. Daniels, O. Farkas, J.B. Foresman, J.V. Ortiz, J. Cioslowski, D.J. Fox, Gaussian 09, Revision D.01, Gaussian, Inc., Wallingford CT, 2013.
[29] a) C.L. Barros, P.J.P. de Oliveira, F.E. Jorge, A. Canal Neto, M. Campos, Mol. Phys. 108 (2010) 1965;
b) F.E. Jorge, A. Canal Neto, G.G. Camiletti, S.F. Machado, J. Chem. Phys. 130 (2009) 064108;
c) A. Canal Neto, F.E. Jorge, Chem. Phys. Lett. 582 (2013) 158.
[30] R.F.W. Bader, Atoms in Molecules: a Quantum Theory, Oxford University Press, Oxford, 1990.
[31] T. Lu, F.W. Chen, J. Comput. Chem. 33 (2012) 580.
[32] S. Bianketti, A.J. Blake, C. Wilson, P. Hubberstey, N.R. Champess, M. Schröder, Cryst. Eng. Commun. 11 (2009) 763.
[33] M.T. Räisänen, N. Runeberg, M. Klinga, M. Nieger, M. Bolte, P. Pyykkö, M. Leskelä, T. Repo, Inorg. Chem. 46 (2007) 9954.
[34] E. Espinosa, E. Molins, C. Lecomte, Chem. Phys. Lett. 285 (1998) 170.
[35] M.V. Vener, A.N. Egorova, A.V. Churakov, V.G. Tsirelson, J. Comput. Chem. 33 (2012) 2303.

II

SELF-ASSEMBLY OF SQUARE PLANAR RHODIUM CAR BONYL COMPLEXES WITH 4,4-DISUBSTITUTED-2,2'-BIPYRI DINE LIGANDS

by

Kalle Kolari, Elina Laurila, Maria Chernysheva, Pipsa Hirva, & Matti Haukka, 2020

Solid State Sci., **2020**, *10*, 106103.

Solid State Sciences 100 (2020) 106103

Contents lists available at ScienceDirect

Solid State Sciences

journal homepage: http://www.elsevier.com/locate/ssscie

Self-assembly of square planar rhodium carbonyl complexes with 4,4-disubstituted-2,2′-bipyridine ligands

Kalle Kolari [a], Elina Laurila [a], Maria Chernysheva [a], Pipsa Hirva [b], Matti Haukka [a,*]

[a] University of Jyväskylä, Department of Chemistry, P.O Box 35, FI-40014, University of Jyvaskyla, Finland
[b] University of Eastern Finland, Department of Chemistry, P.O.Box 111, FI-80101, Joensuu, Finland

ARTICLE INFO

Keywords:
Rhodium
Bipyridine
Carbonyl
Reductive carbonylation
Metallophilicity

ABSTRACT

The impact of non-covalent interactions and reaction conditions on formation and self-assembly of ionic pairs of Rh complexes with 4,4′-disubstituted bipyridine ligands $([Rh(L1)(CO)_2][Rh(CO)_2Cl_2])_n$ **(1)**, $[Rh(L1)_2Cl_2][Rh(CO)_2Cl_2]$ **(2)**, $([Rh(L1)(CO)_2][Rh(CO)_2Cl_2][Rh(L1)(CO)_2]_n([Rh(CO)_2(Cl)_2])_n)$ **(3)**, $([Rh(L2)CO_2]$ $[Rh(CO)_2Cl_2])_n$·EtOH **(4)**, $([Rh(L2)(CO)_2])_n$ $([Rh(CO)_2Cl_2])_n$ **(5)** (L1 = 4,4′-dimethyl-2,2′-bipyridine, L2 = 4,4′-diamine-2,2′-bipyridine) have been studied. Packing of square planar Rh complexes favor formation of one-dimensional chains. In structure **1**, the polymeric chain is formed by the alternating cationic $[Rh(L1)(CO)_2]^+$ and the anionic $[Rh(CO)_2Cl_2]^-$ units leading to a neutral pseudo linear 1D chain with metallophilic contacts. In compound **2**, the square planar $[Rh(CO)_2Cl_2]^-$ anions form only dinuclear anion pairs instead of polymeric chains. Structure **3** consists of an alternative arrangement of cations and anions compared to **1**, the repeating sequence of ions being $[Rh(L1)(CO)_2]^+[Rh(CO)_2Cl_2]^-[Rh(L1)(CO)_2]^+$. The overall positive charge is balanced by outlying $[Rh(CO)_2Cl_2]^-$ counterion. In structures **4** and **5**, only the cationic $[Rh(L2)(CO)_2]^+$ units are involved in formation of the polymeric chains and the positive charge of the chain is balanced by the $[Rh(CO)_2Cl_2]^-$ (**4** and **5**). In structures **1** and **3** the metallophilic interactions have an important role in chain formation. In **4** and **5**, the arrangement of the square planar building blocks is dominated by the hydrogen bonding between the NH_2-substituents of the bipyridine ligand and the chlorides of the anion or solvent of crystallization.

1. Introduction

Supramolecular self-assembly [1,2] is defined as a process where molecular entities are aggregated via reversible [3] non-covalent interactions [4,5] such as π-stacking [6], electrostatic interactions [7], halogen bonding [8], hydrogen [9] bonding and metallophilic interactions [10,11]. Hydrogen bonding is classified as a directional and notable non-covalent interaction in strength [12] and has been widely utilized in crystal engineering [13]. Preparation of organic non-covalent polymers from diamidopyridines and uracil derivatives is an early example of systematic utilization of hydrogen bonding in self-assembly of molecules [10,14]. Similar strategy by modulating the secondary coordination sphere [15] *via* hydrogen bonding has been implemented to self-assembly of discrete metal complexes to form from one-dimensional metallopolymers [9,16–19] to metal-organic frameworks [20–22]. Due to reversibility and the dynamic nature of the hydrogen bond interactions between monomers these polymeric compounds express the variety of properties [23]. Closely related halogen bonds have also been used to link metal complexes into extended polymeric structures [24,25]. It has been shown that halogen bonds can also be used to fine-tune the properties of metal complexes [26]. In the case of square planar metal complexes, metallophilic interactions or metal-π-interactions provide alternative non-covalent tools that can be utilized in building extended structures, especially linear chain compounds [10,11]. It is established that square-planar monomeric units will self-assemble *via* d_z^2-orbital overlap of d^8 metal centers whereas in d^{10} metal ions interactions occur *via* $d_{x^2-y^2}^{22}$ [27,28]. Magnus green salts and Krogman salts are classic examples of metallophilic Pt and Pd chain structures [29,30]. However, metallophilicity is known to occur in a range of metal compounds including iridium and rhodium chains, known as iridium and rhodium blues [31]. Metallophilic contacts have been used for example, to generate semiconductive crystalline materials [30]. Similar chain-like structures have also been obtained with square planar rhodium complexes [10,11]. In these systems intermetallic contacts have an impact on the photophysical properties of the polymeric chains.

* Corresponding author.
E-mail address: matti.o.haukka@jyu.fi (M. Haukka).

https://doi.org/10.1016/j.solidstatesciences.2019.106103
Received 21 June 2019; Received in revised form 17 October 2019; Accepted 23 December 2019
Available online 26 December 2019

Derivatives of 2,2′-bipyridine are commonly used as chelating ligands in coordination chemistry. These types of ligands are able to form strongly coordinated and nearly planar groups, which makes them useful especially for building extended stacks of square planar metal complexes [10,11,32,33]. By decorating the polypyridine ligand with suitable substituents, such ligand can be used for changing the electronic properties of the metal complex as well as supporting secondary non-covalent contacts in the supramolecular assemblies for example *via* π-interactions or *via* hydrogen bonds. Complexes with disubstituted-2,2′-bipyridine ligands containing hydrogen bond donor/acceptor substituents such as hydroxyl [34,35] amino [36], dicarboxylic acid [37], hydroxymethyl [38], hydroxyl [39], and pyrrole [40] groups 4,4′-disubstituted ligands, metal complexes have been used to assemble extended hydrogen bonding networks with co-crystallants [34,35,41] or solvent of crystallization [42].

In the current paper we have investigated the impact of metallophilic interactions, hydrogen bonds, metal-π-interactions and Coulombic interactions as well as the influence of reaction conditions in formation of supramolecular assemblies of square planar pairs of cationic and anionic Rh-complexes $[Rh(L1)(CO)_2]/[Rh(CO)_2Cl_2]$ and $[Rh(L2)(CO)_2]/[Rh(CO)_2Cl_2]$ (Scheme 1).

2. Experimental section

All reagents were used as received. Ethanol solvent (95%) was purchased from Altia Oy, 4,4′-dimethyl-2,2′-bipyridine (99%) from Sigma-Aldrich, and 4,4′-diamino-2,2′-bipyridine (>97%) from Carbosynth. The rhodium reagent was obtained from Alfa Aesar and its Rh content was 38–41%. The reduction gas carbon monoxide (100%) was obtained from AGA. All reductive carbonylation syntheses were performed in 100 mL Berghof autoclaves equipped with PTFE liner. IR-spectrum were recorded with the Bruker Alpha spectrometer with the ATR platinum diamond compartment. Elemental analyses were carried out with Elementar Vario EL III analyzer.

2.1. Crystal structure determination

The crystals of **1** — **5** were immersed in cryo-oil, mounted in a MiTeGen loop and measured at 100–200 K. The X-ray diffraction data were collected on a Rigaku Oxford Diffraction Supernova diffractometer using Mo Kα radiation (λ = 0.70173 Å, compounds 1 and 2) or Cu Kα (λ = 1.54184 Å, compounds 3–5). The CrysAlisPro [43] program package was used for cell refinements and data reductions. The structures were solved by charge flipping (SUPERFLIP) [44] or intrinsic phasing method (SHELXT) [45]. An analytical, gaussian or multi-scan absorption corrections (CrysAlisPro [43]) were applied to all data. Structural refinements were carried out using SHELXL [45] with the Olex 2 [46] and SHELXLE [47] graphical user interfaces. The ethanol of crystallization in **5** was disordered resulting in high anisotropic displacement parameters. However, no disorder model was applied to the solvent molecules during the final refinement. In **5** the NH_2 hydrogen atoms were located from the difference Fourier map and refined isotropically. The OH hydrogen atoms in **4** were located from the difference Fourier map but constrained to ride on their parent oxygen with $U_{iso} = 1.5 \cdot U_{eq}$ (parent atom). Other hydrogen atoms were positioned geometrically and constrained to ride on their parent atoms, with C–H = 0.95–0.98 Å, N–H = 0.88 Å, and $U_{iso} = 1.2–1.5 \cdot U_{eq}$ (parent atom). The crystallographic details are summarized in Table 1.

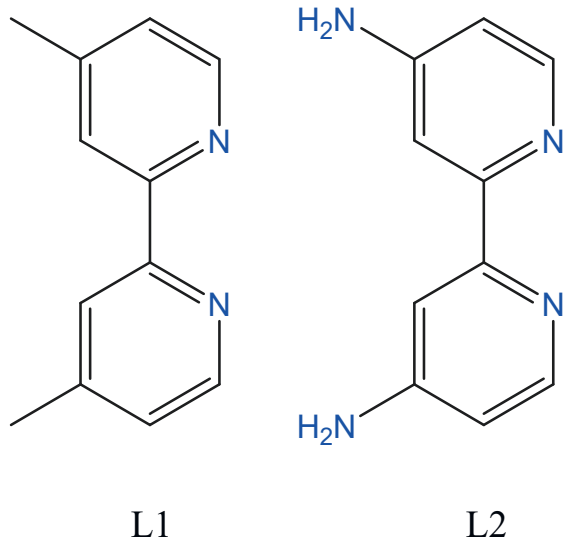

Scheme 1. Schematic presentation of the substituted bipyridine ligands 4,4′-dimethyl-2,2′-bipyridine (L1) and 4,4′-diamino-2,2′-bipyridine (L2).

2.2. Syntheses

2.2.1. Compounds *1* and *2*

A mixture of $RhCl_3 \cdot xH_2O$ (50 mg, 0.2 mmol), 4,4′-dimethyl-2,2′-bipyridine (L1) (20 mg, 0.1 mmol) and 2 mL of ethanol were placed into a Berghof autoclave with PTFE liner. Mixture was stirred for 15 min and then of 2 mL of ethanol was added. The autoclave was pressurized with CO gas to 50 bar and heated at 125 °C for 72 h. After reaction, the autoclave was ramped down with two steps. The first temperature was decreased 10 °C/h for 7 h. Then starting from 55 °C cooling rate was increased to 15 °C/h until room temperature was reached. The orange, crystalline product of $[Rh(L1)(CO)_2]$ $[Rh(CO)_2Cl_2]$ **(1)** (17 mg, 24%) was filtered off and dried in the air overnight. X-Ray quality crystalline material was collected directly from the reaction solution after cooling and no separate crystallization steps were used. Despite drying, the bulk material contained some moisture, which was confirmed by IR-spectroscopy. Elemental analysis for $[Rh(L1)(CO)_2]$ $[Rh(CO)_2Cl_2] \cdot H_2O$ **(1)**: calculated C: 32.52%, H: 2.39% and N: 4.74% found C: 32.22% H: 2.13% and N: 4.56%. IR ν(ATR)/cm-1: 1966 and 1987 (ν(CO), the anionic unit), 2021 and 2067 (ν(CO), the cationic unit). In addition to **1**, few yellow crystals of $[Rh(L1)_2Cl_2][Rh(CO)_2Cl_2]$ were obtained as a side product **(2)**.

2.2.2. Compound *3*

Modification of reaction time and vessel cooldown yielded a few dark orange-red crystals of $[Rh(L1)(CO)_2][Rh(CO)_2Cl_2] \cdot EtOH$ **(3)**. This crystalline material was obtained in 72h reaction and upon cooling reaction vessel first in powered off heating system for 2 h and then in ice bath for additional 2 h. X-Ray quality crystalline material was collected directly from the reaction solution after cooling and no separate crystallization steps were used. Even with fast cooling the compound **1** was the dominating product and compound **3** was obtained only as a minor product. No further analysis of **3** could be carried out due to the low yield of **3**.

2.2.3. Compounds *4* and *5*

Synthesis was performed following similar procedure as in the case of **1** with slight modifications. The amounts of 0.2 mmol (50 mg) of $RhCl_3 \cdot xH_2O$ and 0.1 mmol (21 mg) of 4,4′-diamino-2,2′-bipyridine (L2) was stirred in 2 mL of ethanol for 15 min. Then 2 mL of ethanol was added into the mixture. The autoclave was pressurized with CO gas to 50 bar and heated at 125 °C for 20 h. Again, the reaction vessel was allowed to cool down in two steps (from 125 °C to 65 °C with the cooling rate of 10 °C/h and from 65 °C to room temperature with cooling rate of 15 °C/h). The yellow crystals (11 mg, 75%) with metallic luster were filtered off and dried in the air overnight. Single-crystal X-Ray

Table 1
Crystal data.

	1	2	3	4	5
empirical formula	$C_{16}H_{12}Cl_2N_2O_4Rh_2$	$C_{26}H_{24}Cl_4N_4O_2$ Rh_2	$C_{16}H_{12}Cl_2N_2O_4Rh_2$	$C_{14}H_{10}Cl_2N_4O_4Rh_2$	$C_{32}H_{32}Cl_4N_8O_{10}Rh_4$
fw	573.00	772.11	573.00	574.98	1242.09
temp (K)	120(2)	120(2)	200(2)	100(2)	120(2)
λ(Å)	0.71073	0.71073	1.54184	1.54184	1.54184
cryst syst	Triclinic	Triclinic	Monoclinic	Monoclinic	Triclinic
space group	P-1	P-1	*C*2/*c*	$P2_1/c$	P-1
a (Å)	6.73607(15)	7.8652(2)	10.2239(5)	6.65090(11)	6.7517(5)
b (Å)	6.1636(3)	12.1823(3)	17.6662(11)	23.3367(4)	15.8847(9)
c (Å)	17.6273(3)	16.4622(5)	42.6639(17)	12.01598(18)	20.7118(9)
α(°)	97.2875(14)	100.175(2)	90	90	72.782(5)
β(°)	94.0227(16)	102.055(3)	92.484(5)	99.3009(15)	85.895(5)
γ(°)	97.4129(17)	105.096(3)	90	90	78.957(6)
V (Å^3)	1880.51(6)	1444.04(8)	7698.6(7)	1840.48(5)	2082.2(2)
Z	4	2	16	4	2
ρ_{calc} (Mg/m^3)	2.024	1.776	1.977	2.075	1.981
μ(Kα) (mm^{-1})	2.063	1.544	16.645	17.442	15.511
No. reflns.	67614	23622	12999	21392	13765
Unique reflns.	19097	7466	7771	3883	8392
GOOF (F^2)	1.073	1.032	1.027	1.062	1.041
R_{int}	0.0530	0.0427	0.0554	0.0239	0.0659
R1[a] ($I \geq 2\sigma$)	0.0364	0.0351	0.0638	0.0205	0.0694
w*R*2[b] ($I \geq 2\sigma$)	0.0792	0.0671	0.1608	0.0493	0.1815

[a] $R1 = \Sigma||F_o| - |F_c||/\Sigma|F_o|$.
[b] $wR2 = [\Sigma[w(F_o^2 - F_c^2)^2]/\Sigma[w(F_o^2)^2]]^{1/2}$.

diffraction showed that the crystals of **5** contained ethanol of crystallization. However, the bulk samples used for elemental analysis contained only some moisture matching with [Rh(L2)(CO)$_2$] [Rh(CO)$_2$Cl$_2$]·H$_2$O. Presence of moisture was confirmed by IR-spectroscopy. Calculated: C: 28.36%, H: 2.04% and N: 9.45% found C: 28.64%, H: 1.99%, and N: 9.76%. IR ν (ATR)/cm-1: 2016 and 2017 (ν(CO), the cationic unit), 1983 (ν(CO), the anionic unit). When the reaction mixture was cooled down in a similar way as in the case of **2**, few orange crystals of solvent free [Rh(L2)(CO)$_2$][Rh(CO)$_2$Cl$_2$] **(4)** were obtained. The crystalline product **5** was found to be unstable compared to compound **4** without solvent of crystallization at the ambient conditions due to the slow loss of solvent of crystallization. Again, X-Ray quality crystalline material was collected directly from the reaction solution after cooling and no separate crystallization steps were used.

3. Results and discussion

All syntheses were performed as a one-pot reductive carbonylation of $RhCl_3$ in the presence of the bipyridine ligands in ethanol. With 4,4′-dimethyl-2,2′-bipyridine (L1) linear arrangement of the reduced alternating cationic and anionic square planar Rh-units was preferred (Fig. 1).

The crystal structure of **1** contained two independent cation-anion chains (A and B in Fig. 1) with metallophilic contacts between the Rh-atoms. The Rh···Rh distances varied between 3.3581(2) Å and 3.4172 (2) Å. Both chains were nearly linear with Rh···Rh···Rh angles of 169.977(7)° Å and 166.031(8)° respectively (Fig. 1). The structures resemble closely the previously reported cation-anion chains of [Rh(bpy)(CO)$_2$][Rh(CO)$_2$Cl$_2$] [11], indicating that the methyl substituents on 4,4′- positions on the bipyridine ligands did not have significant impact on stacking cationic and anionic units. However, the shortest intermetallic distance of 3.3174(5) Å, found in [Rh(bpy)(CO)$_2$][Rh(CO)$_2$Cl$_2$], is somewhat shorter than the corresponding distance in **1**. Just like the [Rh(bpy)(CO)$_2$][Rh(CO)$_2$Cl$_2$] crystals, also the crystals of **1** had metallic luster indicating the existence of continuous metal-metal contacts. In addition to polymeric chain structures, few crystals of [Rh

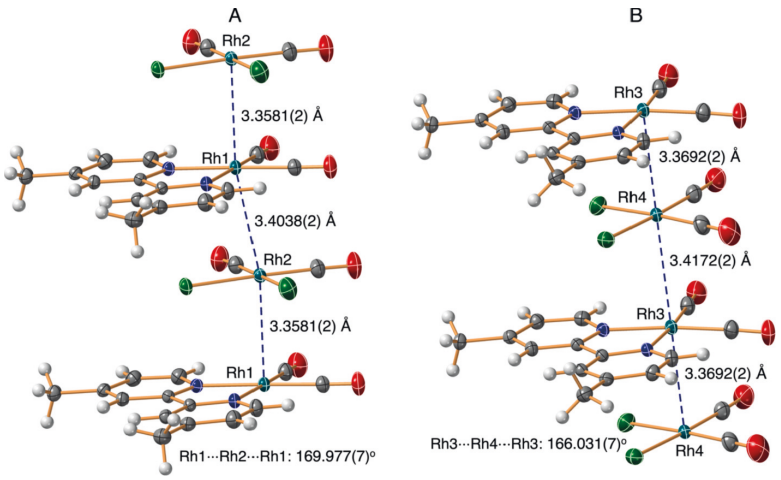

Fig. 1. The two crystallographically independent cation-anion chains, A and B, in **1**.

$(L1)_2Cl_2][Rh(CO)_2Cl_2]$ (**2**) ion pairs (Fig. 2) were also obtained in all reactions as a minor side product. It shows that even if the reaction was carried out under 50 bar CO pressure and the reaction time was 72 h, the reduction of $RhCl_3$ was not complete. In **2**, the square planar $[Rh(CO)_2Cl_2]^-$ anions did form stacked pairs with long Rh···Rh distances (3.9729(5) Å) but not continuous chains (Fig. 2).

The reduction process and the arrangement on the reduced products in crystals were strongly dependent on reaction conditions. The chain compound **1** was obtained only when the reaction solution was cooled down slowly from the reaction temperature of 125 °C to room temperature. If the reaction solution was cooled down rapidly (see the experimental section) the arrangement of Rh-complexes was changed (Fig. 3). Instead of having regular cation-anion chains, the obtained crystalline product consisted of chains with repeating trinuclear cation-anion-cation units with metallophilic contacts between the Rh centers. The positive charge of the repeating trinuclear units were balanced by the $[Rh(CO)_2Cl_2]^-$ anions which were not part of the main chain. The anions formed again stacked pairs with relatively long Rh···Rh contacts of 3.6198(17) Å and interactions between the anionic units are weak (Fig. 3).

The arrangement of ions in **3** is somewhat unusual. Typically, cationic chains consist only of cationic units. The counter anions are then simply balancing the charge as separated anions. In **3** the cationic repeating trinuclear unit Rh1···Rh2···Rh3 contains two square planar cations and one counter anion giving a net charge of +1 to the trinuclear unit. Despite the unusual order of charged building blocks the metal-metal distances in the repeating trinuclear units are comparable with the metal-metal distances in typical metallophilic Rh-chains [45]. The metal-metal distance between the repeating trinuclear units is clearly longer (3.960(13) Å) than the intermetallic distance within the trinuclear unit (3.2299(12) - 3.2798(11)Å) indicating lack of significant metallophilic contacts between the repeating trinuclear units. The separate counter anions in **3** formed dinuclear entities in the crystalline state with the Rh···Rh distance of 3.6198(17) Å. Such a distance is only slightly longer than those reported in the literature for typical anionic dinuclear or polymeric $[Rh(CO)_2Cl_2]^-$ -systems [46–48]. The possible metallophilic interaction between the $[Rh(CO)_2Cl_2]^-$ anions is expected to be at most weak. The directing effect of the metal-metal interactions and formation of metallophilic cation-anion chains seems to be favored by a slow crystallization process. In fast crystallization non-directional coulombic forces and weaker van der Waals interactions start to have a significant role in arranging ionic complexes.

The NH_2 substituent (L2) is not only a stronger electron donor compared to CH_3 -group (L1) but also a good H-bond donor. When the Me-substituted bipyridine was replaced with NH_2-substituted bipyridine, formation of hydrogen bonds favored purely cationic chains

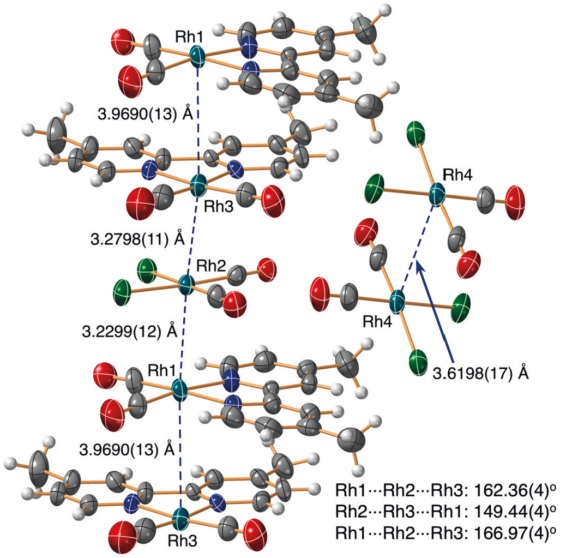

Fig. 3. The chains structure of **3**.

(Figs. 4 and 5). The hydrogen bonding between the chlorido ligands of the anion became the dominating directional force instead of the metallophilicity pushing the anions away from the chain structure (Fig. 4). The steric hindrance affected the arrangement of the cations and instead of metallophilic contacts. Due to the hydrogen bonds the bipyridine ligands of the cationic units are now facing opposite directions and the cation chain is formed *via* metal- π-interactions.

Because of the good H-bond properties of the cations with NH_2-substituted bipyridine ligands, solvent of crystallization had also an important role in the arrangement of ionic units in crystalline state. A strong H-bond acceptor/donor, such as ethanol, could replace the weaker NH···Cl contacts with stronger NH···O and OH···Cl interactions. This pushed the anions further away from the cations allowing the cations to approach differently compare to structure **4**. Now the Rh centers in **5** are nearly linearly aligned and they do form weak metal-metal contacts throughout the crystal (Fig. 5).

4. Conclusions

The organization of the cation/anion pairs of [Rh(4,4′-dimethyl-2,2′-

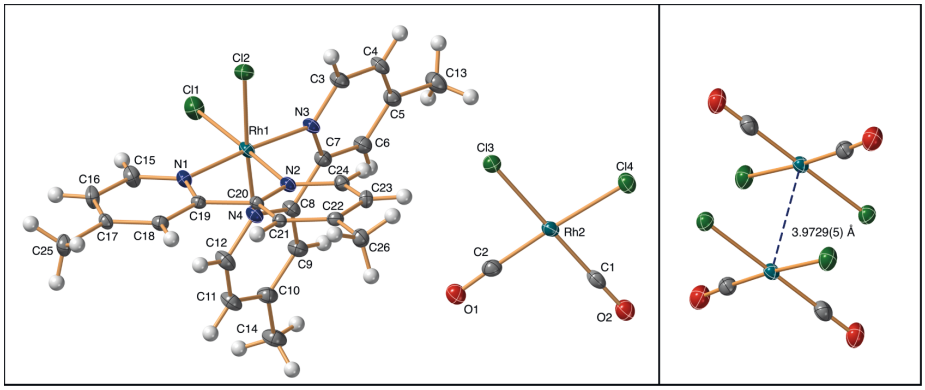

Fig. 2. Left: the asymmetric unit of $[Rh(L1)_2Cl_2][Rh(CO)_2Cl_2]$ **(2)**. Right: The stacked anion pairs in **2**.

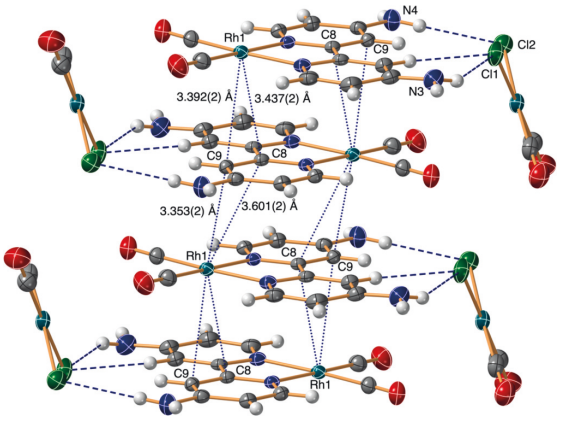

Fig. 4. The chain structure of **4**. Heavy atom distances in selected H-bonds: N3···Cl1#1: 3.669(3) Å, N3···Cl1#2: 3.272(2) Å, N4···Cl2#1: 3.333(2) Å, C9···Cl1#2: 4.044(2) Å. Symmetry transformations used to generate equivalent atoms: #1: x+1, -y+1, -z+2, #2: x+1, y+1/2, -z+3/2).

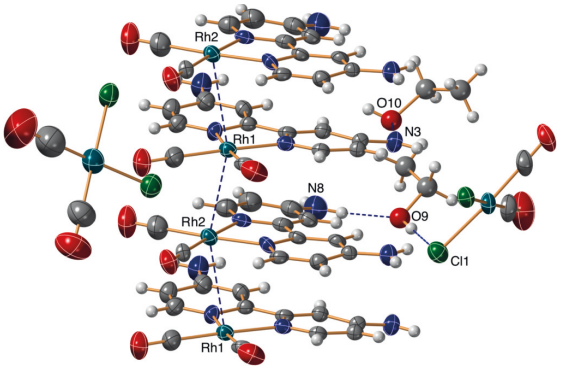

Fig. 5. The chain structure of **5**. Rh1···Rh2: 3.5216(10) Å. Rh1···Rh2#1: 3.3840(10) Å, Rh2#1···Rh1···Rh2: 155.76(3)°. Heavy atom distances in selected H-bonds: N3···O10: 2.80(2) Å, N8···O9: 2.83(3) Å, O9···Cl1: 3.167 (18) Å.

bipyridine)$(CO)_2$]/[Rh $(CO)_2Cl_2$] and [Rh(4,4′-diamine-2,2′-bipyridine) $(CO)_2$]/[Rh$(CO)_2Cl_2$] depend on the interplay between various directional and non-directional non-covalent interactions. In general, the square planar structure of the Rh(I) ions tends to favor stacking of these ionic molecules. In the case of [Rh(4,4′-dimethyl-2,2′-bipyridine) $(CO)_2$]/[Rh$(CO)_2Cl_2$] system, the metallophilic interactions are favoring linear stacks with alternating cations and anions in slow crystallizations. The stacks are further supported by Coulombic forces. In fast crystallizations the non-directional Coulombic forces and other weak van der Waals forces reduces the directing role of the metal-metal interactions. When the 4,4′-dimethyl-2,2′-bipyridine ligand is replaced with a much better H-bond donor ligand 4,4′-diamine-2,2′-bipyridine, hydrogen bonding takes the dominating role in the arrangement of the molecular units. Hydrogen bond formation between the cation and anion leads to linear stacks where the cationic units are facing opposite direction. This prevents sterically the metal-metal contacts and they are replaced with metal-π-interactions. Simultaneously, the anions are pushed away from the chain structure. The solvent of crystallization may also have a strong impact on the arrangement of ionic units. Presence of a good H-bond acceptor/donor, such as ethanol, may replace the hydrogen bonds between the cation and anion with cation-solvent contacts. In such a case the anions may be pushed even further away from the cation stacks allowing metal-metal interactions and aligned stacking of the cationic units. All in all, design of a supramolecular systems is challenging. To be able to fabricate predictable structures requires that all significant interactions must be considered as the potential directing forces.

Declaration of competing interest

There are no interests to declare.

Acknowledgment

Financial support of Magnus Ehrnrooth foundation (K.K), Academy of Finland, project no. 295581 (M H) as well as the European Network on Smart Inorganic Polymers (SIPs) COST CM1302 project.

Supporting information

CCDC 1935018–1935022 contain the crystallographic data for **1**–**5**, respectively. These data can be obtained free of charge via http://www.ccdc.cam.ac.uk/cgi-bin/catreq.cgi, or from the Cambridge Crystallographic Data Centre, 12 Union Road, Cambridge CB2 1EZ, UK; fax: (+44) 1223 336 033; or e-mail: deposit@ccdc.cam.ac.uk.

References

[1] K.C. Bentz, S.M. Cohen, Supramolecular metallopolymers: from linear materials to infinite networks, Angew. Chem. Int. Ed. 57 (2018) 14992–15001, https://doi.org/10.1002/anie.201806912.
[2] L. Yang, X. Tan, Z. Wang, X. Zhang, Supramolecular polymers: historical development, preparation, characterization, and functions, Chem. Rev. 115 (2015) 7196–7239, https://doi.org/10.1021/cr500633b.
[3] M. Schmittel, K. Mahata, Diversity and complexity through reversible multiple orthogonal interactions in multicomponent assemblies, Angew. Chem. Int. Ed. 47 (2008) 5284–5286, https://doi.org/10.1002/anie.200800583.
[4] T. Aida, E.W. Meijer, S.I. Stupp, Functional supramolecular polymers, Science 80 (2012) 335, https://doi.org/10.1126/science.1205962, 813 LP – 817.
[5] P. Xing, Y. Zhao, Multifunctional nanoparticles self-assembled from small organic building blocks for biomedicine, Adv. Mater. 28 (2016) 7304–7339, https://doi.org/10.1002/adma.201600906.
[6] W.-H. Wu, M.-J. Huang, Q. Zeng, W.-R. Xian, W.-M. Liao, J. He, Electrical and magnetic properties of a radical-based Co(II) coordination complex with CH···π and π···π supramolecular interactions, Inorg. Chem. Commun. 103 (2019) 149–153, https://doi.org/10.1016/j.inoche.2019.03.022.
[7] R.O. Fuller, C.S. Griffith, G.A. Koutsantonis, K.M. Lapere, B.W. Skelton, M. A. Spackman, A.H. White, D.A. Wild, Supramolecular interactions between hexabromoethane and cyclopentadienyl ruthenium bromides: halogen bonding or electrostatic organisation? CrystEngComm 14 (2012) 804–811, https://doi.org/10.1039/C1CE05438D.
[8] B. Li, S.-Q. Zang, L.-Y. Wang, T.C.W. Mak, Halogen bonding: a powerful, emerging tool for constructing high-dimensional metal-containing supramolecular networks, Coord. Chem. Rev. 308 (2016) 1–21, https://doi.org/10.1016/j.ccr.2015.09.005.
[9] C.S.A. Fraser, D.J. Eisler, R.J. Puddephatt, Self-assembly of organometallic polymers through hydrogen bonding: a diplatinum(IV) complex with a single bridging halide ligand, Polyhedron 25 (2006) 266–270, https://doi.org/10.1016/j.poly.2005.08.020.
[10] E. Laurila, R. Tatikonda, L. Oresmaa, P. Hirva, M. Haukka, Metallophilic interactions in stacked dinuclear rhodium 2,2′-biimidazole carbonyl complexes, CrystEngComm 14 (2012) 8401–8408, https://doi.org/10.1039/c2ce25385b.
[11] E. Laurila, L. Oresmaa, J. Hassinen, P. Hirva, M. Haukka, Neutral one-dimensional metal chains consisting of alternating anionic and cationic rhodium complexes, Dalton Trans. 42 (2013) 395–398, https://doi.org/10.1039/c2dt31671d.
[12] M. Tadokoro, K. Nakasuji, Hydrogen bonded 2,2′-biimidazolate transition metal complexes as a tool of crystal engineering, Coord. Chem. Rev. 198 (2000) 205–218, https://doi.org/10.1016/S0010-8545(99)00223-4.
[13] B. Moulton, M.J. Zaworotko, From molecules to crystal Engineering: supramolecular isomerism and polymorphism in network solids, Chem. Rev. 101 (2001) 1629–1658, https://doi.org/10.1021/cr9900432.
[14] C. Fouquey, J.-M. Lehn, A.-M. Levelut, Molecular recognition directed self-assembly of supramolecular liquid crystalline polymers from complementary chiral components, Adv. Mater. 2 (1990) 254–257, https://doi.org/10.1002/adma.19900020506.
[15] S.A. Cook, A.S. Borovik, Molecular designs for controlling the local environments around metal ions, Acc. Chem. Res. 48 (2015) 2407–2414, https://doi.org/10.1021/acs.accounts.5b00212.
[16] B. Soltani, H. Nabipour, J.T. Engle, C.J. Ziegler, π···π and hydrogen bonding interactions in the crystal structure of trans-dichloro-tetrakis(1H-indazole-N2)-

nickel(II), Mater. Today Proc. 5 (2018) 15845–15851, https://doi.org/10.1016/j.matpr.2018.05.083.
[17] K. Chkirate, S. Fettach, K. Karrouchi, N.K. Sebbar, E.M. Essassi, J.T. Mague, S. Radi, M. El Abbes Faouzi, N.N. Adarsh, Y. Garcia, Novel Co(II) and Cu(II) coordination complexes constructed from pyrazole-acetamide: effect of hydrogen bonding on the self assembly process and antioxidant activity, J. Inorg. Biochem. 191 (2019) 21–28, https://doi.org/10.1016/j.jinorgbio.2018.11.006.
[18] M. Kose, S.E. Duman, V. McKee, I. Akyol, M. Kurtoglu, Hydrogen bond directed 1D to 3D structures of square-planar Ni(II) complexes and their antimicrobial studies, Inorg. Chim. Acta 462 (2017) 281–288, https://doi.org/10.1016/j.ica.2017.04.005.
[19] V. Sethuraman, N. Stanley, P. Thomas Muthiah, C. Karunakaran, Supramolecular self-assembly via inter-ligands hydrogen bonds in [Cu(H2O)2(NO3)2(tb)] (tb is thiabendazole), Acta Crystallogr. E E. 58 (2002) m392–m395, https://doi.org/10.1107/S1600536802011054.
[20] S. Petriček, Syntheses and crystal structures of metal (Mn, Co, Ni) chloride complexes with 3-hydroxypyridin-2-one and contribution of OH···Cl hydrogen bonds to their structural diversity, Polyhedron 167 (2019) 11–25, https://doi.org/10.1016/j.poly.2019.03.050.
[21] I.A. Baburin, V.A. Blatov, L. Carlucci, G. Ciani, D.M. Proserpio, Interpenetrated three-dimensional hydrogen-bonded networks from metal–organic molecular and one- or two-dimensional polymeric motifs, CrystEngComm 10 (2008) 1822–1838, https://doi.org/10.1039/B811855H.
[22] T.-G. Zhan, T.-Y. Zhou, Q.-Y. Qi, J. Wu, G.-Y. Li, X. Zhao, The construction of supramolecular polymers through anion bridging: from frustrated hydrogen-bonding networks to well-ordered linear arrays, Polym. Chem. 6 (2015) 7586–7593, https://doi.org/10.1039/C5PY01284H.
[23] M. Tuikka, M. Niskanen, P. Hirva, K. Rissanen, A. Valkonen, M. Haukka, Concerted halogen and hydrogen bonding in [RuI2(H2dcbpy)(CO)2]···I2···(CH3OH)···I2···[RuI2(H2dcbpy)(CO)2], Chem. Commun. 47 (2011) 3427–3429, https://doi.org/10.1039/C0CC05726F.
[24] X. Ding, M.J. Tuikka, P. Hirva, V.Y. Kukushkin, A.S. Novikov, M. Haukka, Fine-tuning halogen bonding properties of diiodine through halogen–halogen charge transfer – extended [Ru(2,2′-bipyridine)(CO)2X2]·I2 systems (X = Cl, Br, I), CrystEngComm 18 (2016) 1987–1995, https://doi.org/10.1039/C5CE02396C.
[25] V.V. Sivchik, A.I. Solomatina, Y.-T. Chen, A.J. Karttunen, S.P. Tunik, P.-T. Chou, I. O. Koshevoy, Halogen bonding to amplify luminescence: a case study using a platinum cyclometalated complex, Angew. Chem. Int. Ed. 54 (2015) 14057–14060, https://doi.org/10.1002/anie.201507229.
[26] M. Fontana, H. Chanzy, W.R. Caseri, P. Smith, A.P.H.J.H.J Schenning, E.W. Meijer, F. Gröhn, A soluble equivalent of the supramolecular, quasi-one-dimensional, semiconducting Magnus' green salt, Chem. Mater. 14 (2002) 1730–1735, https://doi.org/10.1021/cm0109793.
[27] J.K. Bera, K.R. Dunbar, 23/2002 the Chemistry of the antibody molecule chain compounds based on transition metal Backbones : new life for an old topic, Angew. Chem. Int. Ed. 41 (2002) 4453, https://doi.org/10.1002/1521-3773(20021202)41:23<4453::AID-ANIE4453>3.0.CO;2-1.
[28] L.H. Doerrer, Steric and electronic effects in metallophilic double salts, Dalton Trans. 39 (2010) 3543–3553, https://doi.org/10.1039/b920389c.
[29] K. Krogmann, Planar complexes containing metal-metal bonds, Angew Chem. Int. Ed. Engl. 8 (1969) 35–42, https://doi.org/10.1002/anie.196900351.
[30] E. Laurila, L. Oresmaa, J. Hassinen, P. Hirva, M. Haukka, Neutral one-dimensional metal chains consisting of alternating anionic and cationic rhodium complexes, Dalton Trans. 42 (2013) 395–398, https://doi.org/10.1039/C2DT31671D.
[31] C. Tejel, M.A. Ciriano, L.A. Oro, From platinum blues to rhodium and iridium blues, Chem. Eur J. 5 (1999) 1131–1135, https://doi.org/10.1002/(SICI)1521-3765(19990401)5:4<1131::AID-CHEM1131>3.0.CO;2-3.
[32] P.W. DeHaven, V.L. Goedken, Crystal and molecular structure of dicarbonyl(2,4-pentanediimine)rhodium(I) tetrafluoroborate, a structure having extended rhodium-rhodium interactions, Inorg. Chem. 18 (1979) 827–831, https://doi.org/10.1021/ic50193a058.
[33] C. Crotti, S. Cenini, B. Rindone, S. Tollari, F. Demartin, Deoxygenation reactions of ortho-nitrostyrenes with carbon monoxide catalysed by metal carbonyls: a new route to indoles, J. Chem. Soc., Chem. Commun. (1986) 784–786, https://doi.org/10.1039/C39860000784.
[34] A.J. Rodríguez-Santiago, N. Cortés, K. Pham, J. Miksovska, R.G. Raptis, 4,4′-Dihydroxy-2,2′-bipyridine complexes of Co(III), Cu(II) and Zn(II); structural and spectroscopic characterization, Polyhedron 150 (2018) 61–68, https://doi.org/10.1016/j.poly.2018.04.039.
[35] M.D. Stephenson, T.J. Prior, M.J. Hardie, New network structures from Cu(II) complexes of chelating ligands with appended hydrogen bonding sites, Cryst. Growth Des. 8 (2008) 643–653, https://doi.org/10.1021/cg700820d.
[36] T. Chand Vagvala, T. Ooyabe, M. Sakai, Y. Funasako, M. Inokuchi, W. Kurashige, Y. Negishi, V. Kalousek, K. Ikeue, Synthesis and characterization of metal-diaminobipyridine complexes as low-cost co-catalysts for photo-sensitized hydrogen evolution, Inorg. Chim. Acta 482 (2018) 821–829, https://doi.org/10.1016/j.ica.2018.07.022.
[37] A.E. Platero-Prats, A. Bermejo Gómez, L. Samain, X. Zou, B. Martín-Matute, The first one-pot synthesis of metal–organic frameworks functionalised with two transition-metal complexes, Chem. Eur J. 21 (2015) 861–866, https://doi.org/10.1002/chem.201403909.
[38] D. Sivanesan, S. Yoon, Functionalized bipyridyl rhodium complex capable of electrode attachment for regeneration of NADH, Polyhedron 57 (2013) 52–56, https://doi.org/10.1016/j.poly.2013.04.011.
[39] C.M. Conifer, R.A. Taylor, D.J. Law, G.J. Sunley, A.J.P.P. White, G.J.P.P. Britovsek, First metal complexes of 6,6′-dihydroxy-2,2′-bipyridine: from molecular wires to applications in carbonylation catalysis, Dalton Trans. 40 (2011) 1031–1033, https://doi.org/10.1039/C0DT01526A.
[40] P. Plitt, D.E. Gross, V.M. Lynch, J.L. Sessler, Dipyrrolyl-functionalized bipyridine-based anion receptors for emission-based selective detection of dihydrogen phosphate, Chem. Eur J. 13 (2007) 1374–1381, https://doi.org/10.1002/chem.200601514.
[41] N. Rigby, T. Jacobs, J.P. Reddy, M.J. Hardie, Metal complexes of 2,2′-Bipyridine-4,4′-diamine as metallo-tectons for hydrogen bonded networks, Cryst. Growth Des. 12 (2012) 1871–1881, https://doi.org/10.1021/cg201512q.
[42] E. Tomás-Mendivil, J. Díez, V. Cadierno, Palladium(II) complexes with symmetrical dihydroxy-2,2′-bipyridine ligands: exploring their inter- and intramolecular interactions in solid-state, Polyhedron 59 (2013) 69–75, https://doi.org/10.1016/j.poly.2013.04.043.
[43] Agilent, CrysAlisPro, Agilent Technologies Inc, Yarnton, Oxfordshire, England, 2013.
[44] L. Palatinus, G. Chapuis, {\it SUPERFLIP} {–} a computer program for the solution of crystal structures by charge flipping in arbitrary dimensions, J. Appl. Crystallogr. 40 (2007) 786–790, https://doi.org/10.1107/S0021889807029238.
[45] G.M. Sheldrick, Crystal structure refinement with {\it SHELXL}, Acta Crystallogr. C 71 (2015) 3–8, https://doi.org/10.1107/S2053229614024218.
[46] O.V. Dolomanov, L.J. Bourhis, R.J. Gildea, J.A.K. Howard, H. Puschmann, {\it OLEX2}: a complete structure solution, refinement and analysis program, J. Appl. Crystallogr. 42 (2009) 339–341, https://doi.org/10.1107/S0021889808042726.
[47] C.B. Hübschle, G.M. Sheldrick, B. Dittrich, {\it ShelXle}: a Qt graphical user interface for {\it SHELXL}, J. Appl. Crystallogr. 44 (2011) 1281–1284, https://doi.org/10.1107/S0021889811043202.

III

SELF-HEALING, LUMINESCENT METALLOGELATION DRIVEN BY SYNERGISTIC METALLOPHILIC AND FLUORINE-FLUORINE INTERACTIONS

by

Kalle Kolari, Evgeny Bulatov, Rajendhraprasad Tatikonda, Kia Bertula, Elina Kalenius, Nonappa, & Matti Haukka 2020

Soft Matter, **2020**,*16*, 2795-2802. DOI: 10.1039/C9SM02186H

Soft Matter

PAPER

View Article Online
View Journal | View Issue

Cite this: *Soft Matter*, 2020, **16**, 2795

Self-healing, luminescent metallogelation driven by synergistic metallophilic and fluorine–fluorine interactions†

Kalle Kolari,[a] Evgeny Bulatov,[a] Rajendhraprasad Tatikonda,[a] Kia Bertula,[b] Elina Kalenius,[a] Nonappa *[bc] and Matti Haukka *[a]

Received 4th November 2019,
Accepted 14th February 2020

DOI: 10.1039/c9sm02186h

rsc.li/soft-matter-journal

Square planar platinum(II) complexes are attractive building blocks for multifunctional soft materials due to their unique optoelectronic properties. However, for soft materials derived from synthetically simple discrete metal complexes, achieving a combination of optical properties, thermoresponsiveness and excellent mechanical properties is a major challenge. Here, we report the rapid self-recovery of luminescent metallogels derived from platinum(II) complexes of perfluoroalkyl and alkyl derivatives of terpyridine ligands. Using single crystal X-ray diffraction studies, we show that the presence of synergistic platinum–platinum (Pt···Pt) metallophilic interactions and fluorine–fluorine (F···F) interactions are the major driving forces in achieving hierarchical superstructures. The resulting bright red gels showed the presence of highly entangled three-dimensional networks and helical nanofibres with both (*P* and *M*) handedness. The gels recover up to 87% of their original storage modulus even after several cycles under oscillatory step-strain rheological measurements showing rapid self-healing. The luminescence properties, along with thermo- and mechanoresponsive gelation, provide the potential to utilize synthetically simple discrete complexes in advanced optical materials.

Introduction

Supramolecular chemistry involving metal–ligand (M–L) coordination-induced self-assembly has opened new avenues in the field of stimulus-responsive soft materials.[1–3] This is attributed to the possibilities to access a diverse range of metal components (metal ions, clusters, and nanoparticles) and rationally designed organic ligands with well-defined coordination sites.[4,5] Among the metal components containing soft materials, self-healing and stimulus-responsive metallogels have gained considerable attention recently.[6,7] The presence of metal components alters the gelation process, gel strength, mechanical properties, and morphological features.[8–11] More importantly, metal components also impart properties such as conductivity, redox activity, magnetism, photophysical properties, antimicrobial properties, and thixotropic behaviour.[12–18] Furthermore, certain metal ions also serve as a source for *in situ* metal nanoparticle formation.[19–22] Therefore, metallogels find potential applications in chiral recognition, light-emitting materials, soft conductive materials, wearable electronics, energy storage, self-healing devices, catalysis, and antimicrobial systems, and can act as artificial enzyme mimics.[23–27] Metallogels contain metal components and organic components with appropriate binding sites. Low molecular weight organic ligands, biopolymers and synthetic polymers having functional groups such as carboxylic acid, amines, thiols and alkynes have been used as coordination sites for a diverse range of mono-, di-, and trivalent metal ions (Ag^{+}, Fe^{2+}, Cu^{2+}, Zn^{2+}, Co^{2+}, Ni^{2+}, Pd^{2+}, Pt^{2+}, Fe^{3+}, and Au^{3+}), metal clusters or nanoparticles,[28–31] wherein a combination of metal chelation and other non-covalent interactions such as H-bonding, van der Waals interaction, electrostatic interaction, π-stacking and metallophilic interactions has been explored to achieve hierarchical self-assembly.[32–34] Metallogels involving low molecular weight organic ligands result in discrete coordination complexes or coordination polymerization upon complexation.[19–22] When the gelation consists of the self-assembly of discrete complexes, the supramolecular interactions between the organic ligands act as the primary driving force, whereas, for coordination polymerization-induced gelation, the metal–ligand interaction forms the main driving force.[35,36] For supramolecular metallogels, the gelation can be

[a] *Department of Chemistry, University of Jyväskylä, P. O. Box 35, FI-40014 Jyväskylä, Finland. E-mail: matti.o.haukka@jyu.fi*
[b] *Department of Applied Physics, Aalto University School of Science, Puumiehenkuja 2, FI-02150 Espoo, Finland. E-mail: nonappa@aalto.fi*
[c] *Department of Bioproducts and Biosystems, Aalto University School of Chemical Engineering, Kemistintie 1, FI-02150 Espoo, Finland*

† Electronic supplementary information (ESI) available: Details on the synthesis of ligands and their platinum complexes, NMR spectra, single crystal X-ray data, additional SEM, TEM micrographs and rheological studies. CCDC 1949029 and 1949030. For ESI and crystallographic data in CIF or other electronic format see DOI: 10.1039/c9sm02186h

induced by adding metal salt into a solution containing organic ligands with appropriate binding sites or by dissolving a pre-made metal complex. In the latter case, the main driving forces are metallophilic (metallopolymerization) interactions along with other supramolecular interactions of organic moieties.

Gold(III) and platinum(II) complexes are known to undergo metallophilic interaction-induced self-assembly.[37,38] Au(III) and square planar Pt(II) complexes also offer unique optoelectronic properties.[39,40] The ability to undergo a dramatic colour change upon self-assembly of Pt(II) complexes is attributed to the presence of Pt···Pt interaction.[41] Therefore, self-assembly of various mononuclear and binuclear Pt(II) polypyridine complexes has been explored. Examples include alkynylplatinum(II) complexes with terpyridine ligands.[42–44] Such complexes due to strong σ-donating alkynyl ligands have been shown to possess interesting aggregation behaviour. Depending on the substituents, chiral and helical morphologies, substitution dependent colour change, luminescence, vapochromism, and vapoluminescence have been reported.[45,46] Such properties occur due to changes in weak metal–metal interactions, π-stacking or hydrogen bonding upon exposure to vapour (analyte).[47] Furthermore, features such as self-assembly-induced luminescence provide promising applications in optoelectronics and in developing vapochromic sensors. Platinum(II) complexes have also been shown to form metallogels showing significant changes in the colour and spectroscopic properties upon sol ⇔ gel transition.[48] Though such systems are known to form various superstructures, metallogelation using Pt···Pt interactions is limited in the literature.

Another important non-covalent interaction is fluorine–fluorine interaction. Fluorinated analogues of hydrocarbons have been shown to exhibit simultaneous hydro- and lipophobicities, altered aggregation behaviour, steric bulk, stiffness, stability, and lower critical aggregation concentration.[49] Therefore, organic ligands containing fluorinated analogues of hydrocarbons offer a unique opportunity to design materials with excellent material properties. Recently, it has been shown that perfluoroalkyl substituted 4-aminophenyl-2,2′,6,2′-terpyridine can act as a metallosupramolecular gelator resulting in rapid self-healing and anion selectivity.[50] The F···F interactions have been shown to affect the rheological and mechanical properties of the metallogels. In this work, we show that Pt(II) complexes of alkyl and fluoroalkyl containing terpyridine derivatives undergo a synergistic Pt···Pt and F···F interaction-driven self-assembly leading to rapid gelation. The compounds also exhibit luminescence properties in their solid state, gel state, and solution state. We demonstrate the rapid self-healing of gels containing low solid contents with recovery up to 87% of their storage modulus values even after several cycles. Morphologically, the gels contain a highly entangled 3D network of helical fibres with both handedness.

Results and discussion

Crystal structures and transformations in the solid state

First, we discuss the synthesis and solid state properties of the complexes studied in this work. The synthesis of ligands **L1** and **L2** and their platinum complexes {[Pt(L1)Cl]Cl} (**1**) and {[Pt(L2)Cl]Cl} (**2**) was carried out following a reported literature procedure (see Fig. 1 and ESI† for details and characterization data).[51,52] Yellowish plate-like single crystals suitable for X-ray diffraction were obtained upon recrystallization of both the metal complexes from hot ethanol. In their solid state structures, the complexes **1** and **2** show cationic square-planar units self-assembled to form dimers (Fig. 1b and c) *via* Pt···Pt interactions with a distance of 3.4096(5) Å for **1** and 3.3031(2) Å for **2**, respectively. These dimer units are further extended to form supramolecular polymeric structures facilitated by π···π contacts of terpyridine core. The cationic charges in both the complexes are compensated by the presence of chloride anions. The chloride counter ions are involved in hydrogen bonding with ethanol molecules (*i.e.* solvate) thus filling voids in crystal packing (Fig. S7 and S8, ESI†). Additionally, terpyridine substituents form lipophilic fluorine and hydrophobic phases in the crystal packing of complexes **1** and **2**, respectively. Due to a severe disorder of perfluorinated substituents, the determination of the definite fluorine–fluorine distances remained a challenge. However, the sphere-packing model for the solid state structure of **1** indicates the presence of intermolecular fluorine–fluorine contacts (Fig. 1d), forming lipophilic phases in the crystal structures. In the case of complex **2**, a similar arrangement is observed, *i.e.* hydrophobic phases are formed due to close packing of substituent chains between adjacent molecules (Fig. 1e).

The yellow crystals of complexes **1** and **2** recrystallized from ethanol underwent a colour change to orange when exposed to air, presumably due to the evaporation of solvent molecules, the crystals of **1** being noticeably less stable (Fig. 2a and Movies S1, S2, ESI†). In both cases, the resulting orange solids are amorphous, as confirmed by powder X-ray diffraction studies (Fig. S9, ESI†). Upon drying under vacuum, a further colour change to dark purple was observed for complex **1**, whereas complex **2** remained orange.

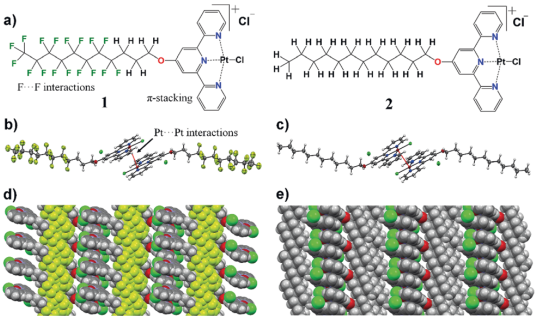

Fig. 1 Chemical structures and single crystal X-ray structures. (a) Chemical structures of gelator molecules {[Pt(L1)Cl]Cl} (**1**) and {[Pt(L2)Cl]Cl} (**2**). (b) X-ray single crystal diffraction-based dimeric structure of gelator **1** showing Pt···Pt interaction and (d) showing higher-order packing driven by F···F interactions. (c and e) X-ray single crystal diffraction-based dimeric structure of complex **2** indicating Pt···Pt interaction and higher-order packing in the solid state.

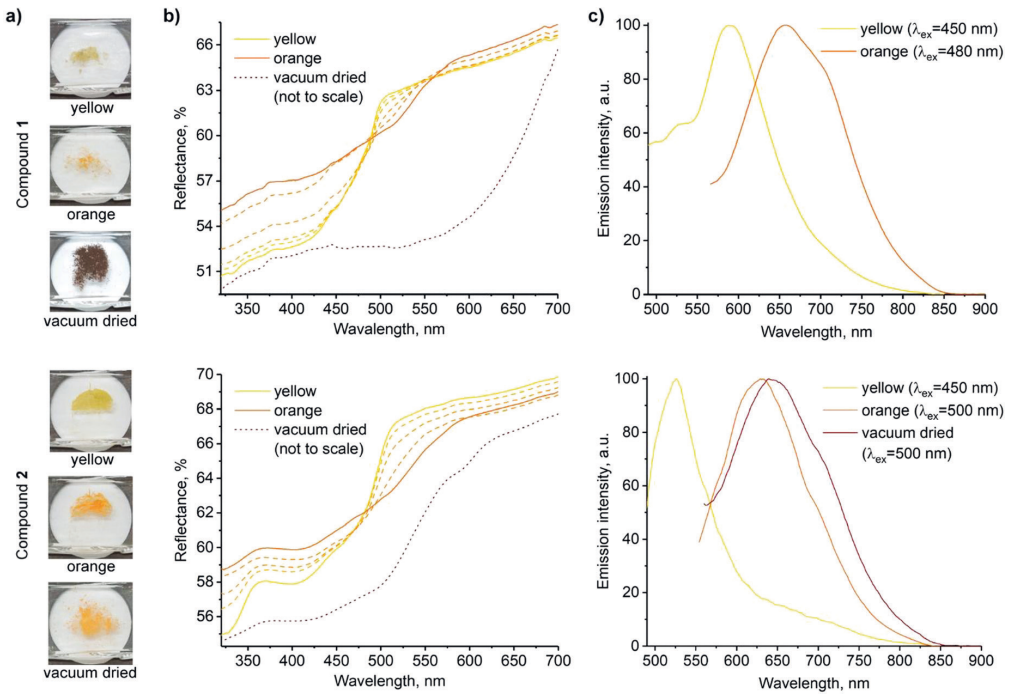

Fig. 2 Solid state forms of **1** (top) and **2** (bottom). (a) Photographs of samples of the three forms used for spectroscopic measurements. (b) Reflectance spectra (transition from yellow to orange forms is shown in dashed lines; spectra of the vacuum dried powders are adjusted to match the scale, and the original spectra are presented in the ESI,† Fig. S10 and S11). (c) Normalized emission spectra (the decrease in emission intensity along with the red shift is demonstrated in ESI,† Fig. S12).

Fig. 2 shows the photographs and corresponding reflectance and normalized emission spectra of solids of **1** and **2** in different forms. The visual colour changes of the solids are manifested in their reflectance spectra by the appearance of shoulders at $\lambda \approx 515$ nm and 530 nm upon transformations from the yellow to air-dried orange forms of **1** and **2**, respectively. At the same time, luminescence emission bands of **1** and **2** decrease in intensity and undergo a redshift ($\lambda_{em} = 590 \rightarrow 650$ and $525 \rightarrow 630$ nm, respectively). Vacuum drying results in a further redshift of reflectance, with a broad reflectance band being formed between $\lambda \approx 500$ and 650 nm in the case of dark purple **1**. However, only a subtle band at $\lambda \approx 600$ nm was observed in the case of orange **2**. The effect of vacuum drying on the luminescence is also much stronger for **1**, which displays no detectable emission, whereas the emission of **2** is only slightly red-shifted compared to the air-dried form (Fig. 2b and c). Intermolecular π···π and Pt···Pt interactions in stacked terpyridine complexes of platinum(II) (Fig. 1) are known to alter the photophysical properties of the complexes. Particularly, metal to ligand charge transfer (MLCT) absorption and emission bands of single molecules change to more red-shifted metal–metal to ligand charge transfer (MMLCT) bands within the stacks. Therefore, the observed redshifts in reflectance and emission spectra of **1** and **2** in the solid state upon drying are attributed to the MMLCT bands. While the amorphous nature of the orange forms prevents direct determination of their molecular arrangements by X-ray diffraction methods, the MMLCT bands indicate the presence of continuous Pt···Pt interactions, in contrast with the dimeric units in the yellow crystalline forms. Similar transformations between yellow and red forms have previously been observed for other terpyridine complexes.[47,53]

Aggregation in solution and gelation

After solid state characterization of complexes **1** and **2**, we studied the self-assembly behaviour in polar organic solvents. A bright yellow solution of complex **1** was obtained in dimethyl sulfoxide (DMSO) at lower concentrations ($C \leq 1$ mM). However, heating was required to dissolve the complex at higher concentrations. Importantly, allowing a supersaturated DMSO solution of complex **1** to attain room temperature resulted in a change of colour to bright red, accompanied by the gelation, which showed resistance to flow upon inversion (Fig. 3a and Movie S3, ESI†). The gelation was observed for a concentration as low as 0.6 w/v% (note: from hereafter, all gelator/solvent w/v% ratios are denoted as %). Similar results were also obtained in *N*,*N*-dimethylformamide (DMF). Complex **1** remained insoluble in water and partially soluble when a mixture of DMSO/water (9 : 1 v/v) was used for gelation. Importantly, no such colour change was observed in ethanol, and the attempts to form gels

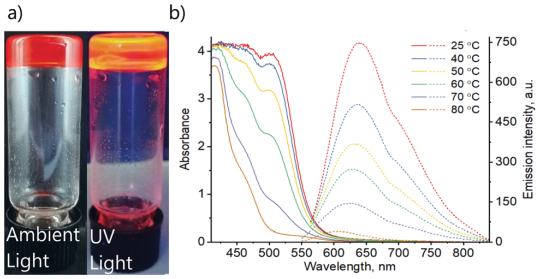

Fig. 3 (a) The photographs of the DMSO gel of complex **1** under ambient light and under UV-radiation. (b) Absorption (solid lines) and emission (dashed lines) spectra of DMSO gel of **1** (0.6%) at various temperatures. Excitation wavelengths λ_{ex} = 550 and 530 nm were used for temperatures 25–60 °C and 70–80 °C accordingly.

produced an unstable gelatinous precipitate. On the other hand, complex **2** only formed an unstable gel in ethanol at concentrations above 1.5% and no gelation or colour change was observed either in DMSO or DMF. Such a difference in the behaviours of **1** and **2** is attributed to their different aggregation capabilities. Apart from the intermolecular π···π interactions between the terpyridine units and Pt···Pt interactions, the aliphatic chains in **1** and **2** further promote aggregation *via* lipophilic stacking, as observed in the crystal structures (Fig. 1d and e). The perfluoroalkyl chain in **1** is expected to cause stronger aggregation due to F···F interactions, as previously reported in the literature.[51] Therefore, the change of colour for complex **1** from yellow to red in solution at higher concentrations and upon gelation is attributed to the appearance of the MMLCT band, associated with the stacking of the terpyridine units assisted by F···F interactions. On the other hand, complex **2** demonstrates much less capability for aggregation.[54–56]

Nuclear magnetic resonance (NMR) spectroscopy has been utilized extensively to study gels.[57–59] In the literature, it has often been shown that the ^{1}H NMR resonance peaks of gels at room temperature show similar chemical shift values to that of the solution state (after gel melting).[60–62] It has been hypothesized that for gels at room temperature, the observed ^{1}H resonance peaks predominantly originate from the free molecules that are not bound to the gel network, whereas the molecules in the aggregated state remain NMR silent.[60,61] We have performed variable temperature (VT) ^{1}H and ^{19}F NMR spectroscopy measurements of the DMSO-d_6 gel of **1** to investigate the sol ⇔ gel transition and interactions involved in the gelation. The ^{1}H NMR resonance signals remained invisible and featureless in temperature range of 30–50 °C, a property that is typical for low molecular weight gels below their melting temperature. This is attributed to increased viscosity and reduced molecular tumbling in the gel state. However, above 60 °C, the signal to noise ratio improved and the aliphatic and aromatic region displayed a clear splitting pattern at 90 °C (see ESI,† Fig. S13a and b). The signals at the same time underwent a slight downfield shift ($\Delta\delta$ between 0.01 to 0.09 ppm) (see ESI,† Table S2). The gel ⇔ sol transition observed in VT ^{1}H NMR experiments is in agreement with the gel melting temperature (T_{gel} = 69 °C) of the 0.6% DMSO gel of **1** determined using an inverted test tube method. Variable temperature ^{19}F NMR spectroscopy measurements displayed broad peaks at 30 °C. A downfield shift in the ^{19}F resonance peaks was revealed upon heating the gel from 30 °C to 90 °C. Furthermore, upon heating, the ^{19}F signals also became sharp and showed an apparent splitting, indicating changes in F···F interactions in the transformation from gel to solution state (ESI,† Fig. S13b). Unlike the VT ^{1}H NMR spectra, the VT ^{19}F NMR spectra showed a clear change in chemical shift values with $\Delta\delta$ between 0.15 and 1.61 ppm (see ESI,† Table S3). Fourier transformed infrared (FT-IR) spectroscopy of complex **1** in its synthetic solid, gel (1%) and solution states (0.4%) was performed to further probe the fluorine–fluorine interactions by monitoring the $\nu_s(CF_2)$ stretching frequencies. The FT-IR spectra of solid powder form revealed the C–F stretching frequency at 1144 cm^{-1} (ESI,† Fig. S14). The gel of complex **1** showed an increased stretching frequency at 1148 cm^{-1}. Finally, further shifting was detected in solution (1153 cm^{-1}). Thus, it can be concluded that fluorine–fluorine interactions are present in solid, gel and solution with decreasing strength, affecting the self-assembly of monomeric units and gelation.

To gain more insights, variable temperature absorption and emission spectroscopic analyses of solution and gel states of complex **1** were carried out (Fig. 3). The absorption spectrum of the DMSO gel (0.6%) of complex **1** shows a peak at λ_{abs} = 500 nm at 25 °C. Importantly, the intensity decreases upon increasing temperature. Similarly, the corresponding emission also decreases in intensity with increasing temperature and shows a blue shift upon heating from λ_{em} = 640 nm at 25 °C to λ_{em} = 600 nm at 80 °C. These observations match well with the changes in photophysical properties of solid **1** upon the transformation from yellow to orange form (Fig. 2b and c). Thus, the absorption and emission bands at λ_{abs} = 500 nm and λ_{em} = 640 nm are accordingly assigned to the MMLCT transitions, which are expected to depend on aggregation and, consequently, temperature. The emission lifetime at room temperature τ = 51 ns suggests the fluorescence nature of the complex. Though such a short excited-state lifetime is not very common for transitions involving Pt(II) centres, previously, it has been reported for a limited number of terpyridine platinum(II) complexes.[55]

Preliminary studies of absorption and emission spectra of the solution of complex **1** in DMSO at various concentrations and various temperatures indicated the formation of more than one type of aggregate. Therefore, an unambiguous interpretation of the spectra remained a challenge. However, the correlation of photophysical properties of **1** in solid and gel states indicates similarities in intermolecular arrangements, namely the formation of continuous chains with stacked terpyridine units and close Pt···Pt contacts within the gel structure. The F···F interactions and packing of the perfluoroalkyl chains also appear to take place, based on the NMR and FT-IR spectra, as well as the non-gelling behaviour of complex **2**. A detailed study of the aggregation behaviour of complex **1** in solution is beyond the scope of this work and will be the subject of a separate study.

Gelation and morphology

The morphological features of self-assembled superstructures in the gel were studied using electron microscopy imaging. First, the scanning electron microscopy (SEM) imaging of DMSO and DMF gels of complex **1** was performed. For SEM imaging, aerogels were prepared using a liquid propane freeze-drying method.[63] Freeze-drying allows minimum drying artefacts during specimen preparation. The representative SEM micrographs of aerogels from DMSO and DMF gels of **1** are shown in Fig. 4.

Interestingly, the SEM micrographs show the presence of helical screw-like fibres with both handedness (*P* and *M*) in DMSO (Fig. 4b and c). Similarly, in DMF, helical fibres with both handedness are observed (Fig. 4e and f; see ESI† for additional SEM images, Fig. S15 and S16). It is well documented in the literature that achiral gelators tend to form helical structures with both handedness.[64,65] Importantly, triazine-containing alkynylplatinum(II) terpyridine complexes with appropriate substituents on terpyridine units have been shown to assemble into a mixture of right- and left-handed helical fibres in DMSO–water mixtures.[66] It has been hypothesized that in such complexes, the terpyridine units are bent with respect to the alkynyl ligand, inducing directional Pt···Pt interactions and π-stacking. Furthermore, such assemblies are also due to dominant hydrophobic–hydrophobic interactions in polar solvents. Based on the X-ray crystal structure of the solids, VT NMR spectroscopy and FT-IR studies of complex **1**, it is evident that there exists a strong F···F interaction in the gel and solid states. Therefore, the presence of Pt···Pt, π···π and F···F interactions results in minimized unfavourable interactions in polar DMSO and drives the formation of helical nanostructures.

From SEM imaging, it is evidenced that the helical fibres with lateral dimensions varying from 100 to 500 nm are composed of smaller fibrils. To further evaluate the nature of the fibrillar structures, a TEM specimen was prepared by drop-casting the freshly prepared hot sol onto holey-carbon film (Fig. 5). TEM micrographs of DMSO gels of **1** clearly show highly entangled fibrillar structures. The fibril diameters varied from 15 to 30 nm with indefinite length. It is important to note that the sample preparation methods for SEM and TEM are different. For SEM, premade gels are freeze-dried to obtain aerogels, whereas TEM studied a drop casted thin film of hot sol. TEM, therefore, allowed the smaller fibrillar structures to be observed. Similarly, the DMF gel of **1** also showed structural features that undergo higher-order assembly into fibres as indicated in the SEM micrographs.

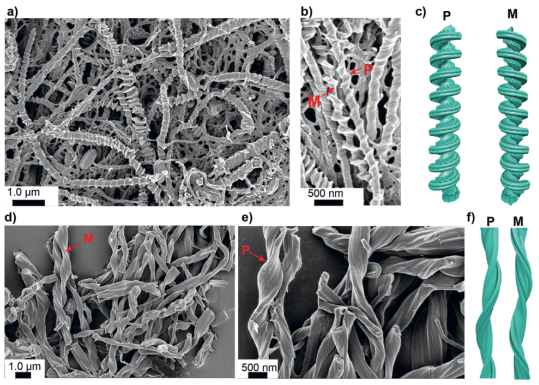

Fig. 4 Scanning electron microscopy. (a and b) SEM micrographs of aerogels from the DMSO gel of **1** (1.0%) showing helical screw-like structures. (c) Schematic illustration of helical screw-like fibres in the DMSO gel of **1**. (d and e) SEM micrographs of aerogels from the DMF gels of **1** (1.0%) showing helical fibre bundles. (f) Schematic illustration of helical fibres in the DMF gel of **1**. For additional SEM images, see ESI† (Fig. S15 and S16).

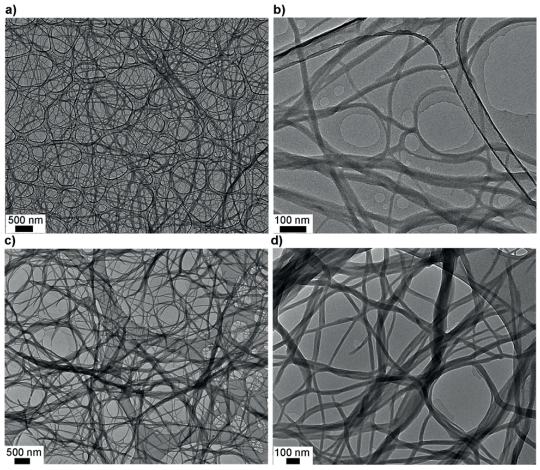

Fig. 5 Transmission electron microscopy. (a and b) TEM micrographs of the dried DMSO gel of **1** (0.6%). (c and d) TEM micrographs of the dried DMF gel of **1** (1.0%). For additional TEM micrographs, see ESI,† Fig. S17 and S18.

Fibrillar structures were also observed when non-gelling complex **2** was dispersed in DMSO or DMF with fibre diameters ranging from 15 to 50 nm.

Rheological properties

Metallogels exhibit unique mechanical properties in rheological experiments such as self-healing and thixotropy.[6,50] The mechanical properties of DMSO and DMF gels of complex **1** were studied using dynamic oscillatory rheological measurements on the 1.0% gels. In all experiments, premade gels were used to study the rheological properties. First, the time sweep experiments were performed to evaluate the stability of the gels and in both cases, the storage modulus (G') is close to an order of magnitude higher than the loss modulus (G''), suggesting that the systems under investigation are indeed gels and remained stable under experimental conditions (see ESI,† Fig. S19). It is also evident that DMF gels of **1** displayed higher stiffness than that of DMSO gels. The average storage modulus (G') values were found to be 90 Pa and 2.0 kPa for DMSO and DMF gels of **1**, respectively.

The rheological properties of soft materials display non-linear behaviour with a rapid decline in their storage modulus above certain strain levels, known as critical strain. Critical strain allows understanding the linearity of a material under

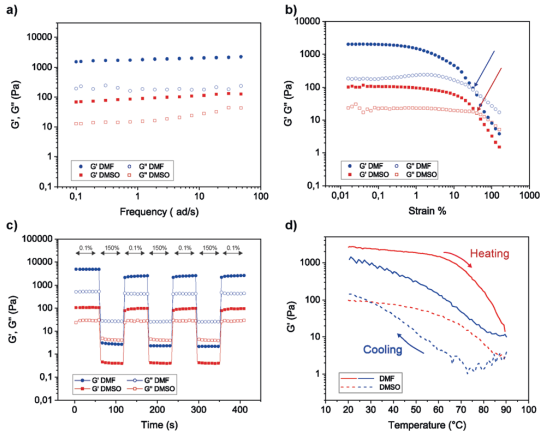

Fig. 6 Rheological measurements: (a) frequency sweep experiments of DMSO and DMF gels (1.0%) of **1**. (b) Strain sweep experiments (arrows indicate the strain% above which the gels break). (c) Step-strain experiments showing the self-recovery by alternately applying 0.1% and 150% strain. (d) The thermoreversible nature of the gels is revealed using temperature sweep cycles. See ESI† for additional rheological data with error bars.

investigation. Below critical strain, the structure of the gels remains intact and applying strain levels above critical strain will disrupt the gel structure. This information is useful in understanding the linear viscoelastic regime of the materials. In our experiments, the DMSO and DMF gels of complex **1** show that the structure remains intact until 32% and 40% strain levels, respectively, above which the materials behaved non-linearly and a cross-over between G' and G'' was observed.

The frequency sweep measurements provide insights about the junction networks and temporary bonds that hold the networks together. This information can be extracted using frequency-dependent storage and loss moduli (Fig. 6b). The rheological and SEM studies suggest the presence of junction networks. Another interesting property of metallogels is self-healing. Rheologically, self-healing can be studied by using step-strain experiments. In the case of step-strain tests, recovery of the gel is observed after shearing. The step-strain rheological measurements were performed to investigate the reversible gel ⇔ sol transition and self-recovery, upon several cycles. For the step strain experiments, controlled strains of 0.1% and 150% were applied for 60 s, respectively (Fig. 6c). The gels showed an immediate response to increased strain by turning into viscoelastic liquids as indicated by the rapid decrease in G' well below that of G''. The application of increased strain also appears to break the structure further during the 60 s experiment, as shown by the slight decreasing elastic modulus values on subsequent cycles. The gels recovered almost instantaneously upon switching to lower strain (0.1%), *i.e.* rapid self-recovery. Importantly, the process can be repeated for several cycles. However, slightly lower elastic moduli after the first high–low strain cycle and gradual build-up are observed, therefore indicating that the structure build-up to the equilibrium state would require longer periods of "rest" (low strain). Importantly, the DMSO gels recovered up to 87% of their original storage modulus values even after four cycles. On the other hand, DMF gels recovered up to 61% of the initial storage modulus upon repeated step-strain cycles. Finally, we studied the thermal properties using temperature sweep experiments. First, the premade gel was heated, and the moduli were followed. Temperature ramps from 20 °C to 90 °C and from 90 °C to 20 °C were measured with 0.1% strain amplitude and 5 °C min^{-1} heating rate. Temperature ramps and step-strain experiments present the average of two measurements. Above 70 °C, a rapid decline in the storage modulus was observed when the 1.0% DMSO and DMF gels begin to melt, in agreement with the visual and variable temperature NMR tests described above. However, the thermoreversibility under rheological measurement is prominent for DMSO gels as they are rather robust. Further, unlike DMSO gels, DMF gels were not robust to transfer and scoop processes, and the solvent was often expelled, which might also explain the observed high modulus.

Conclusions

Self-assembly of discrete metal complexes offers a range of opportunities to construct structurally and functionally unique soft materials using simple synthetic design. More importantly, simple chemical modification of functional units allows a remarkable change in their structure, function, and interactions. These changes also affect the self-assembly behaviour, morphology, and rheological properties at extremely low solid contents. In this work, we have demonstrated that replacement of the alkyl derivative with a fluoroalkyl derivative in terpyridine ligand allows control over the solid state assembly, luminescence properties, and gelation ability of complexes **1** and **2**. Our results show that the presence of synergistic Pt···Pt and F···F interactions is responsible for the rapid gelation of complex **1**. This combination of interactions is also responsible for self-assembly-induced luminescence, rapid gelation, and self-healing. Therefore, this study demonstrates how the influence of metallophilic interactions on luminescence properties can provide insight on intermolecular arrangements and thus potentially allow investigation of supramolecular structures of the gels. The SEM of the cryo-frozen gel of complex **1** displayed an enantiomeric mixture of fibres with screw rotation to left and right. Fibres were up to 200 nm in diameter. The topology of fibres is stabilized with non-covalent interactions including intermolecular platinum–platinum interactions. Additionally, changing the solvent from ethanol to DMSO affects the formation of helical polymeric structures and enables the formation of fibres with screw rotation by affecting the packing of monomeric units.

Conflicts of interest

There are no conflicts to declare.

Acknowledgements

KK and RT acknowledge the kind financial support from the Magnus Ehrnrooth Foundation, and Academy of Finland (M. H. Proj. no. 295581). Academy of Finland's Centre of Excellence in Molecular Engineering of Biosynthetic Hybrid

Materials (HYBER, 2014–2019) and Aalto University Nanomicroscopy Centre (Aalto-NMC) are acknowledged for the use of their facilities.

References

1 *Functional Metallosupramolecular Materials*, ed. J. G. Hardy and F. H Schacher, Royal Society of Chemistry, 1st edn, 2015, pp. 1–446.
2 M. Burnworth, L. Tang, J. R. Kumpfer, A. J. Duncan, F. L. Beyer, G. L. Fiore, S. J. Rowan and C. Weder, *Nature*, 2011, **472**, 334–337.
3 A. J. McConnell, C. S. Wood, P. P. Neelakandan and J. R. Nitschke, *Chem. Rev.*, 2015, **115**, 7729–7793.
4 D. G. Kurth, *Sci. Technol. Adv. Mater.*, 2008, **9**, 014103.
5 R. Dobrawa and F. Würthner, *J. Polym. Sci., Part A: Polym. Chem.*, 2005, **43**, 4981–4995.
6 H. Wu, J. Zheng, A.-L. Kjøniksen, W. Wang, Y. Zhang and J. Ma, *Adv. Mater.*, 2019, **31**, 1806204.
7 Y.-Y. Tama and V. W.-W. Yam, *Chem. Soc. Rev.*, 2013, **42**, 1540–1567.
8 M. Häring and D. D. Díaz, *Chem. Commun.*, 2016, **52**, 13068–13081.
9 C. D. Jones and J. W. Steed, *Chem. Soc. Rev.*, 2016, **45**, 6546–6596.
10 E. Degtyar, M. J. Harrington, Y. Politi and P. Fratzl, *Angew. Chem., Int. Ed.*, 2014, **53**, 12026–12044.
11 H. Svobodová, M. Lahtinen, Z. Wimmer and E. Kolehmainen, *Soft Matter*, 2012, **8**, 7840.
12 J. Ge, E. Neofytou, T. J. Cahill III, R. E. Beygui and R. N. Zare, *ACS Nano*, 2012, **6**, 227.
13 K. Mitsumoto, J. M. Cameron, R.-J. Wei, H. Nishikawa, T. Shiga, M. Nihei, G. N. Newton and H. Oshio, *Chem. – Eur. J.*, 2017, **23**, 1502–1506.
14 J. Kima and D. Lee, *Chem. Sci.*, 2019, **10**, 3864–3872.
15 H. T. P. Anh, C.-M. Huang and C.-J. Huang, *Sci. Rep.*, 2019, **9**, 11562.
16 X. Yu, L. Chen, M. Zhang and T. Yi, *Chem. Soc. Rev.*, 2014, **43**, 5346–5371.
17 H. Liang, Z. Zhang, Q. Yuana and J. Liu, *Chem. Commun.*, 2015, **51**, 15196–15199.
18 V. A. Mallia and R. G. Weiss, *Soft Matter*, 2016, **12**, 3665–3676.
19 R. Tatikonda, K. Bertula, Nonappa, S. Hietala, K. Rissanen and M. Haukka, *Dalton Trans.*, 2017, **46**, 2793–2802.
20 R. Tatikonda, E. Bulatov, Z. Özdemir, Nonappa and M. Haukka, *Soft Matter*, 2019, **15**, 442–451.
21 M. Tautz, C. Saldías, A. D. Lozano-Gorrín and D. Díaz Díaz, *New J. Chem.*, 2019, **43**, 13850–13856.
22 H. Bunzen, Nonappa, E. Kalenius, S. Hietala and E. Kolehmainen, *Chem. – Eur. J.*, 2013, **19**, 12978.
23 B. H. Schroeder, A. Guha, A. Lamoureux, G. V. Renterghem, D. Sept, M. Shtein, J. Yang and M. Mayer, *Nature*, 2017, 214–218.
24 C. Keplinger, J.-Y. Sun, C. C. Foo, P. Rothemund, G. M. Whitesides and Z. Suo, *Science*, 2013, **341**, 984–987.
25 Z. Sun, Z. Li, Y. He, R. Shen, L. Deng, M. Yang, Y. Liang and Y. Zhang, *J. Am. Chem. Soc.*, 2013, **135**, 13379–13386.
26 C.-H. Li, C. Wang, C. Keplinger, J.-L. Zuo, L. Jin, Y. Sun, P. Zheng, Y. Cao, F. Lissel, C. Linder, X.-Z. You and Z. Bao, *Nat. Chem.*, 2016, **8**, 618–624.
27 C. Wei, J. Su, B. He, G.-B. Wen, Y.-W. Lin and Y. Zhang, *Angew. Chem., Int. Ed.*, 2018, **57**, 3504.
28 B. N. Ghosh, S. Bhowmik, P. Mal and K. Rissanen, *Chem. Commun.*, 2014, **50**, 734–736.
29 S. Bhowmik, B. N. Ghosh and K. Rissanen, *Org. Biomol. Chem.*, 2014, **12**, 8836–8839.
30 J. L. Zhong, X. J. Jia, H. J. Liu, X. Z. Luo, S. G. Hong, N. Zhang and J. Bin Huang, *Soft Matter*, 2015, **12**, 191–199.
31 K. Jie, Y. Zhou, B. Shi and Y. Yao, *Chem. Commun.*, 2015, **51**, 8461–8464.
32 S. Datta, M. L. Saha and P. J. Stang, *Acc. Chem. Res.*, 2018, **51**, 2047–2063.
33 L. J. Chen and H. B. Yang, *Acc. Chem. Res.*, 2018, **51**, 2699–2710.
34 Y. Zhang, Q. F. Zhou, G. F. Huo, G. Q. Yin, X. L. Zhao, B. Jiang, H. Tan, X. Li and H. B. Yang, *Inorg. Chem.*, 2018, **57**, 3516–3520.
35 J. Zhang and C. Y. Su, *Coord. Chem. Rev.*, 2013, **257**, 1373–1408.
36 P. Sutar and T. K. Maji, *Chem. Commun.*, 2016, **52**, 8055–8074.
37 E. R. T. Tiekink, *Coord. Chem. Rev.*, 2014, **275**, 130–153.
38 V. Phillips, F. G. Baddour, T. Lasanta, J. M. López-De-Luzuriaga, J. W. Bacon, J. A. Golen, A. L. Rheingold and L. H. Doerrer, *Inorganica Chimica Acta*, Elsevier B.V., 2010, vol. 364, pp. 195–204.
39 A. Sathyanarayana, S. Nakamura, K. Hisano, O. Tsutsumi, K. Srinivas and G. Prabusankar, *Sci. China: Chem.*, 2018, **61**, 957–965.
40 M. H. Y. Chan, M. Ng, S. Y. L. Leung, W. H. Lam and V. W. W. Yam, *J. Am. Chem. Soc.*, 2017, **139**, 8639–8645.
41 A. Aliprandi, M. Mauro and L. De Cola, *Nat. Chem.*, 2016, **8**, 10–15.
42 C. Yu, K. M. C. Wong, K. H. Y. Chan and V. W. W. Yam, *Angew. Chem., Int. Ed.*, 2005, **44**, 791–794.
43 A. Y. Y. Tam, K. M. C. Wong, N. Zhu, G. Wang and V. W. W. Yam, *Langmuir*, 2009, **25**, 8685–8695.
44 C. Po, Z. Ke, A. Y. Y. Tam, H. F. Chow and V. W. W. Yam, *Chem. – Eur. J.*, 2013, **19**, 15735–15744.
45 T. J. Wadas, Q.-M. Wang, Y. Kim, C. Flaschenreim, T. N. Blanton and R. Eisenberg, *J. Am. Chem. Soc.*, 2004, **126**, 16841–16849.
46 M. J. Bryant, J. M. Skelton, L. E. Hatcher, C. Stubbs, E. Madrid, A. R. Pallipurath, L. H. Thomas, C. H. Woodall, J. Christensen, S. Fuertes, T. P. Robinson, C. M. Beavers, S. J. Teat, M. R. Warren, F. Pradaux-Caggiano, A. Walsh, F. Marken, D. R. Carbery, S. C. Parker, N. B. McKeown, R. Malpass-Evans, M. Carta and P. R. Raithby, *Nat. Commun.*, 2017, **8**, 1800.
47 R. Zhang, Z. Liang, A. Han, H. Wu, P. Du, W. Lai and R. Cao, *CrystEngComm*, 2014, **16**, 5531–5542.
48 L. Ao, T.-F. Fu, Z.-C. Gao, X.-L. Zhang and F. Wang, *Chin. Chem. Lett.*, 2016, **27**, 1147–1154.

49 R. J. Baker, P. E. Colavita, D. M. Murphy, J. A. Platts and J. D. Wallis, *J. Phys. Chem. A*, 2012, **116**, 1435–1444.
50 L. Arnedo-Sánchez, Nonappa, S. Bhowmik, S. Hietala, R. Puttreddy, M. Lahtinen, L. De Cola and K. Rissanen, *Dalton Trans.*, 2017, **46**, 7309–7316.
51 P. Du, *Inorg. Chim. Acta*, 2010, **363**, 1355–1358.
52 R. Tatikonda, S. Bhowmik, K. Rissanen, M. Haukka and M. Cametti, *Dalton Trans.*, 2016, **45**, 12756–12762.
53 V. C. H. Wong, C. Po, S. Y. L. Leung, A. K. W. Chan, S. Yang, B. Zhu, X. Cui and V. W. W. Yam, *J. Am. Chem. Soc.*, 2018, **140**, 657–666.
54 S. W. Lai, M. C. W. Chan, K. K. Cheung and C. M. Che, *Inorg. Chem.*, 1999, **38**, 4262–4267.
55 S. E. Hobert, J. T. Carney and S. D. Cummings, *Inorg. Chim. Acta*, 2001, **318**, 89–96.
56 J. A. Bailey, M. G. Hill, R. E. Marsh, V. M. Miskowski, W. P. Schaefer and H. B. Gray, *Inorg. Chem.*, 1995, **34**, 4591–4599.
57 B. Escuder, M. Llusar and J. F. Miravet, *J. Org. Chem.*, 2006, **71**, 7747–7752.
58 Nonappa, M. Lahtinen, B. Behera, E. Kolehmainen and U. Maitra., *Soft Matter*, 2010, **6**, 1748–1757.
59 Nonappa and E. Kolehmainen, *Soft Matter*, 2016, **12**, 6015–6026.
60 Nonappa, D. Šaman and E. Kolehmainen, *Magn. Reson. Chem.*, 2015, **53**, 256–260.
61 V. Noponen, Nonappa, M. Lahtinen, A. Valkonen, H. Salo, A. E. Kolehmainen and E. Sievänen, *Soft Matter*, 2010, **6**, 3789–3796.
62 S. Ikonen, Nonappa, A. Valkonen, R. Juvonen, H. Salo and E. Kolehmainen, *Org. Biomol. Chem.*, 2010, **8**, 2784–2794.
63 K. Bertula, L. Martikainen, P. Munne, S. Hietala, J. Klefström, O. Ikkala and Nonappa, *ACS Macro Lett.*, 2019, **8**, 670–675.
64 S. Y.-L. Leung, K. M.-C. Wong and V. W.-W. Yam, *Proc. Natl. Acad. Sci. U. S. A.*, 2016, **113**, 2845–2850.
65 H. L. K. Fu, C. Po, S. Y. L. Leung and V. W. W. Yam, *ACS Appl. Mater. Interfaces*, 2017, **9**, 2786–2795.
66 H. L. K. Fu, S. Y. L. Leung and V. W. W. Yam, *Chem. Commun.*, 2017, **53**, 11349–11352.

DEPARTMENT OF CHEMISTRY, UNIVERSITY OF JYVÄSKYLÄ
RESEARCH REPORT SERIES

1. Vuolle, Mikko: Electron paramagnetic resonance and molecular orbital study of radical ions generated from (2.2)metacyclophane, pyrene and its hydrogenated compounds by alkali metal reduction and by thallium(III)trifluoroacetate oxidation. (99 pp.) 1976
2. Pasanen, Kaija: Electron paramagnetic resonance study of cation radical generated from various chlorinated biphenyls. (66 pp.) 1977
3. Carbon-13 Workshop, September 6-8, 1977. (91 pp.) 1977
4. Laihia, Katri: On the structure determination of norbornane polyols by NMR spectroscopy. (111 pp.) 1979
5. Nyrönen, Timo: On the EPR, ENDOR and visible absorption spectra of some nitrogen containing heterocyclic compounds in liquid ammonia. (76 pp.) 1978
6. Talvitie, Antti: Structure determination of some sesquiterpenoids by shift reagent NMR. (54 pp.) 1979
7. Häkli, Harri: Structure analysis and molecular dynamics of cyclic compounds by shift reagent NMR. (48 pp.) 1979
8. Pitkänen, Ilkka: Thermodynamics of complexation of 1,2,4-triazole with divalent manganese, cobalt, nickel, copper, zinc, cadmium and lead ions in aqueous sodium perchlorate solutions. (89 pp.) 1980
9. Asunta, Tuula: Preparation and characterization of new organometallic compounds synthesized by using metal vapours. (91 pp.) 1980
10. Sattar, Mohammad Abdus: Analyses of MCPA and its metabolites in soil. (57 pp.) 1980
11. Bibliography 1980. (31 pp.) 1981
12. Knuuttila, Pekka: X-Ray structural studies on some divalent 3d metal compounds of picolinic and isonicotinic acid N-oxides. (77 pp.) 1981
13. Bibliography 1981. (33 pp.) 1982
14. 6^{th} National NMR Symposium, September 9-10, 1982, Abstracts. (49 pp.) 1982
15. Bibliography 1982. (38 pp.) 1983
16. Knuuttila, Hilkka: X-Ray structural studies on some Cu(II), Co(II) and Ni(II) complexes with nicotinic and isonicotinic acid N-oxides. (54 pp.) 1983
17. Symposium on inorganic and analytical chemistry May 18, 1984, Program and Abstracts. (100 pp.) 1984
18. Knuutinen, Juha: On the synthesis, structure verification and gas chromatographic determination of chlorinated catechols and guaiacols occuring in spent bleach liquors of kraft pulp mill. (30 pp.) 1984
19. Bibliography 1983. (47 pp.) 1984
20. Pitkänen, Maija: Addition of BrCl, B_2 and Cl_2 to methyl esters of propenoic and 2-butenoic acid derivatives and ^{13}C NMR studies on methyl esters of saturated aliphatic mono- and dichlorocarboxylic acids. (56 pp.) 1985
21. Bibliography 1984. (39 pp.) 1985
22. Salo, Esa: EPR, ENDOR and TRIPLE spectroscopy of some nitrogen heteroaromatics in liquid ammonia. (111 pp.) 1985

23. Humppi, Tarmo: Synthesis, identification and analysis of dimeric impurities of chlorophenols. (39 pp.) 1985
24. Aho, Martti: The ion exchange and adsorption properties of sphagnum peat under acid conditions. (90 pp.) 1985
25. Bibliography 1985 (61 pp.) 1986
26. Bibliography 1986. (23 pp.) 1987
27. Bibliography 1987. (26 pp.) 1988
28. Paasivirta, Jaakko (Ed.): Structures of organic environmental chemicals. (67 pp.) 1988
29. Paasivirta, Jaakko (Ed.): Chemistry and ecology of organo-element compounds. (93 pp.) 1989
30. Sinkkonen, Seija: Determination of crude oil alkylated dibenzothiophenes in environment. (35 pp.) 1989
31. Kolehmainen, Erkki (Ed.): XII National NMR Symposium Program and Abstracts. (75 pp.) 1989
32. Kuokkanen, Tauno: Chlorocymenes and Chlorocymenenes: Persistent chlorocompounds in spent bleach liquors of kraft pulp mills. (40 pp.) 1989
33. Mäkelä, Reijo: ESR, ENDOR and TRIPLE resonance study on substituted 9,10-anthraquinone radicals in solution. (35 pp.) 1990
34. Veijanen, Anja: An integrated sensory and analytical method for identification of off-flavour compounds. (70 pp.) 1990
35. Kasa, Seppo: EPR, ENDOR and TRIPLE resonance and molecular orbital studies on a substitution reaction of anthracene induced by thallium(III) in two fluorinated carboxylic acids. (114 pp.) 1990
36. Herve, Sirpa: Mussel incubation method for monitoring organochlorine compounds in freshwater recipients of pulp and paper industry. (145 pp.) 1991
37. Pohjola, Pekka: The electron paramagnetic resonance method for characterization of Finnish peat types and iron (III) complexes in the process of peat decomposition. (77 pp.) 1991
38. Paasivirta, Jaakko (Ed.): Organochlorines from pulp mills and other sources. Research methodology studies 1988-91. (120 pp.) 1992
39. Veijanen, Anja (Ed.): VI National Symposium on Mass Spectrometry, May 13-15, 1992, Abstracts. (55 pp.) 1992
40. Rissanen, Kari (Ed.): The 7. National Symposium on Inorganic and Analytical Chemistry, May 22, 1992, Abstracts and Program. (153 pp.) 1992
41. Paasivirta, Jaakko (Ed.): CEOEC'92, Second Finnish-Russian Seminar: Chemistry and Ecology of Organo-Element Compounds. (93 pp.) 1992
42. Koistinen, Jaana: Persistent polychloroaromatic compounds in the environment: structure-specific analyses. (50 pp.) 1993
43. Virkki, Liisa: Structural characterization of chlorolignins by spectroscopic and liquid chromatographic methods and a comparison with humic substances. (62 pp.) 1993
44. Helenius, Vesa: Electronic and vibrational excitations in some

biologically relevant molecules. (30 pp.) 1993

45. Leppä-aho, Jaakko: Thermal behaviour, infrared spectra and x-ray structures of some new rare earth chromates(VI). (64 pp.) 1994
46. Kotila, Sirpa: Synthesis, structure and thermal behavior of solid copper(II) complexes of 2-amino-2- hydroxymethyl-1,3-pr opanediol. (111 pp.) 1994
47. Mikkonen, Anneli: Retention of molybdenum(VI), vanadium(V) and tungsten(VI) by kaolin and three Finnish mineral soils. (90 pp.) 1995
48. Suontamo, Reijo: Molecular orbital studies of small molecules containing sulfur and selenium. (42 pp.) 1995
49. Hämäläinen, Jouni: Effect of fuel composition on the conversion of fuel-N to nitrogen oxides in the combustion of small single particles. (50 pp.) 1995
50. Nevalainen, Tapio: Polychlorinated diphenyl ethers: synthesis, NMR spectroscopy, structural properties, and estimated toxicity. (76 pp.) 1995
51. Aittola, Jussi-Pekka: Organochloro compounds in the stack emission. (35 pp.) 1995
52. Harju, Timo: Ultrafast polar molecular photophysics of (dibenzylmethine)borondifluoride and 4-aminophthalimide in solution. (61 pp.) 1995
53. Maatela, Paula: Determination of organically bound chlorine in industrial and environmental samples. (83 pp.) 1995
54. Paasivirta, Jaakko (Ed.): CEOEC'95, Third Finnish-Russian Seminar: Chemistry and Ecology of Organo-Element Compounds. (109 pp.) 1995
55. Huuskonen, Juhani: Synthesis and structural studies of some supramolecular compounds. (54 pp.) 1995
56. Palm, Helena: Fate of chlorophenols and their derivatives in sawmill soil and pulp mill recipient environments. (52 pp.) 1995
57. Rantio, Tiina: Chlorohydrocarbons in pulp mill effluents and their fate in the environment. (89 pp.) 1997
58. Ratilainen, Jari: Covalent and non-covalent interactions in molecular recognition. (37 pp.) 1997
59. Kolehmainen, Erkki (Ed.): XIX National NMR Symposium, June 4-6, 1997, Abstracts. (89 pp.) 1997
60. Matilainen, Rose: Development of methods for fertilizer analysis by inductively coupled plasma atomic emission spectrometry. (41 pp.) 1997
61. Koistinen, Jari (Ed.): Spring Meeting on the Division of Synthetic Chemistry, May 15-16, 1997, Program and Abstracts. (36 pp.) 1997
62. Lappalainen, Kari: Monomeric and cyclic bile acid derivatives: syntheses, NMR spectroscopy and molecular recognition properties. (50 pp.) 1997
63. Laitinen, Eira: Molecular dynamics of cyanine dyes and phthalimides in solution: picosecond laser studies. (62 pp.) 1997
64. Eloranta, Jussi: Experimental and theoretical studies on some

quinone and quinol radicals. (40 pp.) 1997

65. Oksanen, Jari: Spectroscopic characterization of some monomeric and aggregated chlorophylls. (43 pp.) 1998
66. Häkkänen, Heikki: Development of a method based on laser-induced plasma spectrometry for rapid spatial analysis of material distributions in paper coatings. (60 pp.) 1998
67. Virtapohja, Janne: Fate of chelating agents used in the pulp and paper industries. (58 pp.) 1998
68. Airola, Karri: X-ray structural studies of supramolecular and organic compounds. (39 pp.) 1998
69. Hyötyläinen, Juha: Transport of lignin–type compounds in the receiving waters of pulp mills. (40 pp.) 1999
70. Ristolainen, Matti: Analysis of the organic material dissolved during totally chlorine-free bleaching. (40 pp.) 1999
71. Eklin, Tero: Development of analytical procedures with industrial samples for atomic emission and atomic absorption spectrometry. (43 pp.) 1999
72. Välisaari, Jouni: Hygiene properties of resol-type phenolic resin laminates. (129 pp.) 1999
73. Hu, Jiwei: Persistent polyhalogenated diphenyl ethers: model compounds syntheses, characterization and molecular orbital studies. (59 pp.) 1999
74. Malkavaara, Petteri: Chemometric adaptations in wood processing chemistry. (56 pp.) 2000
75. Kujala Elena, Laihia Katri, Nieminen Kari (Eds.): NBC 2000, Symposium on Nuclear, Biological and Chemical Threats in the 21st Century. (299 pp.) 2000
76. Rantalainen, Anna-Lea: Semipermeable membrane devices in monitoring persistent organic pollutants in the environment. (58 pp.) 2000
77. Lahtinen, Manu: *In situ* X-ray powder diffraction studies of Pt/C, CuCl/C and Cu_2O/C catalysts at elevated temperatures in various reaction conditions. (92 pp.) 2000
78. Tamminen, Jari: Syntheses, empirical and theoretical characterization, and metal cation complexation of bile acid-based monomers and open/closed dimers. (54 pp.) 2000
79. Vatanen, Virpi: Experimental studies by EPR and theoretical studies by DFT calculations of α-amino-9,10-anthraquinone radical anions and cations in solution. (37 pp.) 2000
80. Kotilainen, Risto: Chemical changes in wood during heating at 150-260 °C. (57 pp.) 2000
81. Nissinen, Maija: X-ray structural studies on weak, non-covalent interactions in supramolecular compounds. (69 pp.) 2001
82. Wegelius, Elina: X-ray structural studies on self-assembled hydrogen-bonded networks and metallosupramolecular complexes. (84 pp.) 2001
83. Paasivirta, Jaakko (Ed.): CEOEC'2001, Fifth Finnish-Russian Seminar: Chemistry and Ecology of Organo-Element Compounds. (163 pp.) 2001
84. Kiljunen, Toni: Theoretical studies on spectroscopy and

atomic dynamics in rare gas solids. (56 pp.) 2001

85. Du, Jin: Derivatives of dextran: synthesis and applications in oncology. (48 pp.) 2001
86. Koivisto, Jari: Structural analysis of selected polychlorinated persistent organic pollutants (POPs) and related compounds. (88 pp.) 2001
87. Feng, Zhinan: Alkaline pulping of non-wood feedstocks and characterization of black liquors. (54 pp.) 2001
88. Halonen, Markku: Lahon havupuun käyttö sulfaattiprosessin raaka-aineena sekä havupuun lahontorjunta. (90 pp.) 2002
89. Falábu, Dezsö: Synthesis, conformational analysis and complexation studies of resorcarene derivatives. (212 pp.) 2001
90. Lehtovuori, Pekka: EMR spectroscopic studies on radicals of ubiquinones Q-*n*, vitamin K_3 and vitamine E in liquid solution. (40 pp.) 2002
91. Perkkalainen, Paula: Polymorphism of sugar alcohols and effect of grinding on thermal behavior on binary sugar alcohol mixtures. (53 pp.) 2002
92. Ihalainen, Janne: Spectroscopic studies on light-harvesting complexes of green plants and purple bacteria. (42 pp.) 2002
93. Kunttu, Henrik, Kiljunen, Toni (Eds.): 4th International Conference on Low Temperature Chemistry. (159 pp.) 2002
94. Väisänen, Ari: Development of methods for toxic element analysis in samples with environmental concern by ICP-AES and ETAAS. (54 pp.) 2002
95. Luostarinen, Minna: Synthesis and characterisation of novel resorcarene derivatives. (200 pp.) 2002
96. Louhelainen, Jarmo: Changes in the chemical composition and physical properties of wood and nonwood black liquors during heating. (68 pp.) 2003
97. Lahtinen, Tanja: Concave hydrocarbon cyclophane π-prismands. (65 pp.) 2003
98. Laihia, Katri (Ed.): NBC 2003, Symposium on Nuclear, Biological and Chemical Threats – A Crisis Management Challenge. (245 pp.) 2003
99. Oasmaa, Anja: Fuel oil quality properties of wood-based pyrolysis liquids. (32 pp.) 2003
100. Virtanen, Elina: Syntheses, structural characterisation, and cation/anion recognition properties of nano-sized bile acid-based host molecules and their precursors. (123 pp.) 2003
101. Nättinen, Kalle: Synthesis and X-ray structural studies of organic and metallo-organic supramolecular systems. (79 pp.) 2003
102. Lampiselkä, Jarkko: Demonstraatio lukion kemian opetuksessa. (285 pp.) 2003
103. Kallioinen, Jani: Photoinduced dynamics of $Ru(dcbpy)_2(NCS)_2$ – in solution and on nanocrystalline titanium dioxide thin films. (47 pp.) 2004
104. Valkonen, Arto (Ed.): VII Synthetic Chemistry Meeting and XXVI Finnish NMR Symposium. (103 pp.) 2004

105. Vaskonen, Kari: Spectroscopic studies on atoms and small molecules isolated in low temperature rare gas matrices. (65 pp.) 2004
106. Lehtovuori, Viivi: Ultrafast light induced dissociation of $Ru(dcbpy)(CO)_2I_2$ in solution. (49 pp.) 2004
107. Saarenketo, Pauli: Structural studies of metal complexing Schiff bases, Schiff base derived *N*-glycosides and cyclophane π-prismands. (95 pp.) 2004
108. Paasivirta, Jaakko (Ed.): CEOEC'2004, Sixth Finnish-Russian Seminar: Chemistry and Ecology of Organo-Element Compounds. (147 pp.) 2004
109. Suontamo, Tuula: Development of a test method for evaluating the cleaning efficiency of hard-surface cleaning agents. (96 pp.) 2004
110. Güneş, Minna: Studies of thiocyanates of silver for nonlinear optics. (48 pp.) 2004
111. Ropponen, Jarmo: Aliphatic polyester dendrimers and dendrons. (81 pp.) 2004
112. Vu, Mân Thi Hong: Alkaline pulping and the subsequent elemental chlorine-free bleaching of bamboo (*Bambusa procera*). (69 pp.) 2004
113. Mansikkamäki, Heidi: Self-assembly of resorcinarenes. (77 pp.) 2006
114. Tuononen, Heikki M.: EPR spectroscopic and quantum chemical studies of some inorganic main group radicals. (79 pp.) 2005
115. Kaski, Saara: Development of methods and applications of laser-induced plasma spectroscopy in vacuum ultraviolet. (44 pp.) 2005
116. Mäkinen, Riika-Mari: Synthesis, crystal structure and thermal decomposition of certain metal thiocyanates and organic thiocyanates. (119 pp.) 2006
117. Ahokas, Jussi: Spectroscopic studies of atoms and small molecules isolated in rare gas solids: photodissociation and thermal reactions. (53 pp.) 2006
118. Busi, Sara: Synthesis, characterization and thermal properties of new quaternary ammonium compounds: new materials for electrolytes, ionic liquids and complexation studies. (102 pp.) 2006
119. Mäntykoski, Keijo: PCBs in processes, products and environment of paper mills using wastepaper as their raw material. (73 pp.) 2006
120. Laamanen, Pirkko-Leena: Simultaneous determination of industrially and environmentally relevant aminopolycarboxylic and hydroxycarboxylic acids by capillary zone electrophoresis. (54 pp.) 2007
121. Salmela, Maria: Description of oxygen-alkali delignification of kraft pulp using analysis of dissolved material. (71 pp.) 2007
122. Lehtovaara, Lauri: Theoretical studies of atomic scale impurities in superfluid ^{4}He. (87 pp.) 2007
123. Rautiainen, J. Mikko: Quantum chemical calculations of structures, bonding, and spectroscopic properties of some sulphur and selenium iodine cations. (71 pp.) 2007
124. Nummelin, Sami: Synthesis, characterization, structural and

retrostructural analysis of self-assembling pore forming dendrimers. (286 pp.) 2008

125. Sopo, Harri: Uranyl(VI) ion complexes of some organic aminobisphenolate ligands: syntheses, structures and extraction studies. (57 pp.) 2008
126. Valkonen, Arto: Structural characteristics and properties of substituted cholanoates and *N*-substituted cholanamides. (80 pp.) 2008
127. Lähde, Anna: Production and surface modification of pharmaceutical nano- and microparticles with the aerosol flow reactor. (43 pp.) 2008
128. Beyeh, Ngong Kodiah: Resorcinarenes and their derivatives: synthesis, characterization and complexation in gas phase and in solution. (75 pp.) 2008
129. Välisaari, Jouni, Lundell, Jan (Eds.): Kemian opetuksen päivät 2008: uusia oppimisympäristöjä ja ongelmalähtöistä opetusta. (118 pp.) 2008
130. Myllyperkiö, Pasi: Ultrafast electron transfer from potential organic and metal containing solar cell sensitizers. (69 pp.) 2009
131. Käkölä, Jaana: Fast chromatographic methods for determining aliphatic carboxylic acids in black liquors. (82 pp.) 2009
132. Koivukorpi, Juha: Bile acid-arene conjugates: from photoswitchability to cancer cell detection. (67 pp.) 2009
133. Tuuttila, Tero: Functional dendritic polyester compounds: synthesis and characterization of small bifunctional dendrimers and dyes. (74 pp.) 2009
134. Salorinne, Kirsi: Tetramethoxy resorcinarene based cation and anion receptors: synthesis, characterization and binding properties. (79 pp.) 2009
135. Rautiainen, Riikka: The use of first-thinning Scots pine (*Pinus sylvestris*) as fiber raw material for the kraft pulp and paper industry. (73 pp.) 2010
136. Ilander, Laura: Uranyl salophens: synthesis and use as ditopic receptors. (199 pp.) 2010
137. Kiviniemi, Tiina: Vibrational dynamics of iodine molecule and its complexes in solid krypton - Towards coherent control of bimolecular reactions? (73 pp.) 2010
138. Ikonen, Satu: Synthesis, characterization and structural properties of various covalent and non-covalent bile acid derivatives of N/O-heterocycles and their precursors. (105 pp.) 2010
139. Siitonen, Anni: Spectroscopic studies of semiconducting single-walled carbon nanotubes. (56 pp.) 2010
140. Raatikainen, Kari: Synthesis and structural studies of piperazine cyclophanes – Supramolecular systems through Halogen and Hydrogen bonding and metal ion coordination. (69 pp.) 2010
141. Leivo, Kimmo: Gelation and gel properties of two- and three-component Pyrene based low molecular weight organogelators. (116 pp.) 2011
142. Martiskainen, Jari: Electronic energy transfer in light-harvesting complexes isolated from *Spinacia oleracea* and from three

photosynthetic green bacteria *Chloroflexus aurantiacus*, *Chlorobium tepidum*, and *Prosthecochloris aestuarii*. (55 pp.) 2011

143. Wichmann, Oula: Syntheses, characterization and structural properties of [O,N,O,X′] aminobisphenolate metal complexes. (101 pp.) 2011
144. Ilander, Aki: Development of ultrasound-assisted digestion methods for the determination of toxic element concentrations in ash samples by ICP-OES. (58 pp.) 2011
145. The Combined XII Spring Meeting of the Division of Synthetic Chemistry and XXXIII Finnish NMR Symposium. Book of Abstracts. (90 pp.) 2011
146. Valto, Piia: Development of fast analysis methods for extractives in papermaking process waters. (73 pp.) 2011
147. Andersin, Jenni: Catalytic activity of palladium-based nanostructures in the conversion of simple olefinic hydro- and chlorohydrocarbons from first principles. (78 pp.) 2011
148. Aumanen, Jukka: Photophysical properties of dansylated poly(propylene amine) dendrimers. (55 pp.) 2011
149. Kärnä, Minna: Ether-functionalized quaternary ammonium ionic liquids – synthesis, characterization and physicochemical properties. (76 pp.) 2011
150. Jurček, Ondřej: Steroid conjugates for applications in pharmacology and biology. (57 pp.) 2011
151. Nauha, Elisa: Crystalline forms of selected Agrochemical actives: design and synthesis of cocrystals. (77 pp.) 2012
152. Ahkola, Heidi: Passive sampling in monitoring of nonylphenol ethoxylates and nonylphenol in aquatic environments. (92 pp.) 2012
153. Helttunen, Kaisa: Exploring the self-assembly of resorcinarenes: from molecular level interactions to mesoscopic structures. (78 pp.) 2012
154. Linnanto, Juha: Light excitation transfer in photosynthesis revealed by quantum chemical calculations and exiton theory. (179 pp.) 2012
155. Roiko-Jokela, Veikko: Digital imaging and infrared measurements of soil adhesion and cleanability of semihard and hard surfaces. (122 pp.) 2012
156. Noponen, Virpi: Amides of bile acids and biologically important small molecules: properties and applications. (85 pp.) 2012
157. Hulkko, Eero: Spectroscopic signatures as a probe of structure and dynamics in condensed-phase systems – studies of iodine and gold ranging from isolated molecules to nanoclusters. (69 pp.) 2012
158. Lappi, Hanna: Production of Hydrocarbon-rich biofuels from extractives-derived materials. (95 pp.) 2012
159. Nykänen, Lauri: Computational studies of Carbon chemistry on transition metal surfaces. (76 pp.) 2012
160. Ahonen, Kari: Solid state studies of pharmaceutically important molecules and their derivatives. (65 pp.) 2012

161. Pakkanen, Hannu: Characterization of organic material dissolved during alkaline pulping of wood and non-wood feedstocks. (76 pp.) 2012
162. Moilanen, Jani: Theoretical and experimental studies of some main group compounds: from closed shell interactions to singlet diradicals and stable radicals. (80 pp.) 2012
163. Himanen, Jatta: Stereoselective synthesis of Oligosaccharides by *De Novo* Saccharide welding. (133 pp.) 2012
164. Bunzen, Hana: Steroidal derivatives of nitrogen containing compounds as potential gelators. (76 pp.) 2013
165. Seppälä, Petri: Structural diversity of copper(II) amino alcohol complexes. Syntheses, structural and magnetic properties of bidentate amino alcohol copper(II) complexes. (67 pp.) 2013
166. Lindgren, Johan: Computational investigations on rotational and vibrational spectroscopies of some diatomics in solid environment. (77 pp.) 2013
167. Giri, Chandan: Sub-component self-assembly of linear and non-linear diamines and diacylhydrazines, formulpyridine and transition metal cations. (145 pp.) 2013
168. Riisiö, Antti: Synthesis, Characterization and Properties of Cu(II)-, Mo(VI)- and U(VI) Complexes With Diaminotetraphenolate Ligands. (51 pp.) 2013
169. Kiljunen, Toni (Ed.): Chemistry and Physics at Low Temperatures. Book of Abstracts. (103 pp.) 2013
170. Hänninen, Mikko: Experimental and Computational Studies of Transition Metal Complexes with Polydentate Amino- and Aminophenolate Ligands: Synthesis, Structure, Reactivity and Magnetic Properties. (66 pp.) 2013
171. Antila, Liisa: Spectroscopic studies of electron transfer reactions at the photoactive electrode of dye-sensitized solar cells. (53 pp.) 2013
172. Kemppainen, Eeva: Mukaiyama-Michael reactions with α-substituted acroleins – a useful tool for the synthesis of the pectenotoxins and other natural product targets. (190 pp.) 2013
173. Virtanen, Suvi: Structural Studies of Dielectric Polymer Nanocomposites. (49 pp.) 2013
174. Yliniemelä-Sipari, Sanna: Understanding The Structural Requirements for Optimal Hydrogen Bond Catalyzed Enolization – A Biomimetic Approach.(160 pp.) 2013
175. Leskinen, Mikko V: Remote β-functionalization of β'-keto esters. (105 pp.) 2014
176. 12th European Conference on Research in Chemistry Education (ECRICE2014). Book of Abstracts. (166 pp.) 2014
177. Peuronen, Anssi: N-Monoalkylated DABCO-Based N-Donors as Versatile Building Blocks in Crystal Engineering and Supramolecular Chemistry. (54 pp.) 2014
178. Perämäki, Siiri: Method development for determination and recovery of rare earth elements from industrial fly ash. (88 pp.) 2014

179. Chernyshev, Alexander, N.: Nitrogen-containing ligands and their platinum(IV) and gold(III) complexes: investigation and basicity and nucleophilicity, luminescence, and aurophilic interactions. (64 pp.) 2014
180. Lehto, Joni: Advanced Biorefinery Concepts Integrated to Chemical Pulping. (142 pp.) 2015
181. Tero, Tiia-Riikka: Tetramethoxy resorcinarenes as platforms for fluorescent and halogen bonding systems. (61 pp.) 2015
182. Löfman, Miika: Bile acid amides as components of microcrystalline organogels. (62 pp.) 2015
183. Selin, Jukka: Adsorption of softwood-derived organic material onto various fillers during papermaking. (169 pp.) 2015
184. Piisola, Antti: Challenges in the stereoselective synthesis of allylic alcohols. (210 pp.) 2015
185. Bonakdarzadeh, Pia: Supramolecular coordination polyhedra based on achiral and chiral pyridyl ligands: design, preparation, and characterization. (65 pp.) 2015
186. Vasko, Petra: Synthesis, characterization, and reactivity of heavier group 13 and 14 metallylenes and metalloid clusters: small molecule activation and more. (66 pp.) 2015
187. Topić, Filip: Structural Studies of Nano-sized Supramolecular Assemblies. (79 pp.) 2015
188. Mustalahti, Satu: Photodynamics Studies of Ligand-Protected Gold Nanoclusters by using Ultrafast Transient Infrared Spectroscopy. (58 pp.) 2015
189. Koivisto, Jaakko: Electronic and vibrational spectroscopic studies of gold-nanoclusters. (63 pp.) 2015
190. Suhonen, Aku: Solid state conformational behavior and interactions of series of aromatis oligoamide foldamers. (68 pp.) 2016
191. Soikkeli, Ville: Hydrometallurgical recovery and leaching studies for selected valuable metals from fly ash samples by ultrasound-assisted extraction followed by ICP-OES determination. (107 pp.) 2016
192. XXXVIII Finnish NMR Symposium. Book of Abstracts. (51 pp.) 2016
193. Mäkelä, Toni: Ion Pair Recognition by Ditopic Crown Ether Based bis-Urea and Uranyl Salophen Receptors. (75 pp.) 2016
194. Lindholm-Lehto, Petra: Occurrence of pharmaceuticals in municipal wastewater treatment plants and receiving surface waters in Central and Southern Finland. (98 pp.) 2016
195. Härkönen, Ville: Computational and Theoretical studies on Lattice Thermal conductivity and Thermal properties of Silicon Clathrates. (89 pp.) 2016
196. Tuokko, Sakari: Understanding selective reduction reactions with heterogeneous Pd and Pt: climbing out of the black box. (85 pp.) 2016
197. Nuora, Piia: Monitapaustutkimus LUMA-Toimintaan liittyvissä oppimisympäristöissä tapahtuvista kemian oppimiskokemuksista. (171 pp.) 2016

198. Kumar, Hemanathan: Novel Concepts on The Recovery of By-Products from Alkaline Pulping. (61 pp.) 2016
199. Arnedo-Sánchez, Leticia: Lanthanide and Transition Metal Complexes as Building Blocks for Supramolecular Functional Materials. (227 pp.) 2016
200. Gell, Lars: Theoretical Investigations of Ligand Protected Silver Nanoclusters. (134 pp.) 2016
201. Vaskuri, Juhani: Oppiennätyksistä opetussuunnitelman perusteisiin - lukion kemian kansallisen opetussuunnitelman kehittyminen Suomessa vuosina 1918-2016. (314 pp.) 2017
202. Lundell Jan, Kiljunen Toni (Eds.): 22nd Horizons in Hydrogen Bond Research. Book of Abstracts. 2017
203. Turunen, Lotta: Design and construction of halogen-bonded capsules and cages. (61 pp.) 2017
204. Hurmalainen, Juha: Experimental and computational studies of unconventional main group compounds: stable radicals and reactive intermediates. (88 pp.) 2017
205. Koivistoinen Juha: Non-linear interactions of femtosecond laser pulses with graphene: photo-oxidation, imaging and photodynamics. (68 pp.) 2017
206. Chen, Chengcong: Combustion behavior of black liquors: droplet swelling and influence of liquor composition. (39 pp.) 2017
207. Mansikkamäki, Akseli: Theoretical and Computational Studies of Magnetic Anisotropy and Exchange Coupling in Molecular Systems. (190 p. + included articles) 2018.
208. Tatikonda, Rajendhraprasad: Multivalent N-donor ligands for the construction of coordination polymers and coordination polymer gels. (62 pp.) 2018
209. Budhathoki, Roshan: Beneficiation, desilication and selective precipitation techniques for phosphorus refining from biomass derived fly ash. (64 pp.) 2018
210. Siitonen, Juha: Synthetic Studies on 1-azabicyclo[5.3.0]decane Alkaloids. (140 pp.) 2018
211. Ullah, Saleem: Advanced Biorefinery Concepts Related to Non-wood Feedstocks. (57 pp.) 2018
212. Ghalibaf, Maryam: Analytical Pyrolysis of Wood and Non-Wood Materials from Integrated Biorefinery Concepts. (106 pp.) 2018

DEPARTMENT OF CHEMISTRY, UNIVERSITY OF JYVÄSKYLÄ
DISSERTATIONS PUBLISHED IN THE JYU DISSERTATIONS RESEARCH SERIES

1. Bulatov, Evgeny: Synthetic and structural studies of covalent and non-covalent interactions of ligands and metal center in platinum(II) complexes containing 2,2′-dipyridylamine or oxime ligands. (58 pp.) 2019. JYU Dissertations 70.
2. Annala, Riia: Conformational Properties and Anion Complexes of Aromatic Oligoamide Foldamers. (80 pp.) 2019. JYU Dissertations 84.
3. Isoaho, Jukka Pekka: Dithionite Bleaching of Thermomechanical Pulp - Chemistry and Optimal Conditions. (73 pp.) 2019. JYU Dissertations 85.
4. Nygrén, Enni: Recovery of rubidium from power plant fly ash. (98 pp.) 2019. JYU Dissertations 136.
5. Kiesilä, Anniina: Supramolecular chemistry of anion-binding receptors based on concave macromolecules. (68 pp.) 2019. JYU Dissertations 137.
6. Sokolowska, Karolina: Study of water-soluble p-MBA-protected gold nanoclusters and their superstructures. (60 pp.) 2019. JYU Dissertations 167.
7. Lahtinen, Elmeri: Chemically Functional 3D Printing: Selective Laser Sintering of Customizable Metal Scavengers. (71 pp.) 2019. JYU Dissertations 175.
8. Larijani, Amir: Oxidative reactions of cellulose under alkaline conditions. 2020. JYU Dissertations.